TITLE:	Analysis of seismograph Geophone Coupling Methods for Blasting
OSM Project Number	
Type of Report	Final
Reporting Period Start Date	February 2008
Reporting Period End Date	December 2011
Principal Author(s)	Catherine T. Aimone-Martin and Tye J. Lasich
Date Report was Issued	February 2012
OSM Award Number	S07AF12473

Aimone-Martin Associates, LLC
1005 Bullock Ave.
Socorro, NM 87801

Thomas B. Moser, MS student
Allen B. Kinney, MS student

Disclaimer

ABSTRACT

Surface blasts were studied to compare the response of different geophone attachment methods. This project, funded by the Office of Surface Mining (OSM), will have direct application within all sectors of the blasting industry. A total of 37 blast sites were included in this study resulting in 486 individual seismograph records used for comparison.

Deployment of geophones in the field to measure off-site impacts of blasting vibrations has long been a topic of concern to vibration specialists, regulators, and researchers. Geophones are often placed in or on the ground without consideration of measurement reliability. Vibration measurements inherently possess a high degree of data scatter that, in part, may be attributed to errors associated with geophone manufacture, calibration, and deployment protocols. Inconsistent or erroneous readings may have serious regulatory compliance consequences. Furthermore, blast design modifications systematically employed during blasting to control off-site impacts and structure motions may be hampered by vibration measurements errors with decoupled geophones.

This project employed statistical analyses to compare different sensor attachment methods to the ground to understand ground motion conditions leading to geophone decoupling in terms of peak velocities, accelerations, and frequency components. Attachment methods included burial, spiking, sandbag, and combinations of spiking and burial, and spiking and sandbag, In addition the effects loose sensors placed on the ground and sensor shape were investigated.

Small-scale repeatability tests were conducted to establish a statistical measure of human-induced errors associated with sensor deployment. Human errors were combined with variabilities due to manufacture to form uncertainty bounds to asses outliers.

Large scale production blasts were monitored using different coupling methods in clusters at various scaled distances in which seismographs were connected in series to achieve a common time base of recording. Peak particle velocities (PPV) ranged 0.07 to 2.68 in/s, frequencies ranged 2.4 to 46.5 Hz, and accelerations ranged 0.02 to 1.01 g. Decoupling was identified when relative ratios of measurements exceeded acceptable uncertainty bounds and were verified using other comparisons such as time-history plots and linear regression analysis applied to scatter diagrams and comparative plots of ground motion components.

Sensor burial provided the least data scatter with the lowest measurement error compared with all other attachment methods. A total of 9 blasts out of 25, or 36% of the blasts, indicated decoupling of a non-burial method. Sensors with spikes and sandbags generated, on average, PPVs that were 38% and 54% greater than buried sensors, respectively. Geophones used with sandbags produced the highest scatter in velocity

and frequency amplitudes while spiked sensors exhibited fairly consistent enhancements of PPV and peak frequencies compared with buried sensors.

The use of acceleration as a guideline to select an appropriate geophone coupling methods did not prove as effective as the use of peak frequency. Decoupling of non-buried sensors occurred for only 53% of the blasts when ground motions accelerations were greater than 0.2 g's. Using a frequency criteria, 79% of the blasts showed decoupling when ground motion peak frequencies were greater than 9 Hz.

TABLE OF CONTENTS

Appendix D Summary statistics for human-induced error tests

LIST OF FIGURES

LIST OF TABLES

EXECUTIVE SUMMARY

The purpose of this study was to compare the vibration response of different geophone attachments methods on or within the ground surface at coal mines, quarries, and construction blast sites. Coupling methods included geophones that were buried, placed loose on the surface, used spikes or sandbags on the surface, combined spiking and sandbags, and combined spiking and burial. Seismographs placed in clusters with sensors of various attachment methods were co-triggered to enable time-history comparisons. Clusters were placed at varying scaled distances from each blast to quantify the attenuation characteristics of different coupling methods.

Geophone coupling was studied on a small-scale using signature hole tests at a constant scaled distance and during full-scale production blasts. Single blast hole tests were conducted to measure human-induced variabilities among a large number of geophones, each deployed by a different person, and included sensor that were buried, spiked, overlain by a sandbag, and spiked with a sandbag. Uncertainty analysis was performed on peak particle velocities (PPV) to compute a relative standard error (RSE) and establish human deployment errors for common sensor attachments. This error was added to known geophone manufacture and calibration errors ($\pm$5%). The resulting combined RSE, computed using National Institutes of Standards and Technology methods, were $\pm$ 3.30%, $\pm$ 4.74%, $\pm$ 10.15%, and $\pm$ 7.11% for burial, spiking, sandbag, and combined sandbag and spiking, respectively. These values formed error bounds used to identify outliers when full-scale production vibration measurements fell outside expected uncertainty limits.

Error analysis further made use of the concept referred to as relative PPV defined as the ratio of PPV for each selected method divided by the PPV of the buried sensor within each cluster. In this study, it was assumed that a well-compacted, buried sensor represented 100% coupling and formed the basis of comparison for all other methods.

Large-scale blasts took place in 8 states with a variety of field conditions and blasting methodologies for 37 blasts generating 486 seismograph records. Ground motions were evaluated by component and in terms of peak particle velocity (PPV), acceleration, and frequency. PPVs ranged from 0.07 to 2.68 in/s, frequencies ranged from 2.4 to 46.5 Hz, and accelerations ranged from 0.02 to 1.01 g.

Germaine to this study was the wealth of data and findings for geophone attachment to compare with guidelines based on ground acceleration. Between 0.2 g's and 1.0 g's, geophone spiking is recommended by the International Society of explosives Engineers based on finding of the U.S. Bureau of Mines. However, the International Society of Rock Mechanics discourages spiking. Observations and calculations presented in this study are intended to be used as a guide to seek alternative criteria to minimize the chances of geophone decoupling.

A variety of visual and statistical techniques were applied to the data to determine when decoupling may occur based on peak component velocities and PPV, peak frequency,

and computed acceleration. These included overlaying ground motion time-histories for different methods. Linear regression analysis was used to compare PPV, peak frequency and acceleration among coupling methods and also applied to scatter plots in which time-correlated component velocity amplitudes were graphed. Linear regression was useful to detect decoupling and the degree to which data correlated.

Study findings comparing sensor performance using the most common attachment methods relative to well-coupled buried sensors are outlined as follows:.

- The use of surface spiking and sandbags can overestimate PPV by 38% for spiking, and 54% with sandbags (average values).
- In general, ground frequencies below 9 Hz may result in lower velocity amplitudes for spiked sensors while above 9 Hz, spiked sensor velocities are more likely to exhibit higher readings than for buried sensors.
- The use of spiking lowers frequencies in the vertical (V) direction and increases frequencies in the horizontal components.
- The use of spikes may only be appropriate at ground frequencies less than 9 Hz regardless of velocity amplitude.
- The use of spikes when burying sensors does not appear to have any performance advantage over a well-coupled buried sensor without spikes.
- Repeated tests measuring human-deployment errors verified that the use of sandbags resulted in the highest standard error among all methods tested.
- Sandbags used to cover geophones on the ground exhibited highly random behavior and caused time lags in peaks and velocity amplification in horizontal components.
- The use of sandbags when ground motion PPV is expected to be over 0.2 in/s with a peak frequency over 13 Hz should be discouraged.
- Adding spikes to a geophone covered with a sandbag does not contribute any added benefits to coupling.

Based on error analysis for four common attachment methods at 25 blast sites, the following was observed:

- 36% of the blasts exhibited decoupling relative to buried sensors in each category of spiked, sandbag, and combined spiked and sandbag sensors.
- 66% of sandbag relative PPV measurement fell outside error bounds.
- The ability of using acceleration criteria to recognized errors outside uncertainty bounds is poor; above 0.2 g’s only 53% of site exhibited decoupling while 47% did not.
- Correlations between buried sensor frequency and decoupling indicated peak ground motion frequency may be a good indicator of decoupling; above 9 Hz buried sensor peak frequency, 79% of the blast exhibited decoupling.

Other findings of interest include the following:

- Decoupling may lead to non-compliance at high PPV and intermediate frequencies.
- There appears to be little correlation between geophone performance and soil properties for buried and spiked geophones while wet cohesive soils produced high frequency wavelets superimposed on lower frequencies for horizontal motions that were not indicative of decoupling.
- Attenuation models based on coupling methods were statistically the same.

1. INTRODUCTION

Current industry practice in the use of seismographs for monitoring blasts includes a wide range of geophone coupling protocols that can result in erroneous and inconsistent ground vibration readings. Improper coupling methods can produce erratic readings that may be misconstrued as geological anomalies rather than poor sensor coupling.

Geophone “decoupling” can occur during blast-induced ground motions when the sensor is allowed to slip along the ground surface, rotate on the surface about spikes acting as pivot points, or bounce independent of the ground movement. Geophones decoupled from true ground movement can greatly underestimate ground vibrations. Conversely, sensor movement independent of the ground can result in higher than expected velocity measurements and exceed regulatory compliance limits.

It is not easy to account for the many variables influencing vibrations measurement, such as environmental effects, measurement equipment, and measuring techniques. Other complications involve the blast site itself. Highly variable site conditions (seismic source and transmission medium properties) may produce little or no discernable differences in time-histories between two or more coupling methods. In contrast, similar conditions can produce widely varying results even when sensors are rigidly attached to the moving ground.

Clearly in such studies of methodology, it is not possible to define the “best” procedure resulting in accurate and repeatable measurements. The true value of ground vibration can only be estimated by measurement subjected to random effects that introduce uncertainty in measurements. Understanding the sources of measurement variability and quantifying errors associated with uncertainty is the first step in identifying when poor coupling might occur.

1.1 Scope of Study

This study compares the performance of different geophone coupling methods by using a variety of statistical methods and correlation plots to determine under what circumstance sensors may become decoupling. The identification and measurement of decoupling during full-scale coal mine, quarry and construction blasting was central to this study.

To set the framework for analysis, two important baseline concepts were addressed. The first was to quantify sources of measurement errors introduced by the equipment (manufacture and calibration errors) and introduced by human deployment (human-induced errors). Equipment error bounds have been determined by seismograph manufactures. However, human deployment errors were determined in this study using small-scale, single blast (signature) holes and a large number of geophones. Error analysis was performed for each coupling method and used to demonstrate when decoupling is suspected from full-scale production blasts seismograph monitoring.

The second concept was to established geophone burial in the ground as the basis for

comparisons with all other surface attachments methods. Simple visual and statistical tools were used to identify possible geophone decoupling. These methods included plots of velocity time histories by geophone component, scatter plots, and linear regression correlation among measurements from different geophone coupling methods and uncertainty analysis to set error bounds on ground velocity measurements. Such comparative tools serve as a guide for seismograph users to avoid practices that may produce unreasonable or unexpected values.

1.2 Study Relevance

This project is an excellent example of research with high technology transfer potential because most end-users are persons deploying seismographs for regulatory compliance monitoring at mine and construction blast sites. Individuals benefiting from this study are drilling and blasting contractors (e.g. shot service companies), mine operators, construction managers, vibration consultants, regulators, independent third party consultants and design engineers. Each of these individuals possesses varying degrees of training and education in proper seismograph field deployment procedures.

It is further expected that the International Society of Explosives Engineering (ISEE) through the Blast Vibration and Seismograph Section may consider the findings of this study and incorporate recommendations for identifying sources of measurement error and reporting confidence intervals into the existing ISEE Field Practice Guidelines for Blasting Seismographs (ISEE 2009)

Lastly, uncertainly analysis procedures described in this report should be applied to all field measurements. The ability to understand and quantity error sources in any kind of measurement is the first step toward minimizing uncertainty. The future trend in scientific measurements will soon require defining systematic or random errors and conveying a level of confidence in data. Blast vibration measurements are often required to show compliance with regulations that limit amplitudes. Therefore, blasting seismograph users have a professional obligation to report measurement technique that minimized uncertainty.

2. PREVIOUS WORK

Preliminary work was conducted in the area of geophone coupling by the U.S. Bureau of Mines (USBM) and others. The Bureau study, RI 8506 (Stagg and Engler, 1980), compared 18 different seismograph models during lab and field-tests to measure amplitude, frequency response, and duration characteristics. Field blasting was conducted at quarries, coal mines, and construction sites to capture ground motions over a wide spectrum of frequencies. Coupling methods included geophones placed on the surface, buried, spiking, and sand bagged. Distortions in time histories were noted for improper coupling that was not described. Distortions included peaks at different times and up to $\pm$ 60% difference in peak amplitudes when comparing a surface mount (undefined) with a buried sensor. Recommendations for geophone placement were based on acceleration levels. At acceleration over 1.0 g, geophone burial in soil and

gluing or bolting to rock surfaces was recommended while for accelerations between 0.2 and 1.0 g, geophones spiking was recommended to prevent slippage. Regardless of ground accelerations, burial was recommended as the best coupling method.

The International Society of Rock Mechanics (ISRM, 1992), adopted the U.S. Bureau of Mines recommendations with the caveat that spiking is discouraged. It was noted spikes served as an anchor and transducers acted as inverted pendulums resulting in erroneous readings for radial and transverse components. Attachment to a hard surface by means of double-sided tape or quick setting cements were recommended when expected accelerations were greater than 1.0 g.

In 1999, the International Society of explosives Engineers Blast Vibration and Seismograph Section adopted recommendations in RI 8506 as guidelines for sensor coupling without modification in the ISEE Field Practice Guidelines for Blasting Seismographs. In 2009, Guidelines were revised without change for coupling recommendations for burial, sandbagging and spiking methods. In each addition is noted that a combination of both spiking and sandbagging gives even greater assurance that good coupling is obtained.

Grogan (1998) summarized recommendation guidelines for geophone coupling by manufacturers of seismographs and professional organizations. He noted placing a sandbag on top of sensors may be somewhat controversial due to inconsistent readings and recommended geophone burial at a depth of 15 cm (6 in) or more.

Robertson (1993) suggested improperly placed sandbags may cause geophones to rotate about a horizontal plane. No field data was provided in support of these observations but rather a static analysis of forces was performed to determine the direction of resultant forces acting on the sensor. Robertson addressed how the location of the geophones centroid is changed by the distributed weight of a sand bag leading to skewed data readings. He also demonstrated how the geophone base with or without spikes can rotate or slip founded on coefficients of friction and accelerations.

Blair (1995) discussed the use of a standard mount with an optimum mass factor that limits ground coupling problems. By knowing the soil density and shear wave velocity, sensor mount dimensions for an embedded mounted can be determine to obtain acceptable vibration measurements over the frequency range of interest. He showed with field work that spiking can over estimate vibration levels by 46%

Armstrong (2001) further investigated block mounts using accelerometers and found burial gave an acceptable 10% discrepancy at all vibration levels tested while spiked mounts showed greater than 30% variation. No data was provided in the thesis for review.

Wheeler (2004) investigated seismometer coupling during five field tests near a limestone quarry using three seismographs per test. The three methods included burial, spiked with a sand bag, and loose on the surface. Peak component velocities ranged

from 0.045 to 1.5 in/s and resulting accelerations far below 1.0 g. Wheeler determined geophone burial provided the best coupling to record ground vibrations because it showed the narrowest spread amongst recorded measurements. His conclusions provided corroboration with those of the USBM.

No studies have been conducted to date that incorporate a wide range of reported frequencies and ground accelerations for various scaled distances. In addition, there has not been a comprehensive study that includes all possible coupling scenarios nor the variation in propagation characteristics of different coupling methods. Additional factors that have not previously been considered are varying soil types, thickness of overlying bedrock, or the effects of geologic features, which might influence blast induced vibration intensity and trajectory resulting in erroneous geophone coupling results.

3. EXPERIMENTAL METHODS

3.1 Site Locations and Characteristics

Measurement of ground vibrations were conducted at 18 blasting operations, 25 blast sites, in eight states as shown in Figure 1. The study focus was on coal mines in Kentucky, West Virginia, Illinois, Ohio, Indiana, and Wyoming, quarries in Michigan and Ohio, and construction sites in New Mexico. Non-coal sites were selected to ensure a wide range of ground motion frequencies for analysis as coal mine blasting tends to generate low frequency ground motions. A total of 38 blasts were monitored during this study resulting in 486 seismograph records.

Site conditions represented a range of surface soils characteristics and thicknesses. Site soils ranged from silty sands with varying amount of gravels to clays and organic silts with water contents ranging from 3% to 36%. Soil thickness overlying rock varied

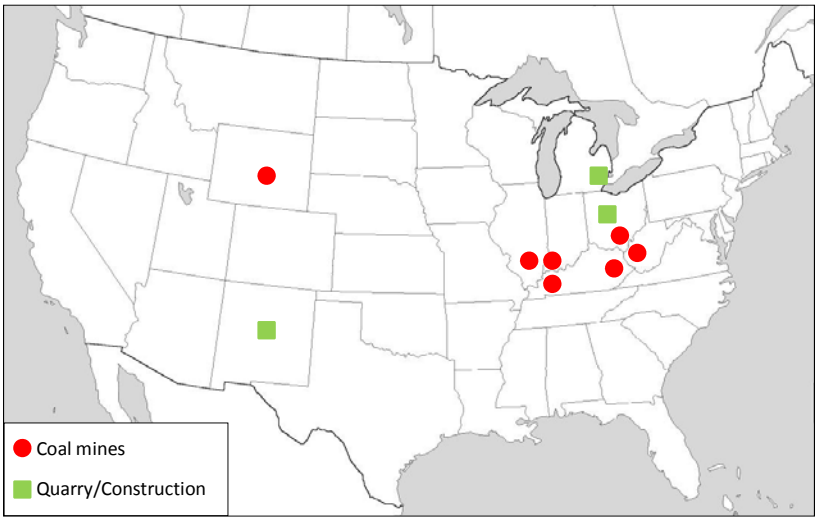

Figure 1 Site map showing the locations of study sites at coal mines, quarries and construction projects

from 2 to 40 ft. Testing included frozen ground and various thickness of grass and vegetation cover.

Table 1 lists the blast design parameters employed at each study site. The range of borehole diameters were from three to 12.3 inches while average hole depths ranged from five to 157 ft. Burdens and spacings ranged from four to 38 ft and four to 40 ft, respectively. The range of the number of rows was from one through 33, with three to 57 holes per row. The types of explosives included regular and heavy ANFO, 50/50 and 60/40 blends, 20% CarboPrill™, and Emulsion 60/40. The charge weights per delay ranged from 6 to 20,364 lbs.

3.2 Field Test Procedures

Field tests comprised small-scale single blast hole, or “signature”, tests to assess human-induced deployment errors and reproducibility of coupling methods and production-scale blast tests to evaluate decoupling potential for single deployment events. Tests were conducted with clusters of geophones. Each cluster was positioned at various scaled distances and co-triggered using special cables to compare sensor performance on a common time base. This approach was valuable for visual comparisons of time histories to show differences among peak amplitudes and frequency content.

3.2.1 Signature cluster tests

Three series of signature blasts were conducted using one-pound charges of Kinestik™ to measure human-induced variabilities among ground motion responses for a large number of co-triggered geophones and four different coupling methods. Methods used are considered to be the most commonly practiced and included clusters of geophones that were buried, spiked, overlain with a sandbag, and spiked with a sandbag. For each method, time histories were compared and relative standard errors associated with human deployment were calculated.

Tests 1 and 2 were conducted with geophones placed at the same nominal scaled distance of 100 ft/lb$^{1/2}$. Sensors remained in place for two blasts for each deployment method to assess repeatability. A total of 16 geophones, shown in Figure 2, were deployed by16 different persons per test for a total of 8 blasts. This translates to 128 different human deployments for statistical error analyses. The maximum component vibration ranged 0.07 to 0.105 in/s.

Test 3 included 4 different blasts, one for each of four coupling methods, using 19 co-triggered geophones, at a scaled distance ranging between 21 to 29 ft/lb ^{½}. The maximum component vibration ranged 0.54 to 2.0 in/s.

Table 1 Summary of blast designs at study sites

Shot ID	Shot ype[1]	Number of holes	Hole diameter	Average depth	Top stem	Burden	Spacing	Number of rows	Holes per row	Explosives[2]	Charge weight per delay
			(in)	(ft)	(ft)	(ft)	(ft)				(lbs)
Coal											
KY-1	production	29	6.8	50	10	16	16	5	6	ANFO	154
KY-2		15	6.8	49	10	16	16	5	3		154
KY-3	production/PS	56	7.9	69	9	18	21	6	7-14		1104
KY-4	PS	16	7.9	73	14	10	10	1	16	60/40 blend	134
KY-5	production	51	7.9	56	11	16.5	17	7	8	ANFO	134
IL-1		37	9.9	43	11	26	27	6	6	20% CarboPrill	841
IL-2		21	9.9	20	11	20	20	3	7		197
IN-3		41	9.9	93	9	21	27	7	6		2298
WY-1	production cast	39	9.0	73	17	28	28	3	13	60/40 blend	1992
WY-2		80	9.0	51	16	28	28	5	16		1237
WY-3		50	10.6	59	24	33	40	5	10	50/50 blend	3601
WY-4		396	12.3	103	56	35	32	5	79		17,701
WY-5		342	12.3	157	32	30	36	6	57		20,364
WY-6	coal	60	11.0	74	28	36	36	6	10		7056
WY-7	production	78	11.0	55	21	38	42	3	26		3504
OH-2		12	7.9	59	16	20	20	3	4	Heavy ANFO	469
OH-3		14	7.9	59	14	20	16	3	4		773
OH-4		100	7.9	20	12.5	18	18	9	10		549
OH-5		34	6.8	42	10	18	18	5	8	ANFO	343
OH-6		8	7.9	72	20	20	20	3	3		934
KY-6		75	7.9	57	7	18	18	8	8		378
KY-7		45	7.9	60	9	18	18	5	9		919
KY-8		50	6.7	26	10	16	16	4	13		211
WV-1		160	10.6	34	10	27	27	8	20	60/40 blend	6957
WV-2		71	7.8	26	10	18	18	5	14	ANFO	467
WV-3		50	7.8	22	10	18	18	2	25		647
Quarry											
MI-1	production	19	4.5	29	6	12	14	2	9	ANFO	124
MI-2		26	4.5	29	6	12	12	2	13		81
MI-3		21	4.5	29	6	12	12	2	10		82
MI-4		9	4.5	29	6	12	12	1	9		82
OH-1		39	6.5	101	13	16	19	4	10	Heavy ANFO	1490
Construction											
NM-1	mass-excavation	450	3	6	4	5	4	9	35	ANFO	33
NM-2		526	3	6	4	5	4	16	33		149
NM-3		548	3	6	4	5	4	30	21		150
NM-4		651	3	9	6	5	4	33	23		150
NM-5		332	4	24	8	9	9	12	28		336
NM-6		448	4	33	7	9	9	18	26		277
NM-7		58	3	5	4	4	4	3	19		4

[1] PS – pre-split

[2] CarboPrill™ - 80% ANFO and 20% coal

Blend – emulsion/ANFO given in percentage of each

Figure 2 Co-triggered seismographs used in signature cluster tests

3.2.2 Full-scale production tests

Three to eight standard tri-axial geophones deployed with different coupling methods were co-triggered by connecting seismographs in series and placed in one to five clusters at varying scaled distances along linear arrays away from blasts. Velocity time histories and peak amplitudes from geophone responses were compared within clusters to assess indication of possible decoupling. The purpose of using arrays was to determine if coupling method played a role in attenuation characteristics of vibrations as a function of distance.

Most clusters consisted of the three primary coupling methods that included buried, spiked, and sandbagged geophones. In many cases, additional geophones included other methods of attachments such as spiking with a sand bag, burying a spiked sensor, and loose on surface.

3.2.2 Attachment methods

The steps to attaching geophones are shown in Figures 3 and 4 for burial, spiking, and sand bagging geophones. Buried sensors were placed in holes dug six inches deep, compacting soil around and on top of the sensor. Spiked sensors were firmly pushed in the ground on a flattened area of ground surface until the sensor based made full ground contact at the base. Sandbags with 20 lbs of loose sand were draped over sensors placed on the ground to ensure the bag made contact with the ground on all sides. All sensors were adjusted with a bubble level.

In Figure 5, a cluster of six units are connected in series with serial cables linking each to a master triggering unit. The trigger unit was set to start recording ground motion time histories when the ground pulse exceeded a pre-set trigger level. This trigger in turn triggered all other “slave” units to start recording at the same time. Figure 6 shows seismographs grouped in clusters of three forming a linear array for a small blast.

Figure 3 Procedure used for geophone burial: digging hole six to eight inches (upper left). backfilling and tamping in lifts (lower left) and backfilling hole (lower right)

Figure 4 Procedure for geophone deployment for the spiking and sandbagging: clean and level the surface, positioning geophone (upper left), press spiked into the ground until sensor base is flush with ground surface (upper right); sand bag placement properly draped over and around sensor (bottom)

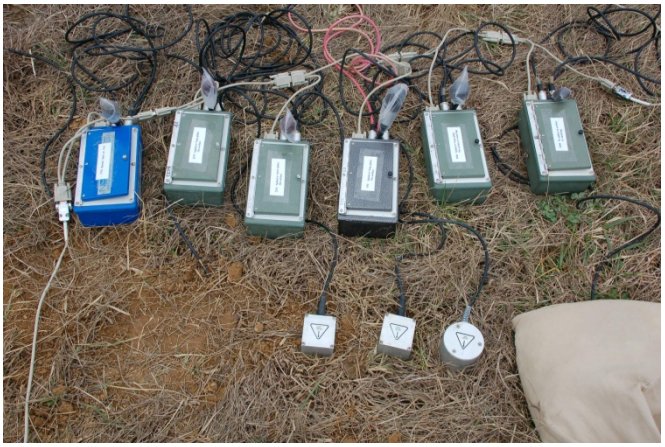

Figure 5 Primary cluster of seismographs linked in series for common trigger time

Figure 6 Clusters of three seismographs placed in a linear array and linked in series for common triggering

Each cluster positioned at various scaled distances was co-triggered to compare sensor performance on a common time base. This approach was valuable for visual comparisons of time histories to show differences among peak amplitudes and frequency content.

3.3 Methods of Analyses

Methods used to assess coupling performance included visual comparisons of velocity time histories, detailed analysis of summary statistics, and error analysis to quantify measurement uncertainties based on human influences in deploying any one coupling

method. No single analytical technique or data plot proved satisfactory to evaluate decoupling because of the many complexities arising from measuring ground motions from blasting. Therefore, several statistical methods were used and compared to identify and verify outliers or anomalous behavior that indicated possible geophone decoupling.

Uncertainty analysis was included as one method to assess coupling performance for any one single deployment method. Measurement error bounds were computed for human deployment for selected coupling methods and added to known manufacture and calibration errors. Peak vibrations using common attachment methods for single field blast site events were compared with the burial method used as a basis of comparison. This relative comparison was evaluated within error bounds to establish conditions under which decoupling most likely occurred for full-scale blasting. Geophone performance for common coupling method was normalize to the burial method because the performance of buried geophone was consistent and exhibited the least variability in terms of measured PPV.

3.3.1 Visual and statistical comparisons of relative responses

Preliminary data comparisons involved the use of time-history plots prepared in spreadsheet format to note the time location of positive and negative peaks by component (R, radial or longitudinal, V, vertical, and T, transverse). Seismograph software was used to convert event files to ASCII format. Time histories for records of co-triggered sensors (with the same time base) were visually inspected by overlaying time histories on the same plot to observe and compute differences among peak amplitudes relative to peaks obtained for the buried geophone. It was assumed geophone burial provided good and accurate “confined” coupling and this assumption was supported by error analysis. Therefore, peaks for other coupling mounts were compared with the peak for the buried method to determine the relative percentage change between burial and other methods. In this manner, attachment methods that produced possible horizontal slippage, rotation, or surface bounce were readily apparent.

Scatter plots of positive and negative velocity peaks over time were prepared and proven useful to determine statistical correlation between time histories for similar components between two sensors of different mounting. The linear regression correlation coefficient, R^2, was used to indicate the degree of agreement between methods. In most cases this was done to compare common coupling methods with geophone burial as the baseline method.

3.3.2 Baseline error analysis

Prior to field measurements at full-scale blast sites, a series of single hole blasts were conducted using a large number of seismographs to assess measurement uncertainty inherent to all mounting techniques. Because “accuracy” is hard to define for vibration measurements, the “best” or most accurate measurement value closest to the true

value may be defined as the measurement with the least error determine from repeated tests. Thus, error analysis was performed to quantify measurement differences for each geophone deployment method and determine which method represented the least variabilities.

Error analysis involves the use of the relative standard error (RSE) as an indicator of uncertainty computed as the standard error of the mean (SEM) divided by the data mean. For "n" measurements, SEM is computed as the standard deviation divide by the square root of the sample number.

Three error sources associated with peak component amplitudes as measured by any one coupling method were identified. These include the following

- manufacture and calibration, RSE_{mc},
- human errors introduced during sensor deployment for any one coupling method based on the standard deviation for a large number of repeated trails or observations, RSE_h , and
- errors associated with the coupling method itself during a one-time deployment and used to assess decoupling.

The combined standard uncertainty can be calculated for the first two error sources using the method described by the National Institutes of Standards and Technology (NIST) given by Taylor and Kuyatt, 1994, where

$$\text{combined standard uncertainty} = \pm \sqrt{RSE_{mc}^2 + RSE_h^2} \qquad (1)$$

This combined uncertainty is considered to represent "baseline error bounds" above or below which ground motion velocities for a one-time geophone deployment can be compared.

a. Geophone manufacture and calibration, RSE_{mc}

Instrumentation measurement errors associated with manufacture and calibration can be established and represented with a constant value. Geophone manufacture and calibration errors are currently being considered by the International Society of Explosives Engineers (ISEE) Standards Committee (Wheeler, 2004; Wheeler, personal communication). Wheeler cites a draft proposal by the ISEE Standards Committee specifying geophone accuracy as it relates to factory manufacture and calibration. The specification would allow the velocity measurement difference between any two seismograph systems to be $\pm$ 5% or measure $\pm$ 0.02 in/s, whichever is greater.

The National Institutes of Standards and Technology (NIST) quantified uncertainly of measurements in terms of the relative standard error of the mean (Taylor and Kuyatt, 1994). According to the NIST guidelines for evaluating and expressing uncertainty of NIST measurements, the standard uncertainty of calibration data can be estimated as a

Type B (or systematic) uncertainty for a uniform probability distribution with upper and lower limits from -a to +a. Hence, the best estimate of a measurement quantity is $(a_+ + a_-)/2$ and uncertainty is defined as

$$\frac{\pm a}{\sqrt{3}} \tag{2}$$

The error bound for the ISEE calibration standard is+5% and -5% for the frequency response of a geophone. Thus, the uncertainty is

$$\frac{\pm 5\%}{\sqrt{3}}$$

or $\pm$ 2.9%.

b. Human-induced errors, RSE_h

Human errors introduced in measurements during sensor deployment for any chosen coupling method are random and measurable using trial field tests. NITS considers the evaluation of uncertainty using statistical analyses of a series of random observations as a Type A evaluation of uncertainty. A number of blast measurements “n” were made using one method deployed by a large number of persons and statistics applied to the data set to quantify the data mean, standard deviation, confidence intervals, and relative standard error introduced by the method itself. Thus, errors for buried, spiked, sandbag, and combined spiked and sandbag sensors were determined and added to the manufacture error.

c. One-time deployment errors introduced during blast vibration monitoring

Measurement errors for a one-time deployment using clusters of geophones comparing coupling methods were analyzed in terms of peak particle velocity (PPV). PPV was selected as the basis for comparison for two reasons. PPV is most often used for compliance measurement. Further, in many cases the PPV resided in the same component (either vertical or radial) among sensors in any one cluster.

A dimensionless “deployment ratio” was used to compare coupling performance with baseline errors for one-time deployment and defined as relative PPV, where

$$\text{relative PPV} = \frac{\text{PPV from coupling method "n"}}{\text{PPV from burial method}} \tag{3}$$

and methods “n” may be spiking, sandbagging, loose on the ground, or a combination of spiking and sandbagging. Based on human error testing, the buried method provided the least errors and was used as a basis to identify possible decoupling for all other surface mounts.

The resulting plot from this analysis is similar to that shown in Figure 7 in which surface mounted sensors are compared to buried sensors for 16 blasts at different sites. In this generic example, the PPV ratio is defined as the PPV for the surface mount divided by the PPV for the buried sensor. The upper and lower bounds of baseline error in this example are presumed to be ±10%, or 1+10% (1.1) and 1-10% (0.9) and are shown with blue dashed lines on either side of unity.

The unusual high relative PPV value at mine site 2 fell far outside the acceptable baseline bounds and therefore signifies possible decoupling. For this example, the unusual high value reflects poor mounting for the surface mounted sensor at the site 2. By comparing relative PPV based on components, shown in Figure 8, it is apparent that both horizontal components (radial, R, and transverse, T) exhibited peaks that were outside error bounds and hence decoupling is suspected. This indicates that the surface sensor was not adequately constrained and may have moved laterally relative to the ground movement.

This analysis approach is similar to that used by Adhikari, et al. (2005). Adhikari considered both instrumental and human errors, using an assumed ±10% combined standard uncertainty applied to PPV ratios, to compare sensors with different mounting methods. No field measurements were performed to support this error bound and the buried sensor was used as the baseline of comparison.

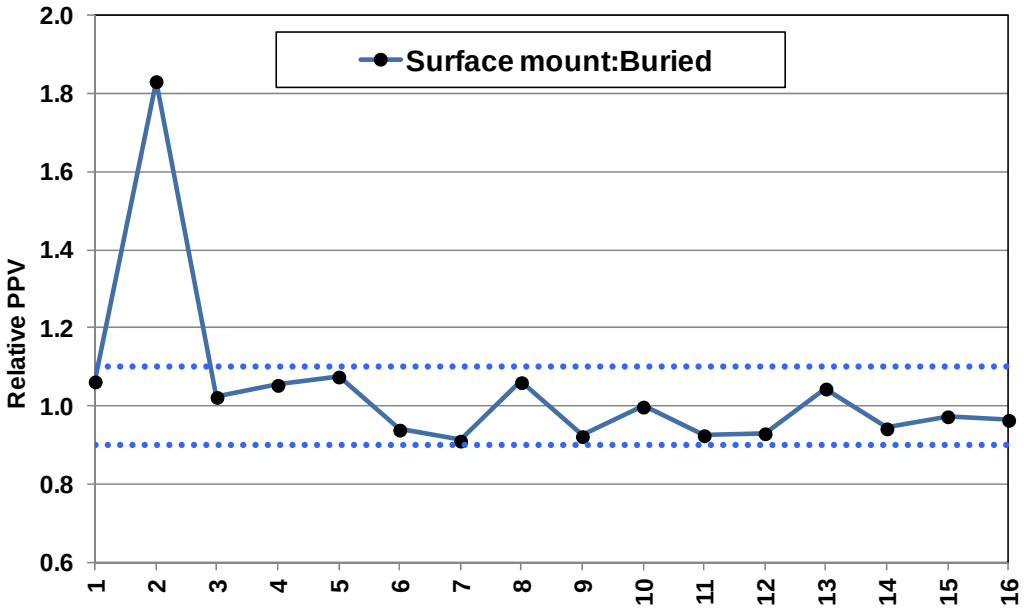

Figure 7 Relative PPV for surface mount compared with buried geophones at 16 sites

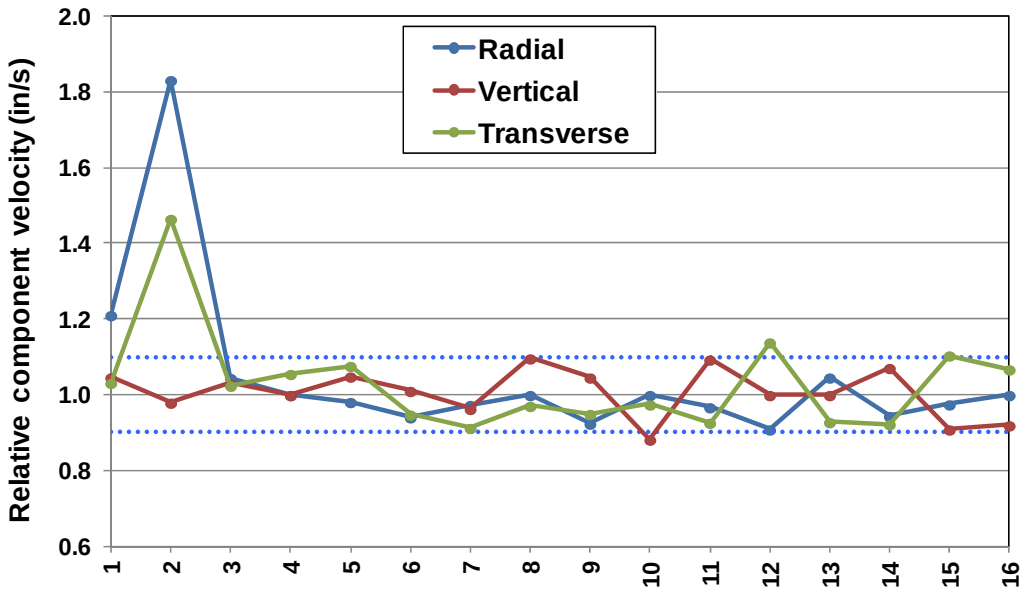

Figure 8 Relative component velocity for surface mount compared with buried geophones at 16 sites

4. RESULTS AND DISCUSSION

4.1 Results Summarized in Appendices

The results of this study are found in a large number of tables and plots that are found in a separate volume of appendices. A list of appendices is as follows:

- Appendix A - Summaries of vibration measurements
- Appendix B -Time history comparisons
- Appendix C - Blast site data for regression analysis
- Appendix D - Summary statistics for human-induced error tests

Appendix A contains tables organized by blast site ID along with the date and time of each full-scale production blast identified in Table 1. Geophones deployed in clusters are identified by seismograph serial number and coupling method within a cluster number at various scaled distances. Single sensors at other locations were often buried and used to characterize site specific attenuation. Peak values for each geophone component are given in terms of component velocity, zero-crossing frequency at the peak, Fast Fourier Transform (FFT) predominant or average frequency, displacement and acceleration. All data were obtained using seismograph software. GPS coordinates of the blast and each cluster are also provided.

Appendix B contains time histories plotted by cluster at various scaled distances to compare coupling methods. For each cluster, times histories for radial (or longitudinal), vertical, and transverse components are given. In some cases PPV plots are provided.

Time histories are plotted at two different time scales on each page. The top figure shows a larger time window of the waveforms while the bottom figure shows a smaller window containing peak values for each coupling method. The positive and negative peak values listed on the bottom figures are given in the same order as the order indicated in the plot legend (e.g. in the order of geophone coupling methods listed) and show the peak velocity for each component.

If the peak component or PPV values are unique from the rest they are numerically identified. However, a dash ("-") is used as a placeholder wherever the peak values are the same as another already listed at another peak. It should be pointed out, peak values (positive or negative) among different coupling methods may occur at different times and at varying frequencies. Horizontal dashed lines are drawn to represent the location of these peak values offset in time from other peaks within a cluster when this occurs.

At the top of the list of peak velocity values (either negative or positive) is a percentage number. This number represents the percent difference between the absolute value of the highest and lowest peaks when the peaks occur at the same nominal time. Within each cluster, the largest percentage difference was computed using the following equation:

$$\%difference = \frac{\left|velocity_{\max}\right| - \left|velocity_{\min}\right|}{\left|velocity_{\min}\right|} * 100\% \qquad (4)$$

As an example, the percent difference is computed for the following peak values for different coupling methods:

0.786
0.785
0.701
0.821
0.772

The highest value is 0.821 and the minimum is 0.701. Therefore the percentage difference is [(0.821 – 0.701) / 0.701] x 100% or 17.1%.

Appendix C provides tables of PPV, peak frequency, acceleration, and component containing the PPV for blast sites in which regression analysis was performed. Tables include mean and standard deviation both in traditional units for each attribute and as a percentage of the mean (in percent). Data in these tables were used for regression analysis to identify possible outliers and decoupling.

Appendix D contains summary statistics for each test series involving a large number of geophones each deployed by individual person to measure human-induce errors for each decoupling method. Summarized are data mean ($\bar{x}$) and standard deviation (s) values for peak component velocity, frequency, and FFT frequency and peak particle

velocity (PPV) for each test and burial method.

4.2 Small-Scale Signature Blasts

4.2.1 Summary statistics

Table 2 shows the minimum, maximum, mean, and standard deviation for PPV and mean peak frequencies for the four methods in each test. The confidence intervals shown are for the mean PPV values. Relative standard error of the mean for human deployment (RSE_h) is also given.

PPVs ranged 0.07 to 0.105 in/s for test series 1 and 2 combined, while in test series 3, PPVs ranged 0.315 to 1.40 in/s. Peak frequencies (e.g. frequencies at the PPV) ranged 15.5 to 28.4 Hz (tests 1 and 2) and 19.6 to 46.5 Hz (test 3).

Table 3 gives the percentage of the total measurements in each test series in which the PPV resided in any one of three components. When the PPV was less than 0.1 in/s, the PPV represented the V component with the exception of the sandbag application. Heavy sandbags tended to act as a momentum “trap” and laterally drag the geophone on the ground surface, reducing the vertical motion. The variability of ground motion peaks between the V and T components for test series 1 and 2 when using a sandbag to cover a surface mounted geophone is attributed to human-induced errors in placing the bag itself even at low ground motion amplitudes.

When PPV values were greater than 0.3 in/s in test series 3, a large percentage of the ground motion shifted to the radial, R, component. No peaks occurred in the transverse, T, direction during signature tests most likely due to the lack of shear wave energy development.

4.2.2 Baseline error analysis for human deployment

Human-induced relative standard error (RSE_h) are shown for test series representing the low PPV and high PPV range tests in Table 4 to show that human deployment errors increased when ground vibration amplitudes increased.

The combined relative standard error used to assess decoupling is given in Table 4 and computed using equation (1). The relative standard error for geophone manufacture and calibration (RSE_{mc}) was taken as 2.9% from equation (2) and combined with RSE_h for test series 3. This range of PPV values best replicate full-scale production blasts where deployment errors are most likely to occur.

Table 2 Summary statistics for three series of small-scale, single hole blasts for test series 1 and 2 (top) and series 3 (bottom)

Test Series 1 and 2 combined: Scaled distance range 106 - 122 ft/lb $^{1/2}$ Number of data = 32 per method								
Coupling Method	Peak Particle Velocity			Mean frequency	Standard deviation (standard error)	Relative standard error of the mean	95% Confidence interval	
	maximum	minimum	mean				(+) 95%	(-) 95%
	(in/s)	(in/s)	(in/s)	(Hz)	(in/s)	(%)	(in/s)	(in/s)
buried	0.090	0.070	0.0786	16.8	0.0061	1.37	0.081	0.077
spiked	0.085	0.075	0.0788	17.2	0.0030	0.68	0.080	0.078
sand bag	0.105	0.080	0.0895	17.3	0.0067	1.32	0.092	0.087
spiked and sand bag	0.105	0.080	0.0925	17.9	0.0058	1.11	0.095	0.091

Test series 3: Scaled distance range 21 - 30 ft/lb $^{1/2}$ Number of data = 16 per method								
Coupling Method	Peak Particle Velocity			Mean frequency	Standard deviation (standard error)	Relative standard error of the mean	95% Confidence interval	
	maximum	minimum	mean				(+) 95%	(-) 95%
	(in/s)	(in/s)	(in/s)	(Hz)	(in/s)	(%)	(in/s)	(in/s)
buried	1.400	1.140	1.257	34.3	0.0867	1.58	1.296	1.218
spiked	0.535	0.315	0.401	23.2	0.0638	3.75	0.431	0.372
sand bag	2.000	0.580	1.118	34.0	0.4744	9.73	1.331	0.905
spiked and sand bag	0.780	0.475	0.414	23.0	0.1140	6.49	0.467	0.362

Table 3 Percentage of peak components representing the peak particle velocity (PPV) for four coupling methods (values are in percent)

Test series	Buried			Sandbag			Spiked			Sandbag and Spiked		
	R	V	T	R	V	T	R	V	T	R	V	T
1	0	100	0	0	68.8	31.3	0	100	0	0	100	0
2	0	100	0	0	12.5	87.5	0	100	0	0	100	0
3	89.5	10.5	0	31.6	68.4	0	50	50	0	22.2	77.8	0

Table 4 Summary of error analysis for human-induced deployment for three test series and resulting combined relative standard error using Test 3 data

Coupling method	Human-induced relative standard error (RSE_h) (%)		Combined relative standard error, RSE (%)
	Tests 1 and 2 combined	Test 3	
	PPV range: 0.075-0.105 in/s	PPV range: 0.315-1.40 in/s	
Buried	±1.37	±1.58	± 3.30
Spiked	±0.68	±3.75	± 4.74
Sandbag	±1.32	±9.73	±10.15
Spiked and sandbag	±1.11	±6.49	± 7.11

4.2.3 Time history comparisons

Comparative time histories for each test series are given in Figures 9 and 10. The reader is reminded these reduced-scale field tests do not represent full-scale production blasts but rather single holes blasts. As such, the time histories are less complex than production blasts and allow comparisons of ground motion energies within a narrow frequency range.

Based on the above analysis, waveform comparisons are shown only for V and R components. T components did not provide useful information based on complexities in shear wave characteristics producing highly variable time histories that cannot be correlated for multiple geophones.

Figure 9 shows representative time history comparisons to show reproducibility between coupling methods for test series 1 and 2 low amplitude signature tests. Only V components are shown where the PPV resides as both R and T were far lower in amplitude. Ground motion accelerations did not exceed 0.027 g's and all time histories were nearly identical for sensors remaining in place between the two blasts. Therefore there was no difference in coupling methods at low velocity amplitudes and repeatability based on source effects appeared to be good at low amplitudes. This comparison was not performed at higher vibration amplitudes.

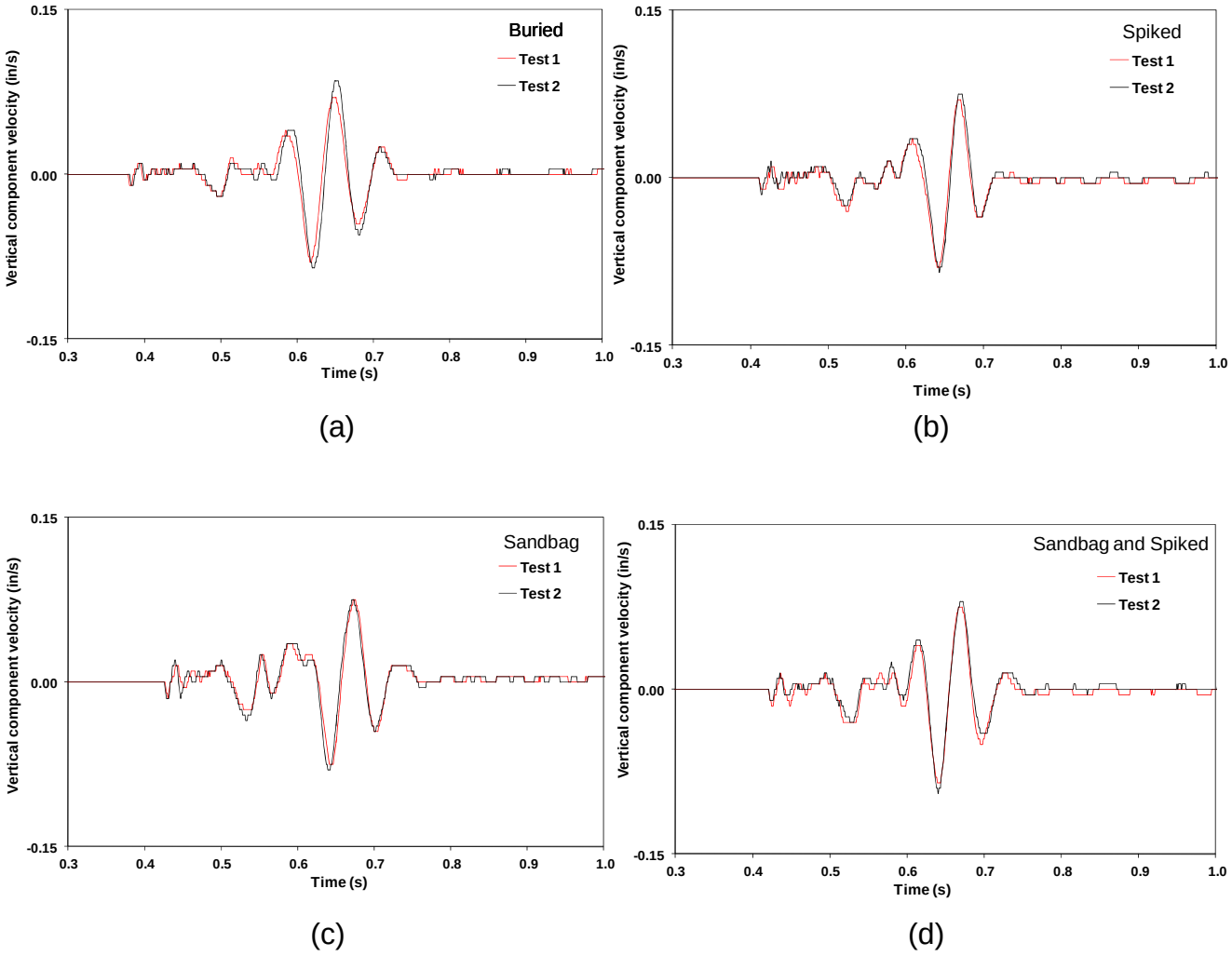

Figure 9 Vertical components for four coupling methods each deployed by different persons during two small-scale test blasts for (a) buried, (b) spiked, (c) sandbag, and (d) sandbag and spiked geophones; sensors remained in place between tests

Comparative V and R time histories and frequency content (FFT plots) for representative sensors deployed during test series 3 and common coupling methods are show in Figures 10 and 11, respectively. Five of the 19 sensors deployed for the same blast are plotted. Each sensor, labeled A through E, was mounted by 5 different persons. The purpose of this comparison was to determine the variabilities among sensors deployment in the same manner so that human influences of placement are better understood.

For the most part, buried sensors showed little variation in velocity time-history plots indicating consistency with geophone site preparation among five individuals.

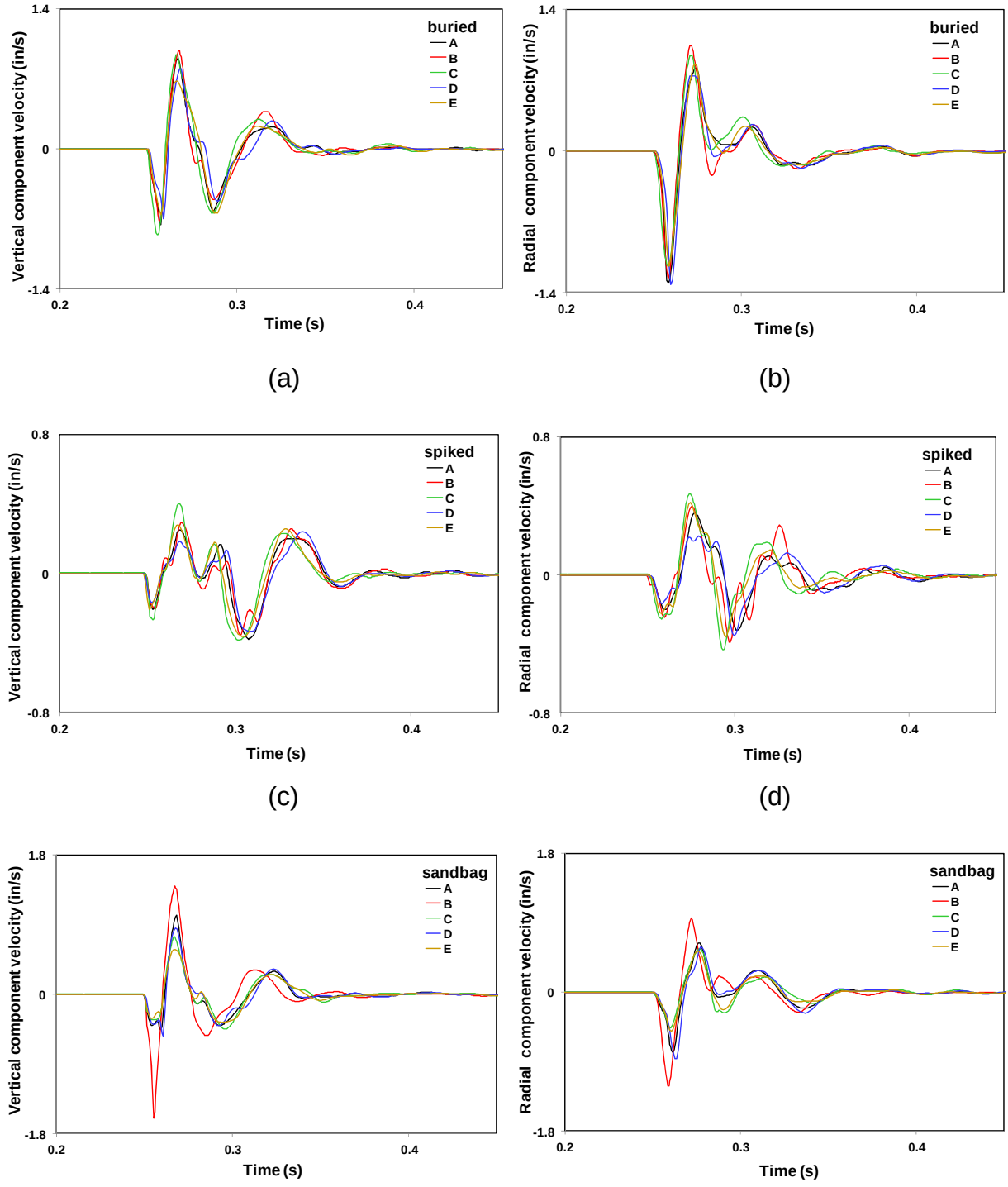

Figure 10 FFT plots for five representative sensors in test series 3

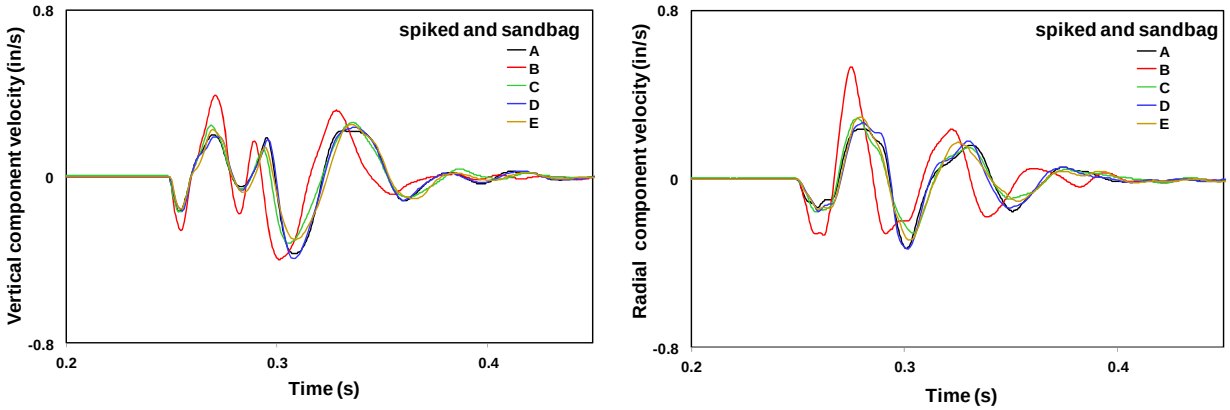

(g) (h)

Figure 10 (cont.) FFT plots for five representative sensors in test series 3

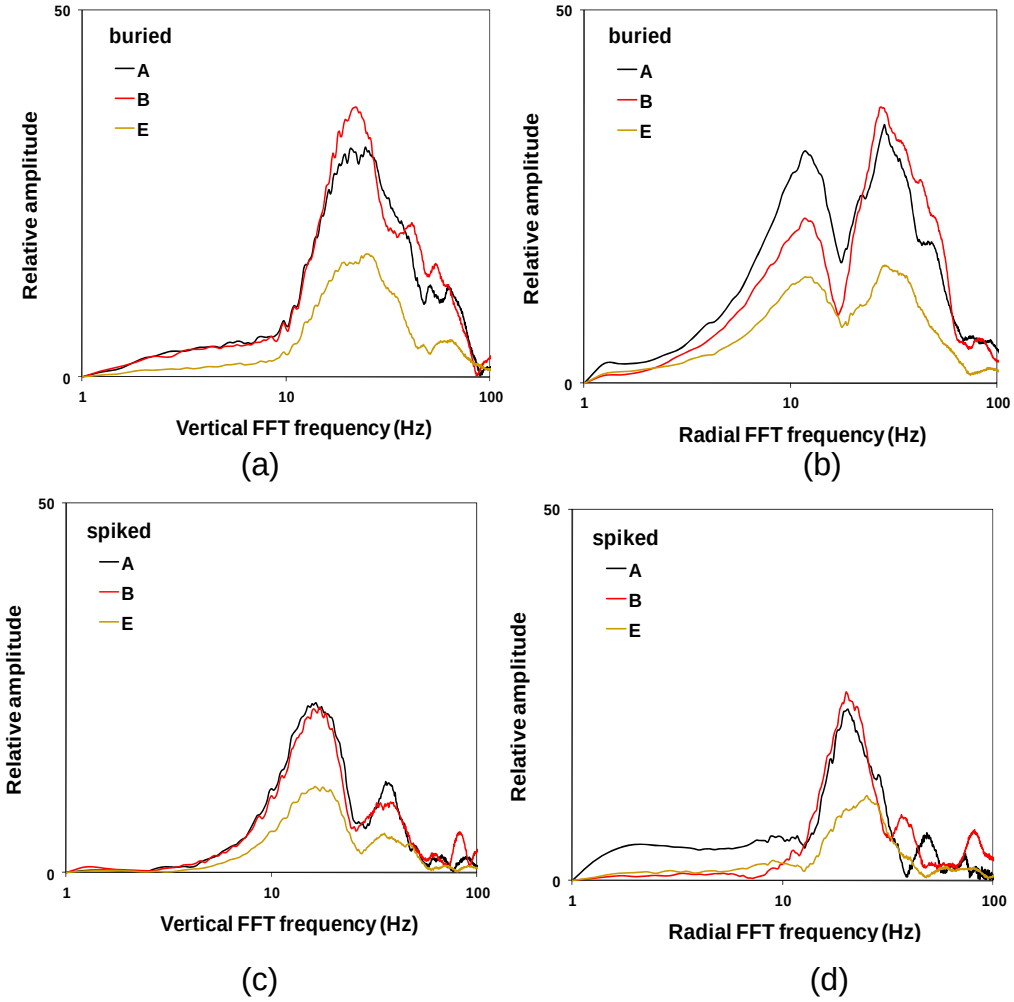

(a) (b)

(c) (d)

Figure 11 Vertical and radial FFT plots for three representative sensors in test series 3

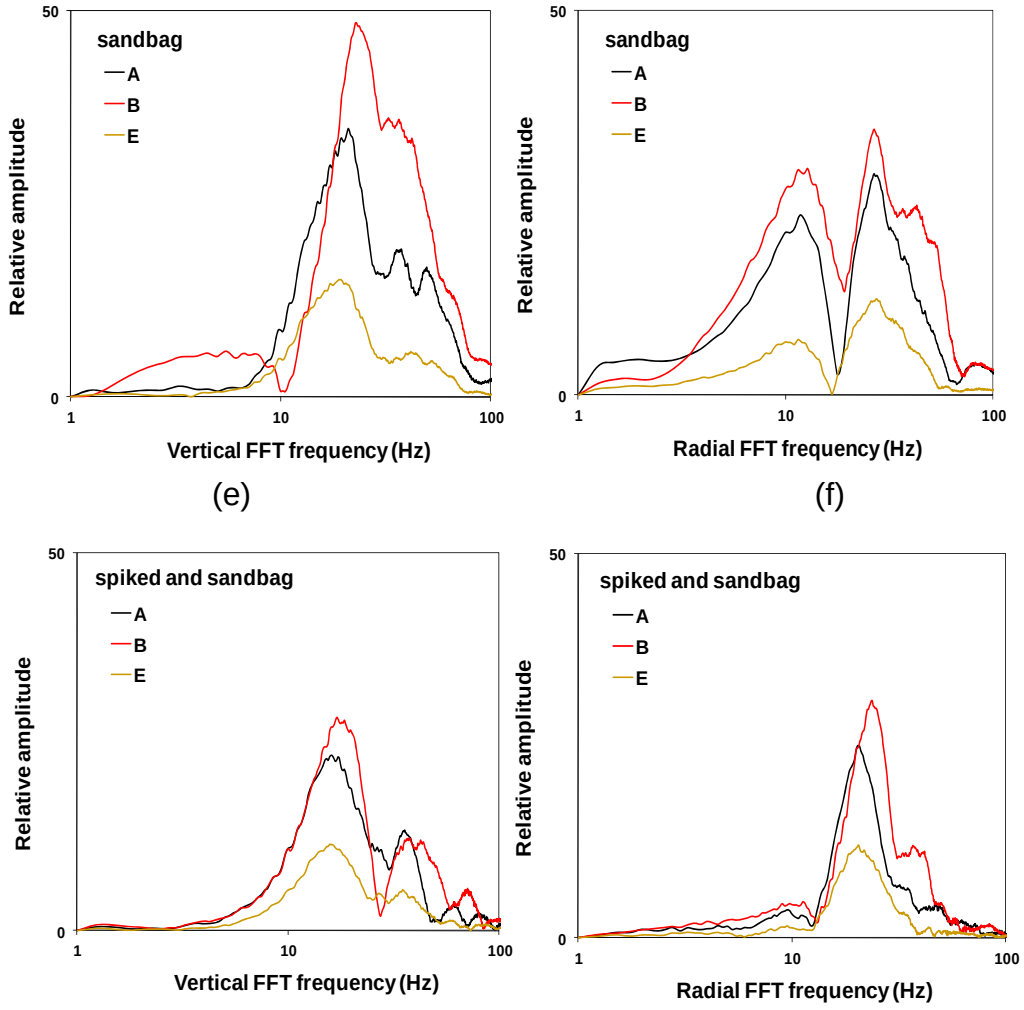

Figure 11 (cont.) Vertical and radial FFT plots for three representative sensors in test series 3

Spiked sensor placement shows a 129% enhancement for sensor C vertical response. Sensor D exhibited minute oscillations superimposed on low frequency peaks indicating possible lack of coupling of the spiked sensor base with the ground. This observation is more apparent in the R component.

The persons preparing the sandbag and spiked and sandbag B sensors for two blasts produced time histories that were far different from the other four sensors with differences between the highest and lowest velocities of 408% for V and 108% for R component for sandbag and spiked and sandbag, respectively. All sensors were recently calibrated and, assuming identical calibration and manufacturing variances, the difference can be attributed to human influence.

The influence of coupling method on peak acceleration was unexpected in light of the U.S. Bureau of Mines findings (Stagg and Engler, 1980) and ISEE recommendations (2009). Recommendations for appropriate coupling method are based on an a priori estimate of ground motion acceleration. However, calculated accelerations associated with the component peaks in Figure 9 are highly influenced by coupling methods used. To illustrate this fact, the following accelerations calculated using seismograph software for sensor B component peaks are as follows:

	Calculated acceleration (g's)		Component
	V component	R component	containing the PPV
Buried	0.64	0.85	R
Spiked	0.24	0.25	R
Sandbag	1.43	0.69	V
Spiked and sandbag	0.25	0.24	R

The situation is clearly confusing. If a sandbag was used, resulting in a peak acceleration of 1.43 g's, one would conclude the ISEE guidelines were not followed and the sensor should have been buried. However, the buried sensor accelerations indicate spiking could have been used to prevent slippage (e.g., spiking is acceptable for accelerations less than 1.0 g's). Yet the spiked sensor produced component accelerations near 0.2 g's which implies no burial or attachment may be necessary.

The frequency spectrum plots for three sensors given in Figure 11 show similarities. The relative amplitude represents the amount of ground motion energy contained within the range of frequencies compared with the component with the highest energy. Sensors A and B represent consistent energy levels for buried and spiked sensors in contrast to anomalous behavior for sensor E. The bi-modal frequency peaks for buried and sandbag sensors represent the first and second time history oscillations, each with distinct frequencies (the second being lower than the first) as indicated in Figure 9. Spiked sensor time histories exhibited one predominate yet lower frequency for 3 cycles. This comparison is shown in Figure 12 using sensor B to plot frequency content by method. Spiked sensors (with and without a sandbag) responded with the lowest ground motion energy and exhibited slightly lower frequencies in both components compared with buried and sandbagged sensors.

The regulatory implications of selecting the wrong burial method are illustrated with a sixth sensor not shown in previous examples but exhibiting the same comparison between burial and sandbag during test series 3. Figure 13 shows time histories for three components during two different blasts at the same scaled distance. Peak velocity amplification using the sandbag compared with geophone burial is evident. It is presumed the same amount of ground motion energy at the measurement locations was generated for each test shot.

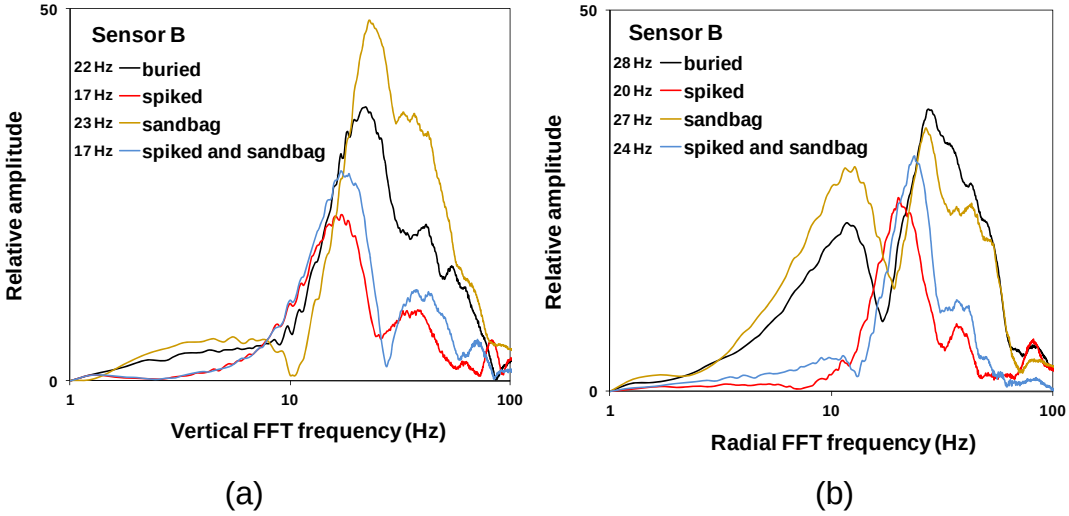

(a) (b)

Figure 12 FFT plot comparisons for sensor B (a) V and (b) R components and four coupling methods

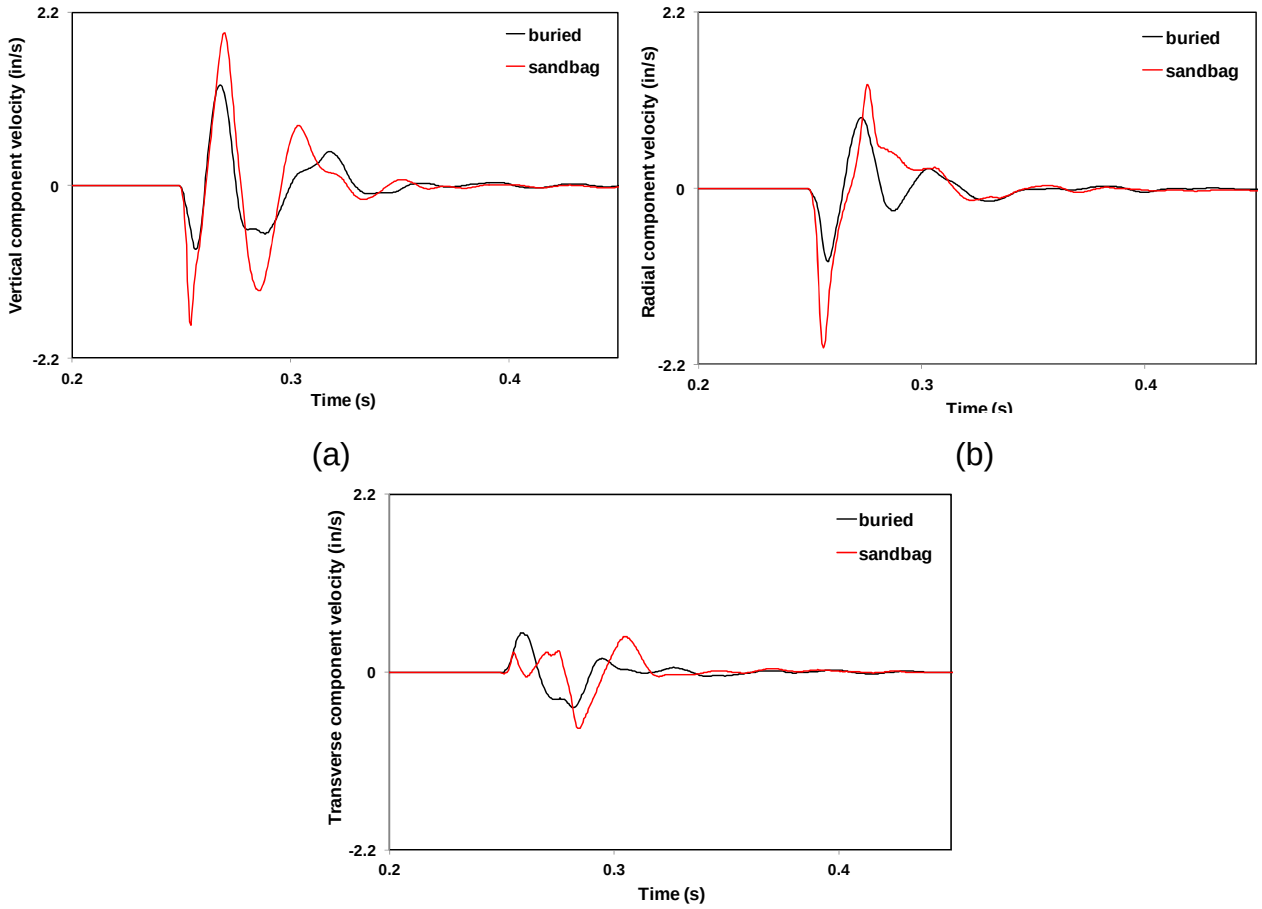

(a) (b)

(c)

Figure 13 Vertical (a), radial (b), and transverse (c) components for a sensor deployed using two coupling methods with ground accelerations measured between 0.8 g's (buried) and 2.0 g's (sandbagged)

The tendency for sandbags to cause a “lag” time in peaks compared with peak times for buried sensors is shown for the T component. The momentum carried by the sandbag mass subjected to horizontal movement is large compared with the moment of the smaller mass geophone. As such, the sandbag tends to “drag” the sensor along the ground surface resulting in a slight time delay and enhancement in positive and negative peaks shown in Figure 13(c). This creates a slight shift in the time of peaks for the sandbagged sensor compared with the buried sensor whose motion is assumed to be in sync with the ground vibration energy.

Electing to place a sandbag over a sensor as opposed to burial can affect the outcome of compliance monitoring. Table 5 is a summary of peak R and V component velocities For the time histories given in Figure 13 and includes the PPV and zero-crossing frequency at the PPV. The PPV and peak frequency for these measurements are plotted within the frequency-based Office of Surface Mining (OSM) vibration standards. The geophone coupled with the sandbag results in a plotted data point that is out of compliance with OSM standards while the buried senor is shown within compliance.

Table 5 Summary of vertical (V) and radial (R) components, PPV and frequency at the PPV for buried and sandbag methods

Coupling method	Peak component velocity		PPV	Peak frequency
	V	R		
	(in/s)	(in/s)	(in/s)	(Hz)
buried	1.28	-0.92	1.25	35.3
sandbag	1.94	-2.00	2.00	27.6

The following findings are summarized based on the above observations:

1. Buried and sandbag sensors exhibit the highest periodic energy and average frequency
2. The use of spikes can lower the vertical frequency component and increases horizontal radial frequency component
3. The use of sandbags may cause a time lag in periodic peak amplitudes compared with buried sensor peaks with velocity amplifications occurring in the horizontal component.
4. Based on the wide range of calculated accelerations from vertical and radial vibration measurements using different coupling methods for the same blast, it may not be possible to select an appropriate attachment method based on anticipated ground motion acceleration.

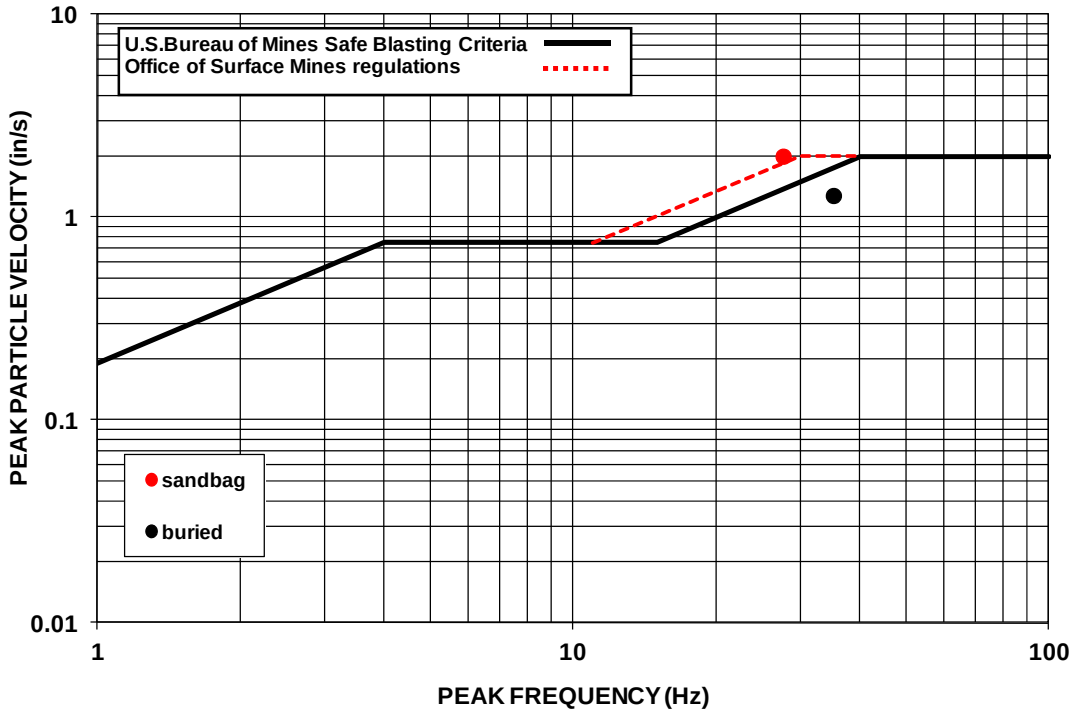

Figure 14 Peak particle velocity versus frequency at the PPV plotting compliance data for buried and sandbag sensors.

4.3 Full-scale Production Blasts

Thirty-seven large-scaled product blasts were monitored using various geophone coupling methods. A total of 486 time-histories were plotted and shown in Appendix B. Representative time-history plots from Appendix B were organized in this section to compare coupling methods in terms of component and peak particle velocities, frequency, and acceleration amplitudes. Data from a total of 12 representative blast sites that include coal mining (10), quarry (1), and construction (1) sites were analyzed in detail. Blast examples represent a range of PPV and frequency values and were selected using linear regression analysis in which coupling methods were compared with the buried geophone method as the baseline. The 12 sites represent about one-third of the complete data set.

4.3.1 Data organization and analysis

Production blast data were grouped in four comparison sets as shown in Table 6 with the fifth being a subset of the fourth. Comparisons groups included the following:

- geophones buried and placed loose on the ground surface,
- by sensor shape, using spiked round and square geophones,
- buried, spiked and combined spiked and buried geophones, and
- geophones buried, spiked on the surface, covered with a sandbag on the surface and a combination of spiked with a sandbag on top (the last blast site NM-7 using only buried, spiked, and sandbag).

Data used for analysis were derived from geophone clusters located at scaled distances ranging from 8.8 to 134 ft/lb$^{1/2}$. Blast sites selected provided various combinations of low to high frequencies as well as PPV amplitudes. Thus, blasts were grouped according to data amplitude ranges shown in Table 7. By selecting various combinations of velocity and frequency, a range of ground motion accelerations were identified. For instance, sites were selected with high PPV and high peak frequencies (and thus high accelerations) or low frequency and high PPV, as well as low PPV and high frequency could be identified. In addition, blasts generating high calculated accelerations were examined for possible decoupling as an indicator of higher than expected velocities or peak frequencies.

Data plots within each comparison set include time histories for each velocity component and scatter plots constructed from time-correlated peak amplitudes (positive and negative) between two different attachment methods. Linear regression analysis was applied to obtain the best-fit line and correlation coefficient (R^2) indicating agreement or lack thereof between two methods within the same cluster.

Table 6 Summary data for production blast sites used for comparative analyses

Comparisons	Site ID	Coupling method	Radial			Vertical			Transverse			PPV component
			velocity	frequency	acceleration	velocity	frequency	acceleration	velocity	frequency	acceleration	
			(in/s)	(Hz)	(g's)	(in/s)	(Hz)	(g's)	(in/s)	(Hz)	(g's)	
loose on the ground surface versus buried	OH-4	loose	0.90	27.0	0.59	0.68	27.0	0.52	0.56	17.0	0.31	R
		buried	0.66	16.0	0.21	0.60	34.0	0.38	0.44	16.0	0.17	R
	KY-2	loose	0.64	39.0	0.42	0.70	32.0	0.49	0.59	18.0	0.25	V
		buried	0.49	9.0	0.23	0.48	16.0	0.23	0.42	16.0	0.17	R
	KY-8	loose	0.28	24.3	0.13	0.19	23.2	0.09	0.25	28.4	0.11	R
		buried	0.21	13.4	0.08	0.17	14.6	0.07	0.16	28.4	0.07	R
	WY-5	loose	2.68	4.4	0.52	1.88	3.1	0.33	1.84	2.4	0.42	R
		buried	2.52	4.3	0.49	1.68	3.0	0.30	1.92	2.4	0.42	R
	OH-1	loose	1.26	10.4	0.36	0.86	30.1	0.38	0.96	11.3	0.36	R
		buried	0.92	8.5	0.29	0.52	23.2	0.24	0.92	11.9	0.27	R
sensor shape	KY-2	round	0.98	56.8	1.01	0.49	14.6	0.25	0.74	19.6	0.57	R
		square	0.54	14.6	0.41	0.50	15.0	0.25	0.51	18.9	0.35	R
	OH-2	round	0.64	6.1	0.18	0.47	11.1	0.14	0.55	8.6	0.20	R
		square	0.68	6.3	0.19	0.46	10.8	0.13	0.58	8.6	0.19	R
buried, spiked, combined spiked and buried	IL-1	buried	0.78	3.8	0.38	1.22	30.1	0.63	1.06	13.0	0.43	V
		spiked	1.34	26.9	0.66	1.34	34.0	0.74	1.62	15.0	0.85	T
		spiked and buried	0.78	28.4	0.36	1.08	28.1	0.52	1.14	21.3	0.44	T
	IN-1	buried	0.54	6.1	0.15	0.50	6.4	0.32	0.59	7.4	0.13	T
		spiked	0.54	5.9	0.27	0.41	15.0	0.32	0.65	7.6	0.24	T
		spiked and buried	0.58	5.8	0.15	0.43	6.4	0.28	0.54	7.4	0.15	R
	KY-4	buried	0.39	8.3	0.17	0.45	56.8	0.42	0.78	7.4	0.29	T
		spiked	0.43	51.2	0.44	0.57	85.3	0.66	0.84	64.0	0.88	T
		spiked and buried	0.38	8.1	0.15	0.43	64.0	0.39	0.78	7.4	0.23	T
	KY-5	buried	0.70	32.0	0.34	0.64	51.2	0.57	0.74	21.3	0.27	T
		spiked	1.08	42.6	0.81	0.72	56.8	0.68	0.78	25.6	0.48	R
		spiked and buried	0.66	30.1	0.30	0.58	51.2	0.53	0.74	22.2	0.27	T
buried, spiked, sandbag, and combined spiked and sandbag	IL-1	buried	0.78	3.8	0.38	1.22	30.1	0.63	1.06	13.0	0.43	V
		spiked	1.34	26.9	0.66	1.34	34.0	0.74	1.62	15.0	0.85	T
		sandbag	0.98	15.5	0.29	1.16	28.4	0.72	1.88	11.6	0.45	T
		spiked and sandbag	0.90	17.0	0.34	1.18	30.0	0.80	1.80	13.0	0.53	T
	WV-2	buried	1.26	12.4	0.57	1.22	28.4	0.54	1.00	21.3	0.38	R
		spiked	1.30	16.5	0.49	1.10	25.6	0.48	0.84	21.3	0.34	R
		sandbag	1.26	13.4	0.59	1.12	26.9	0.50	1.02	19.6	0.39	R
		spiked and sandbag	1.32	16.5	0.51	0.00	0.0	0.00	0.98	15.0	0.38	R
	KY-8	buried	0.21	13.4	0.08	0.17	14.6	0.07	0.16	28.4	0.07	R
		spiked	0.27	23.2	0.11	0.17	14.6	0.07	0.21	30.1	0.09	R
		sandbag	0.28	16.0	0.10	0.25	32.0	0.14	0.21	26.9	0.09	R
		spiked and sandbag	0.28	13.4	0.11	0.22	32.0	0.12	0.19	26.9	0.08	R
	WY-5	buried	2.52	4.3	0.49	1.68	3.0	0.30	1.92	2.4	0.42	R
		spiked	2.40	4.3	0.56	1.80	3.0	0.33	1.76	2.6	0.46	R
		sandbag	2.44	4.4	0.53	1.76	3.0	0.30	1.80	2.4	0.42	R
		spiked and sandbag	2.52	4.4	0.53	1.84	3.0	0.33	1.80	2.4	0.44	R
	OH-1	buried	0.92	8.5	0.29	0.52	23.2	0.24	0.92	11.9	0.27	T
		spiked	0.94	12.1	0.36	0.47	26.9	0.27	1.02	12.4	0.34	T
		sandbag	0.98	9.8	0.32	0.60	23.2	0.24	1.06	13.1	0.33	T
		spiked and sandbag	0.90	8.6	0.27	0.46	24.3	0.24	1.00	12.4	0.33	T
buried, spiked, sandbag	NM-7	buried	0.90	34.1	0.56	0.42	23.2	0.27	0.47	39.3	0.38	R
		spiked	1.24	32.0	0.74	0.52	36.5	0.42	0.93	36.5	0.66	R
		sandbag	0.94	34.1	0.57	0.49	30.1	0.25	0.40	34.1	0.32	R

Table 7 General categories for analysis of full-scale tests based on ranges of peak particle velocity (PPV) and frequency at the PPV

PPV amplitude category	PPV (in/s)	Frequency (Hz)
Low	< 0.4	<10
Medium	0.4 to 0.9	10 to 20
High	> 0.9	>20

4.3.2 Distribution of peak amplitudes for component velocity, frequency and acceleration

Figure 14 provides histograms for peak component attributes of velocity, V_c, frequency, f, and calculated acceleration, A, for all coupling methods combined for the 12 tests. Summary statistics are found in Table 8 (mean, median, standard deviation, and data range within one standard deviation) and in Table 9 (indicating the percentage of all blasts that the attribute specified resides in a given component) to help explain histograms.

Comparing these attributes helps to explain variabilities among components to identify possible outliers among coupling methods. Outliers, or extreme values shown in histograms for all attributes, tend to lie on the high side of the mean or median. Outliers may indicate unusual site characteristics, measurement errors associated with human deployment, or explain the performance of the coupling method itself in response to unusually high ground motion velocity or frequencies.

Statistics in Table 8 show the R component with similar mean and median but with a high standard deviation, indicating a uniform distribution of data values with higher variability compared with the V component. Vertical component data is skewed to the right with a lower standard deviation similar to the T component. Comparing peak frequencies by component, values in the V direction are uniformly distributed but carry the highest amplitudes in comparison with the horizontal components. Outliers are indicated for velocity in the R component and in the V component for frequency.

An inspection of mean and median peak component velocities shows the highest values occur in the R component where the PPV resides more than 55% of the time. The likelihood that decoupling may be indicated by the R component is supported by the radial component outliers shown in Figure 15(a). The lowest mean amplitude occurs in the V component where the PPV resided 11% of the time.

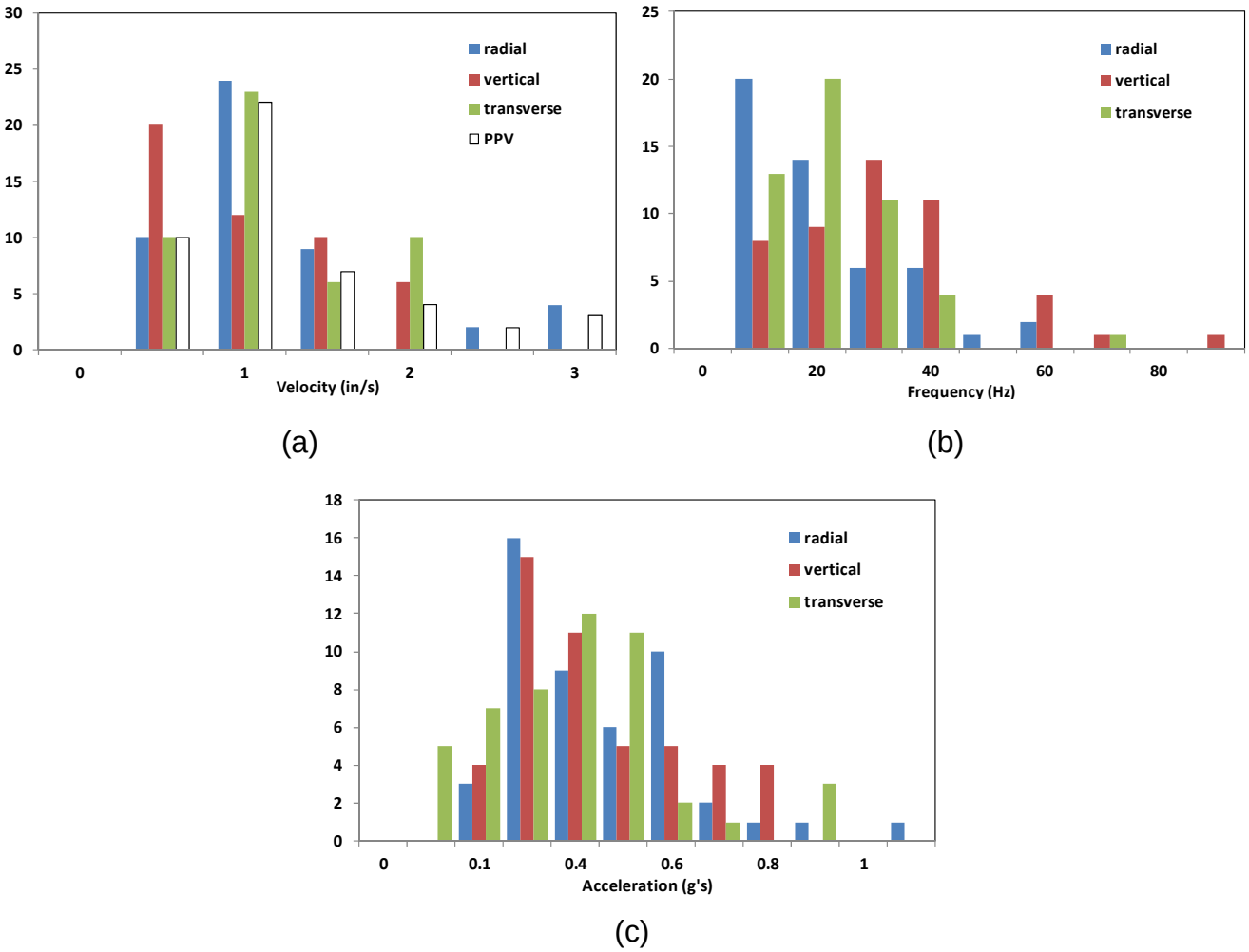

Figure 15 Distribution of peak component velocity and PPV (a), frequency (b) and acceleration (c) amplitudes for 13 representative blasts

Table 8 Data mean and variation of velocity, frequency, and acceleration by component for all coupling methods and 13 representative blasts

Attribute	Radial				Vertical				Transverse			
	mean	median	standard deviation	data range	mean	median	standard deviation	data range	mean	median	standard deviation	data range
Velocity (in/s)	0.99	0.90	0.66	0.33 - 1.65	0.79	0.58	0.50	0.29 - 1.29	0.91	0.84	0.52	0.39 - 1.43
Frequency at the peak (Hz)	17.0	13.4	13.0	4.0 - 30.0	25.8	26.3	17.2	8.6 - 43.0	17.1	15.0	11.6	5.5 - 28.7
Acceleration (g's)	0.38	0.36	0.21	0.17 - 0.59	0.37	0.32	0.20	0.17 -0.57	0.35	0.34	0.19	0.16 - 0.54

Table 9 Percentage of representative blasts where values occur in the various component for all coupling methods

Percentage of blasts that attribute occurs in the various components (%)			
Attribute	Radial, R	Vertical, V	Transverse, T
Peak particle velocity (PPV)	55.8	11.5	32.7
Maximum frequency (f_{max})	12.5	83.3	4.2
Minimum frequency (f_{min})	58.3	0	41.7
Maximum acceleration (A)	52.5	37.3	10.2

The highest or maximum frequencies (or zero-crossing frequency at the component peaks) were found 83% of the time in the V component while the lowest percentage (4.2%) was found in the T direction.

The combinations of slightly higher frequencies and lower velocities in the V component shown in Table 9 compared with lower frequencies and higher velocities in the horizontal directions have the same effect on acceleration. This is because acceleration is proportional to velocity times frequency. As such, the mean and standard deviation of peak accelerations are similar for all components. As such, observing unusually high calculated accelerations may indicate an outlier. However, the basis of this (either high frequency or high vibration) needs to be evaluated.

4.3.3 Implications associated with possible outliers

In the case of frequency, it was noted that two extreme values above 60 Hz appear as outliers for the V component (Figure 15 b). Upon inspection in Table 6, these occurred during the same blast for two spiked sensors (one being combined spiked and buried). If the definition of an outlier is expanded to include frequency values above 50 Hz, six sensors are noted. It happens that all six data were recorded during two blasts (KY4 and KY5) at the same coal mine site using buried, spiked, and combined spiked and buried. Sensors were deployed in surface soils classified according to the Unified Soil Classification System (USCS) as an ML or silt of low plasticity with 72% fines and 27.5% water content.

The first blast was a pre-split shot generating high frequencies (0.57 in/s for the spiked sensor V component) based on short delay timing. The second blast occurring two minutes later was a production blast generating high frequencies (0.72 in/s for the spiked sensor V component). Sensors were only deployed once. All six high frequency data, ranging from 51 to 85 Hz in the V component, are contained in the highest 95th percentile (e.g., 95.8% of the data among all 49 events reside below these values).

Deciding why this site is unique becomes difficult particularly when the next highest V component frequency was far lower (36.5 Hz) for a spiked sensor measured in sandy soils of low moisture content at a construction blast. The difficulty then becomes deciding if the unusually high V component frequencies measured at the coal mine site are unique based on the type of blast (construction versus coal), site transmission characteristics (e.g., soil type), deployment method, or if the person(s) deploying the sensors contributed to these high values for all three methods.

The following observations made regarding the statistical distribution of time-history data:

- Studying the statistical distribution of characteristic time-histories attributes such as component peak velocities, peak frequencies, and maximum accelerations along with PPV for all blast sites and all coupling methods may indicate the behavior of possible outliers where decoupling could exist

- Data presented on the high side of the histograms are random with respect to components and there is no clear trend relating high accelerations with either frequency or velocity high values

- The use of acceleration as a single attribute to identify outliers using simple statistic tools may be difficult because one does not know if the acceleration is based on velocity amplification or high frequency due to possible decoupling

4.3.4 Correlation plots of coupling methods

Plots and diagrams are presented in this section for comparison groups identified in Table 6. Correlation plots for blast site data are given in terms of PPV, peak frequency, and acceleration, evaluated using linear regression analysis supplemented with time-histories, to allow closer inspection of possible outliers or decoupled sensors. Appendix C contains data used for correlation plots.

a. Loose sensor place on the ground compared with a buried sensor (22 sites)

Five of the 22 sites were selected to compare a buried sensor with a sensor lying loose on the ground without attachment. This comparison is relatively simple but shows some important characteristics when comparing combinations of high and low frequencies and velocities that may affect computed accelerations.

Figure16 shows correlation plots of peak velocity, frequency, and accelerations for all 22 sites. Equations for the regression analysis best-fit trend lines are given along with the correlation coefficient (R^2). A red dashed line is drawn in each plot to indicate the trend of perfect correlation (R^2 of 1.0). If a buried sensor is assumed to represent

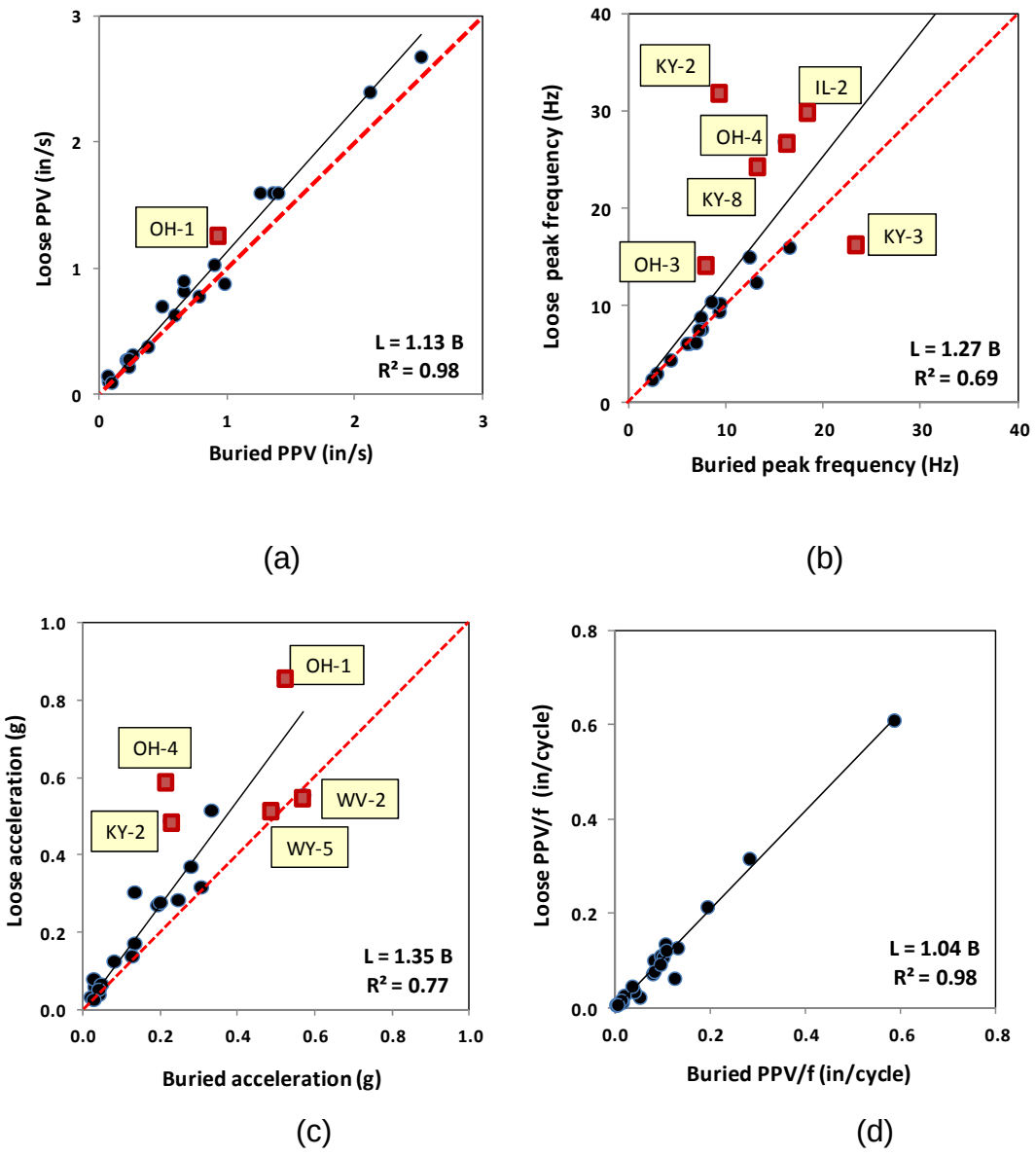

Figure 16 Response of loose versus buried sensors for PPV (a), peak frequency (b), computed acceleration (c) and PPV/f ratio at 22 sites

perfect coupling and a sensor placed on the ground surface without attachment is taken as possibly decoupled, then data that fall above this line indicate possible decoupling using the “loose” method.

In all cases, the ratio of peak attributes between loose and buried sensors range 1.13 to 1.35 (as indicated by the linear slope) with the least correlation in terms of frequency (R^2 of 69%). A few blast sites falling outside trend lines are indentified by site ID.

PPV comparisons are remarkably similar particularly up to 0.4 in/s with a high R^2 of 98%

for all sites irrespective of frequency. However, peak frequencies for loose sensors are between two to three times greater than for buried sensors. The variation in frequency is reflected in the acceleration comparisons.

Comparing the performance of sensors placed loosely on the ground with buried sensors shows the following:

- The tendency for loose sensors to "decouple" may not occur until ground motion peak frequencies exceed around 12 Hz based on the one-to-one correspondence between loose and well-coupled sensors.

- Amplification of loose sensors is surprising low and consistent over a wide range of buried PPV values.

- Inspection of accelerations show that even at 0.03 g's, loose sensor accelerations can be 2 to 3 times that for the buried sensor.

- When considering a function of ground displacement, or ratio of PPV/frequency shown in Figure 16(d), loose sensors responded nearly identical to buried sensors when PPV values were very high at low frequencies as well as low PPV at high frequencies. Note, 95% of the PPV values resided in horizontal components.

Time histories and scatter plots for five sites indicating possible outliers for frequency and acceleration plot in Figures 16 (b) and (c) are shown in Figures 17 through 21. These sites include KY-2, OH-4, WY-5, OH1, and KY-8. Scatter plots show regression equations in terms of loose as a function of buried and designated for R, V, and T components.

Data scatter indicated by R^2 for any component signifies correlation between positive and negative velocity peaks over time. When the differences between loose and buried peaks are uniform, even though the correlation is low, the shape of the scatter plots takes on the form shown for the T component in Figure 17(b) for KY-2. The plot shape can show which phase (positive of negative) velocity amplifications may occur. Extreme positive and negative values take on their own trend away from $R^2 = 1$ in which differences in peak values are consistent and frequency components agree.

In contrast, lags noted in the R time histories peaks for site OH-1 for the loose sensor compared with the buried sensor result in a highly random scatter plot in Figure 20(b). A similar plot is show for the T component where time lag is not as severe. The V plot shape and low correlation is attributed to random differences in peak values.

When PPV is high and peak frequencies are low (average 3.2 Hz), as is the case of site WY-5, there is a nearly one-to-one correspondence of peak velocities between loose and buried sensors and scatter plot component correlations are close to 1.0 shown in Figure 19(b). High frequencies superimposed on peaks are apparent for the both

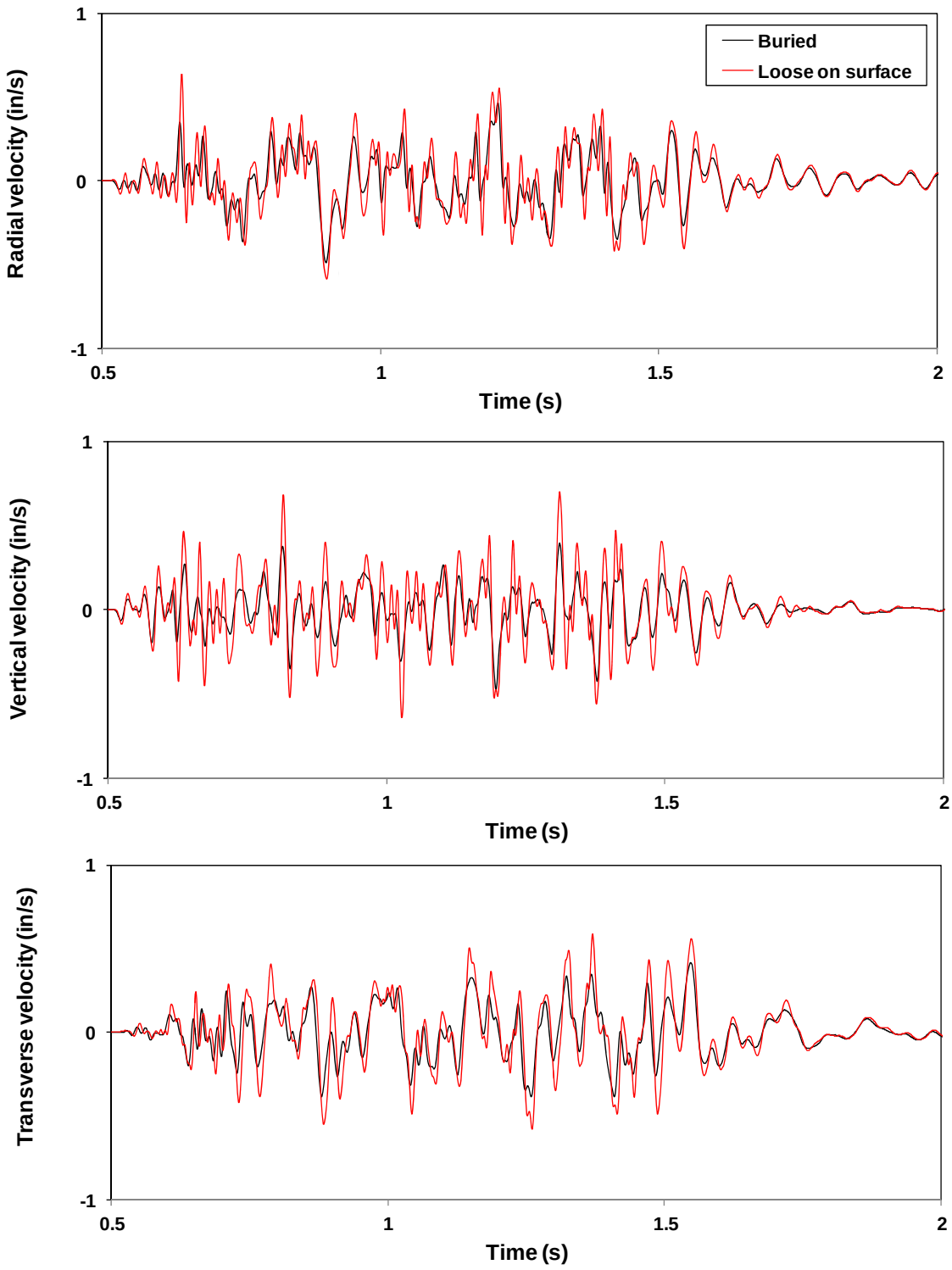

(a)

Figure 17 Component time histories (a) and scatter plots (b) for site KY-2

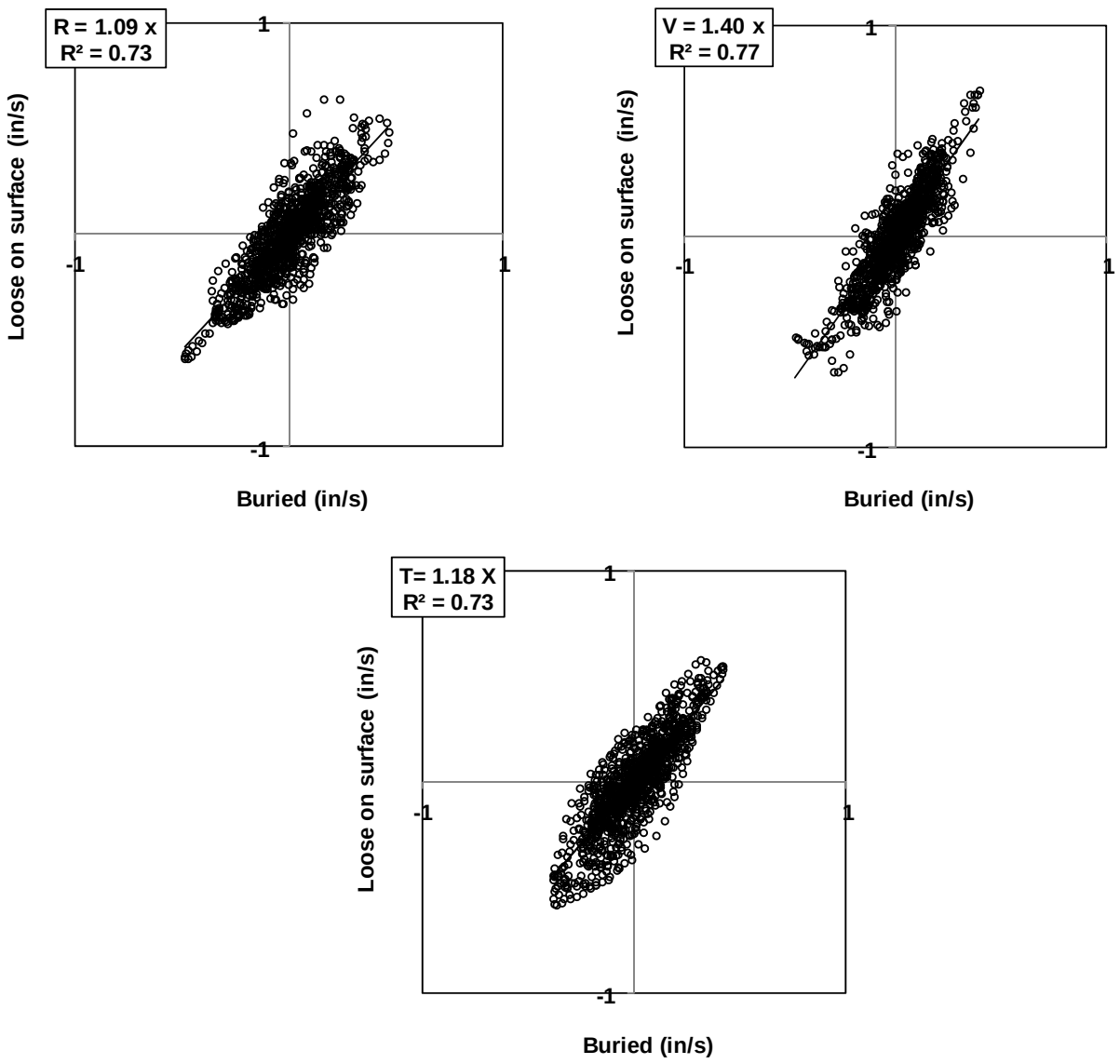

(b)

Figure 17 (cont.) Component time histories (a) and scatter plots (b) for site KY-2

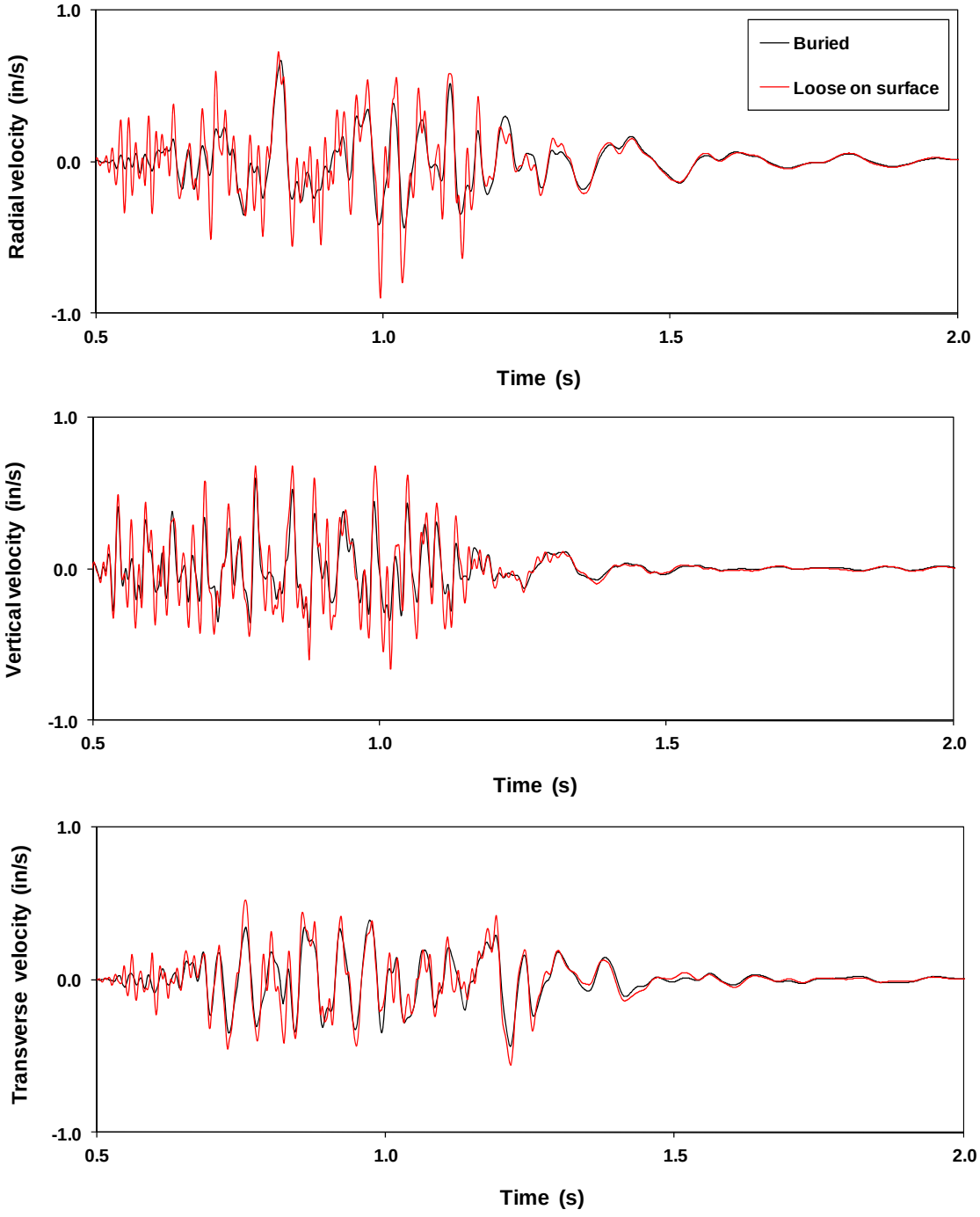

(a)

Figure 18 Component time histories (a) and scatter plots (b) for site OH-4

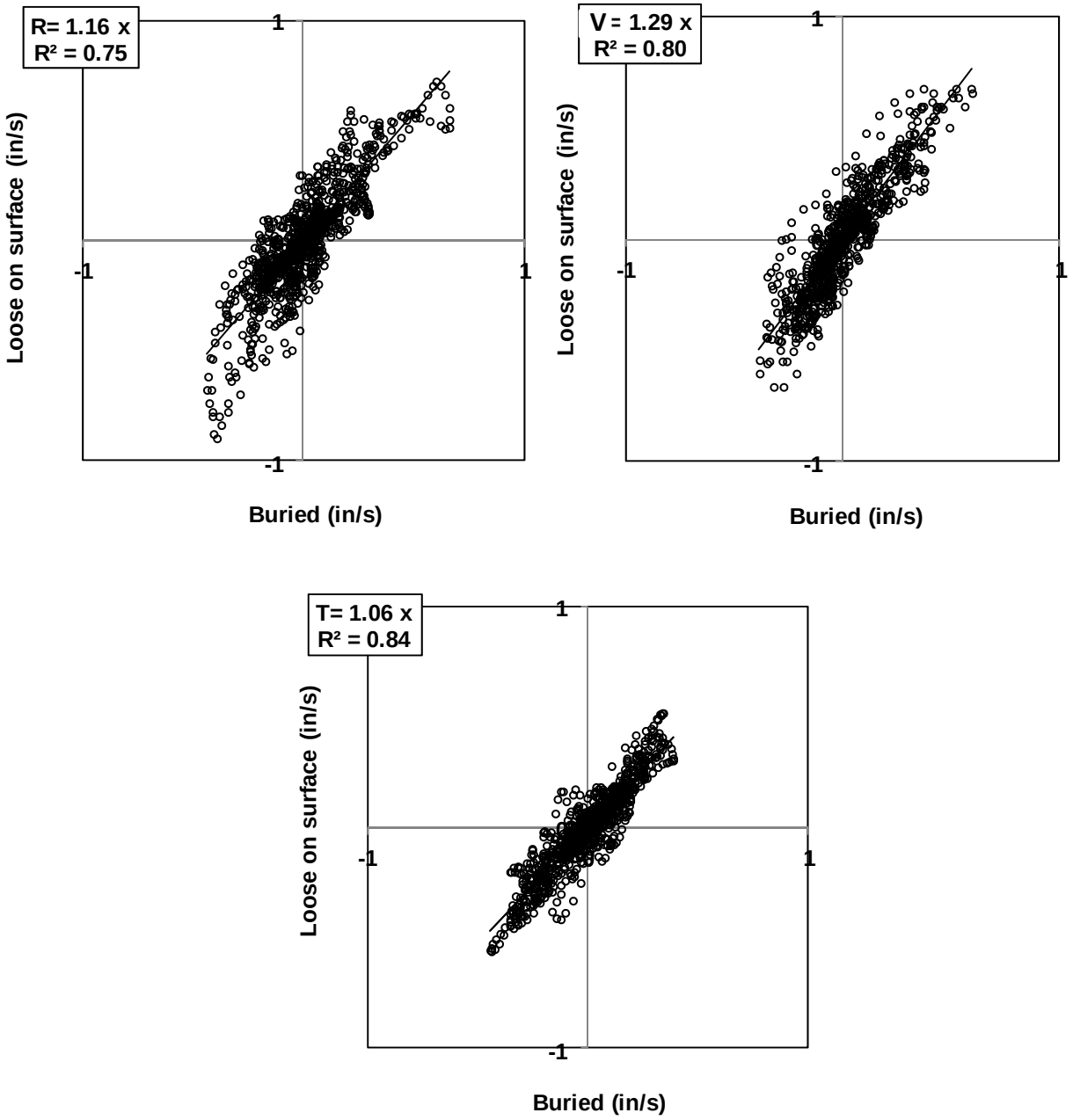

(b)

Figure 18 (cont.) Component time histories (a) and scatter plots (b) for site OH-4

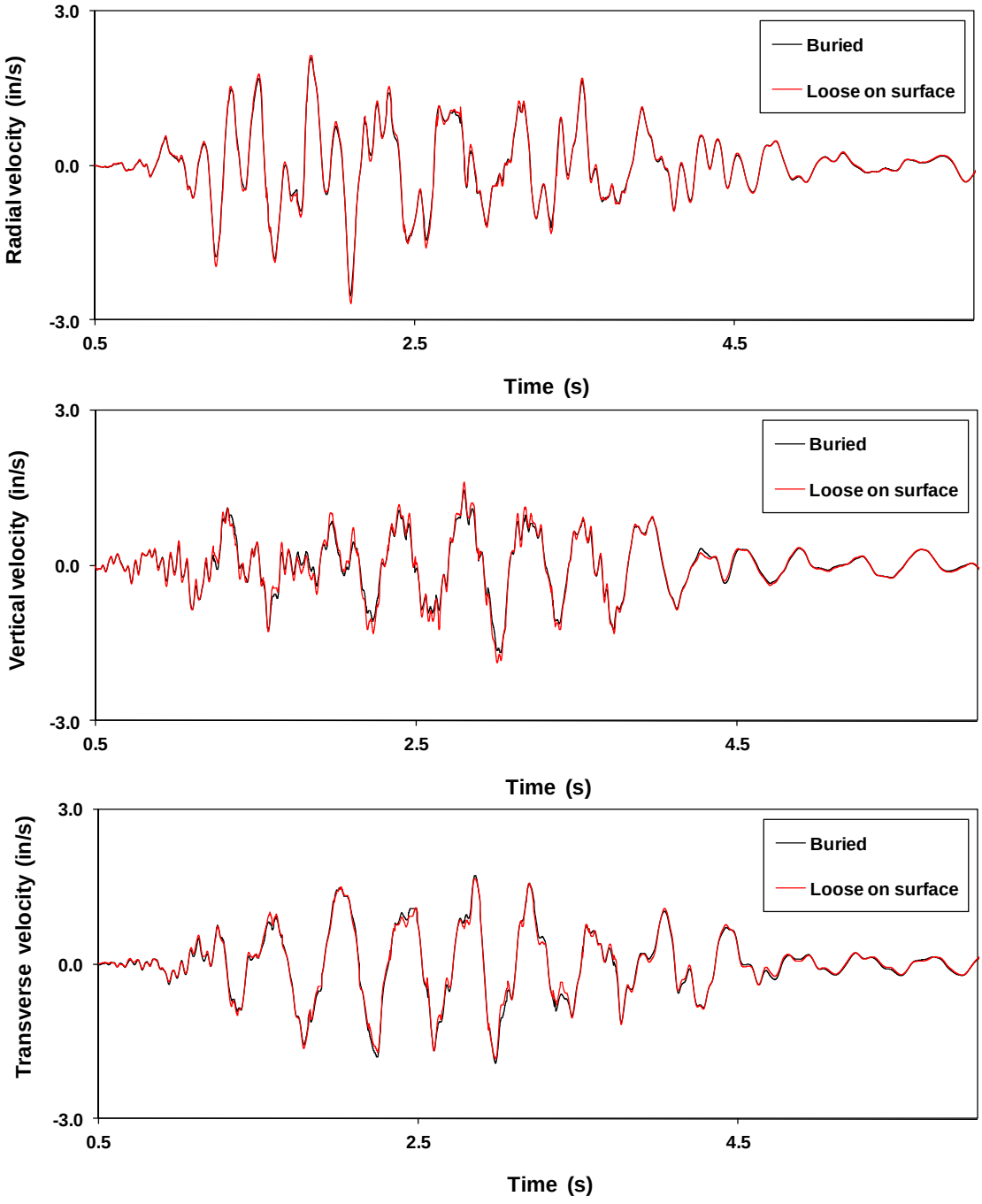

(a)

Figure 19 Component time histories (a) and scatter plots (b) for site WY-5

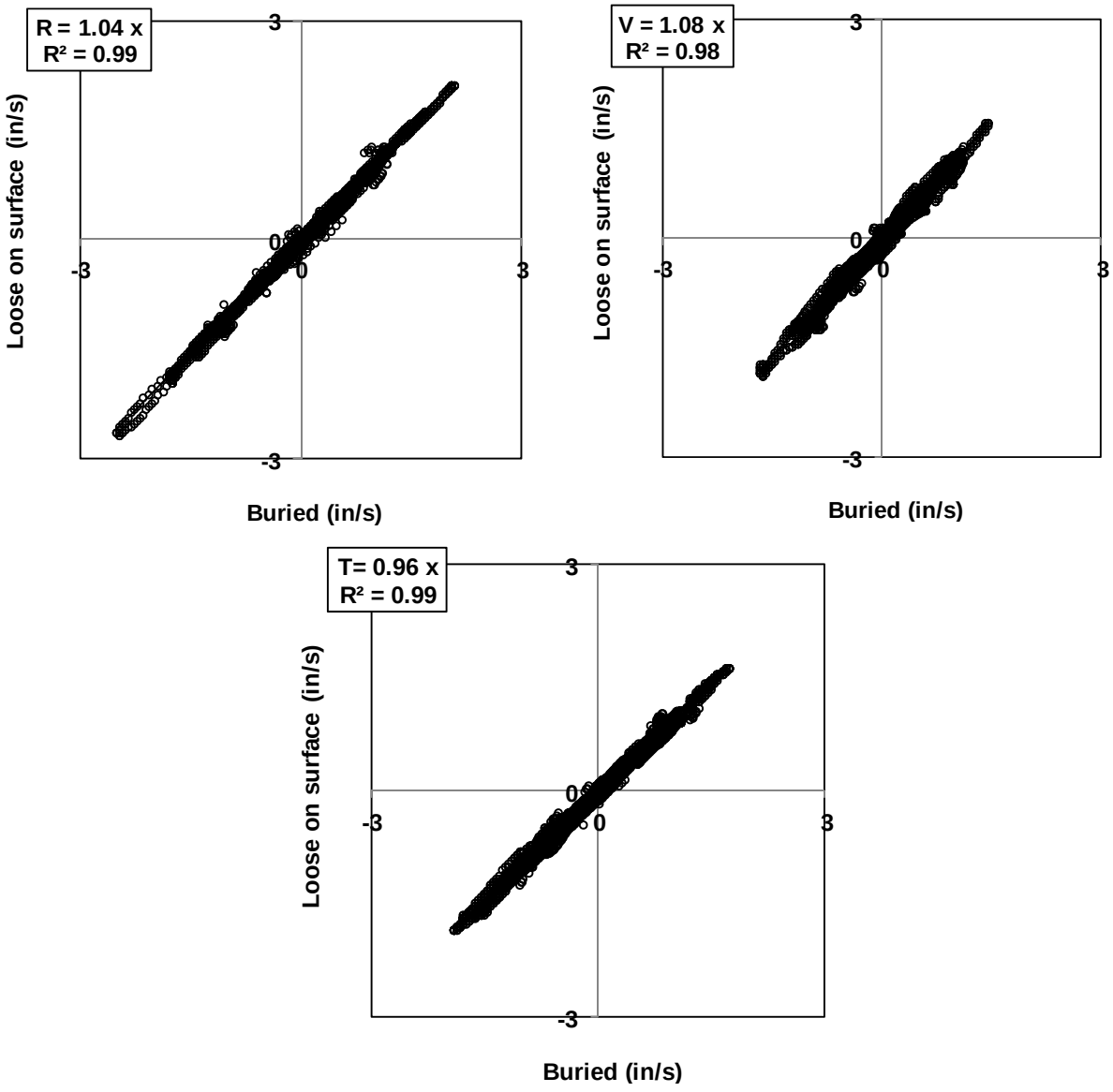

(b)

Figure 19 (cont.) Component time histories (a) and scatter plots (b) for site WY-5

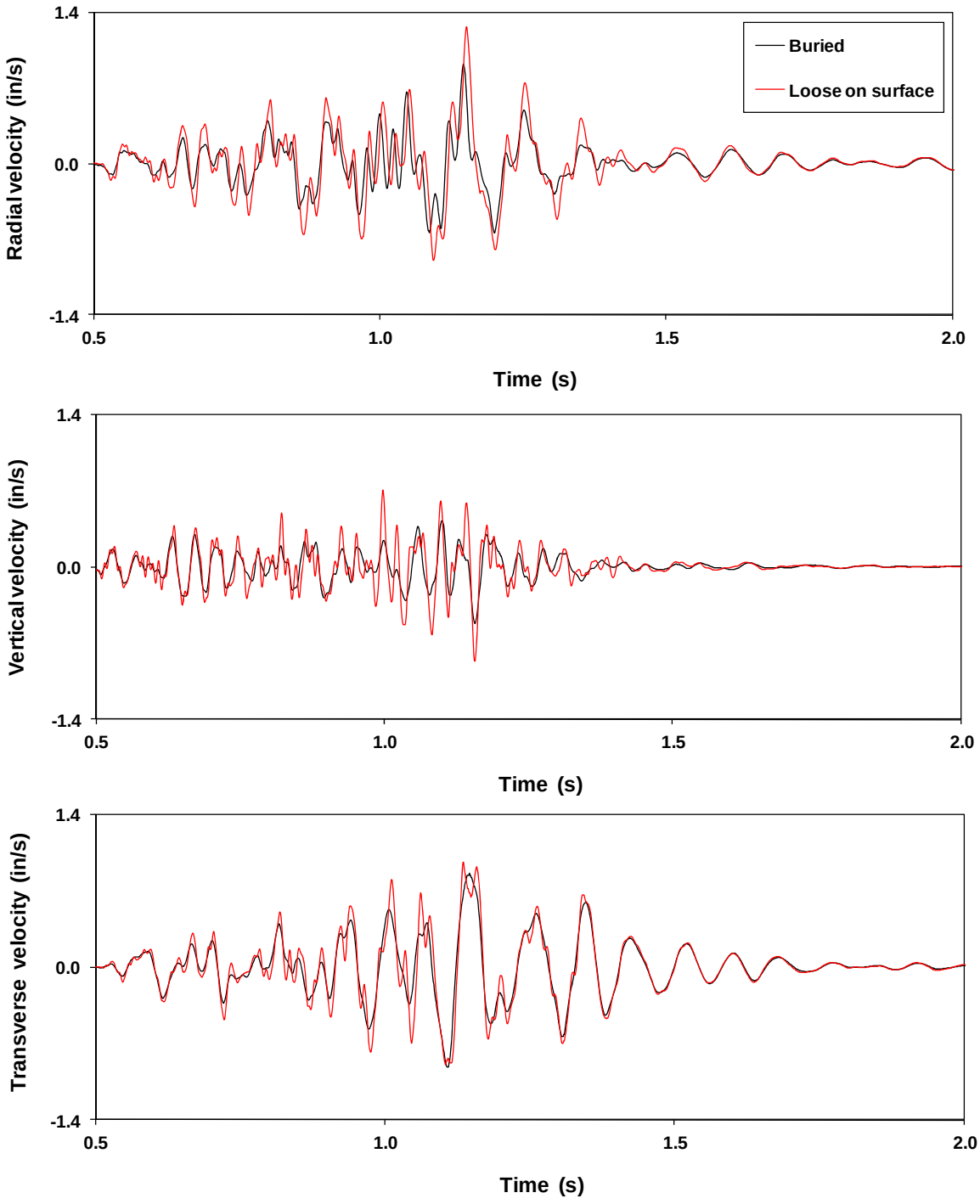

(a)

Figure 20 Component time histories (a) and scatter plots (b) for site OH-1

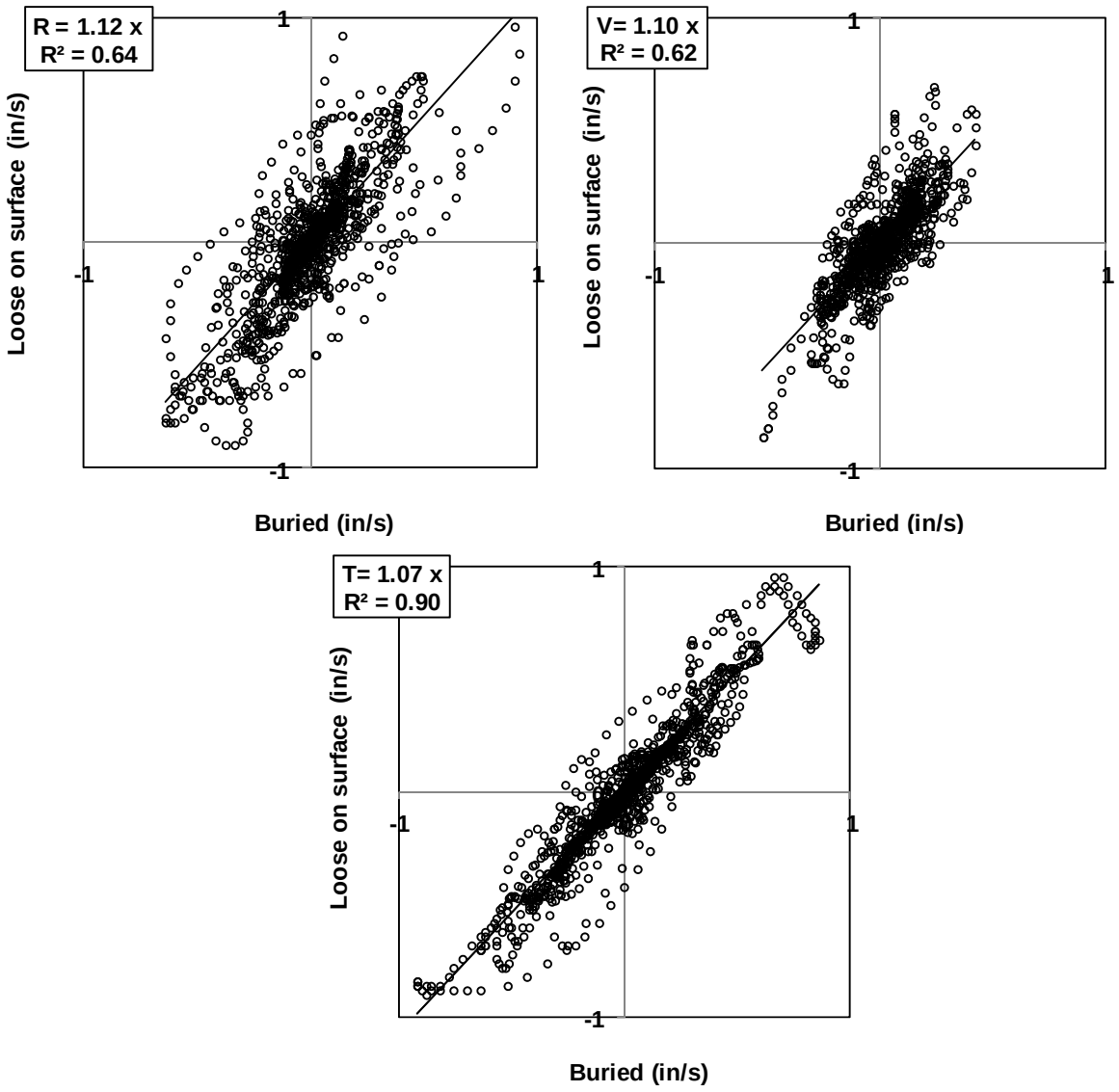

(b)

Figure 20 (cont.) Component time histories (a) and scatter plots (b) for site OH-1

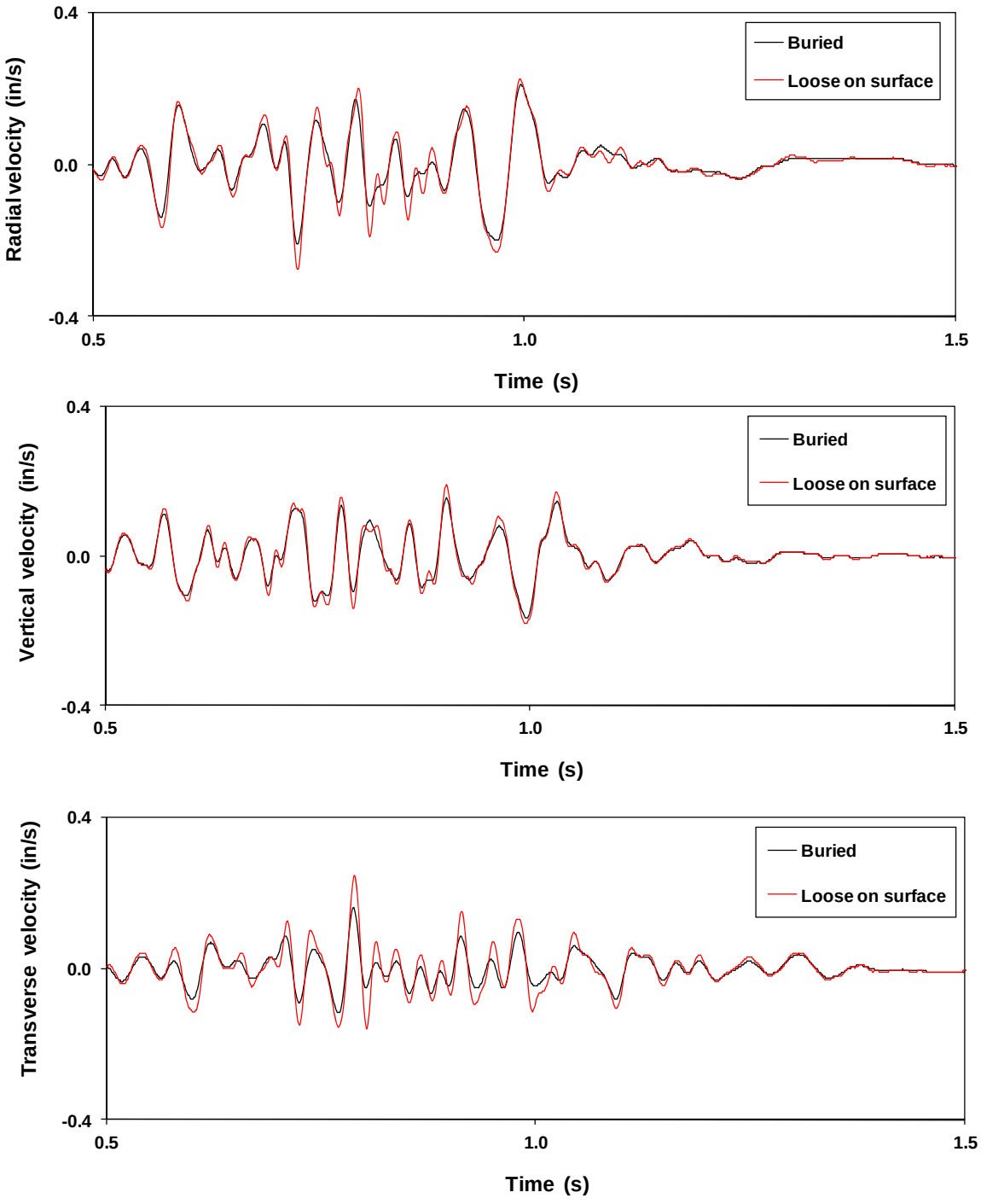

(a)

Figure 21 Component time histories (a) and scatter plots (b) for site KY-8

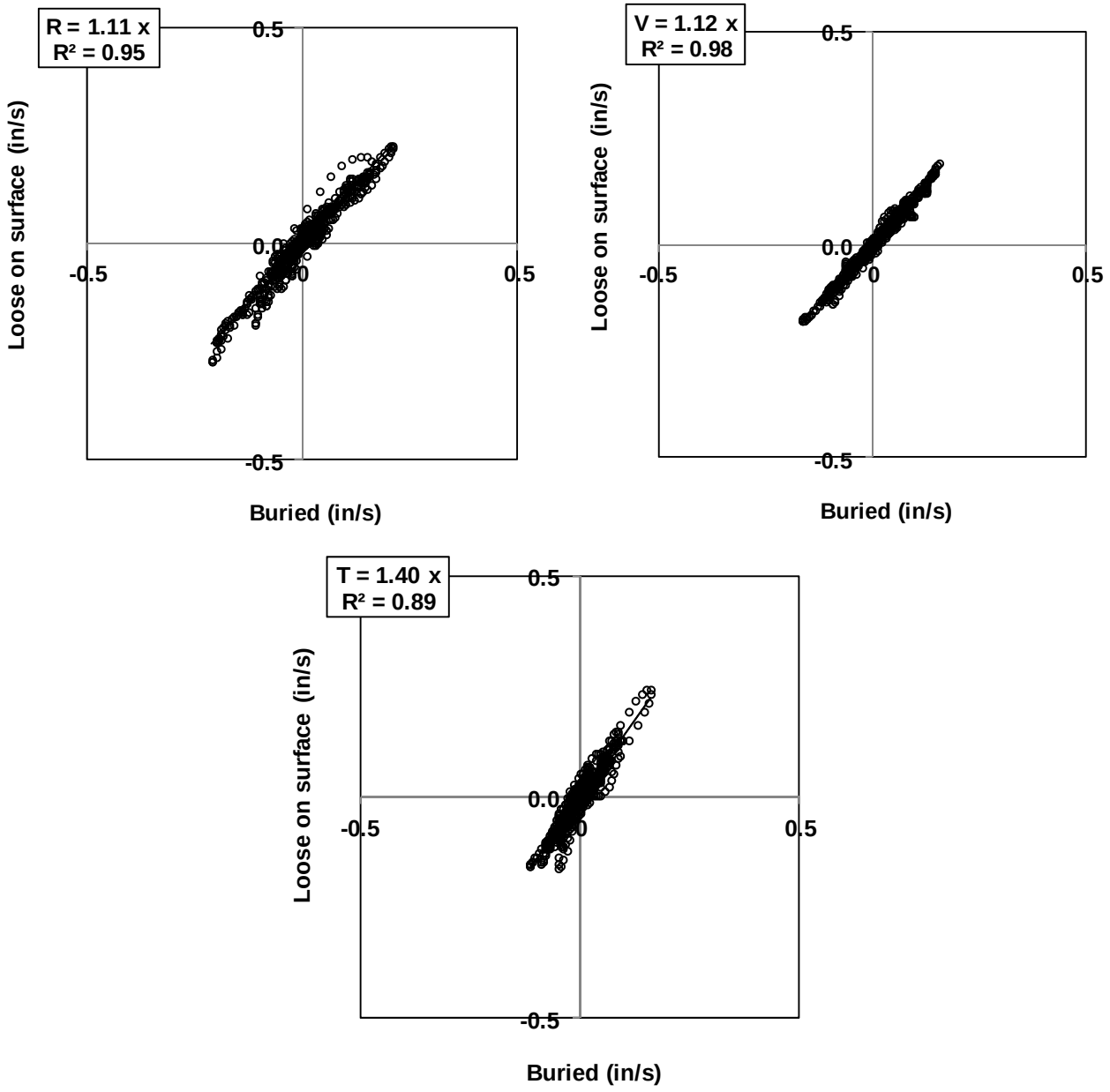

(b)

Figure 21 (cont.) Component time histories (a) and scatter plots (b) for site KY-8

sensors in the V direction and do not represent decoupling but rather may result from the fast delay times along the rows relative to the long row-to-row delay timing for the blast design.

The effects of apparent T component moderately high frequency around 28 Hz for both the buried and loose sensors at the low velocity amplitude site KY-8 in Figure 21(b) shows loose sensor amplification. The scatter plot best-fit slope of 1.4 is the highest for all comparisons and may be attributed to decoupling based on frequency.

In comparison OH-4 exhibits moderate to high frequency and velocity amplitudes and poorer correlation in the R and V components relative to the T direction. Shown in Figure 18(b), the scatter plot ratio of loose to buried peaks averaged 1.29 in the V direction where frequencies are the high for both coupling methods.

The following observations are made:

- When buried sensor peak frequencies were greater than 12 Hz, the ratio of loose to buried PPV ranged 1.31 to 1.43 (average 1.37).

- For the low frequency site WY-5, the difference between lose and buried sensors peak velocities was small (6% difference for PPV in the R component).

- Amplification of peaks in terms of PPV appears to be driven by ground motions frequencies rather than velocity while the PPV is generally carried in the R component for both coupling methods.

b. Sensor shape (16 sites)

The performance of round and square geophones attached to spikes were compared. It was not expected that sensor shape alone could be a major influence on decoupling. However, this comparison provided the opportunity to evaluate spiked sensor front edge shape effects and the “rocking” motion in the R direction that may occur with improperly mounted spiking.

Figure 22 are plots of PPV, peak frequency, and computed peak acceleration for spiked sensors at 16 site blasts in which square and square sensor motions were correlated. In this instance, the regression best-fit was applied to all sites excluding the obvious outliers (KY-1, KY-2 and OH-4). The resulting line slopes are unity for PPV and frequency and 1.07 for acceleration. Both KY-2 and OH-4 were compared in the previous example and identified as possible outliers.

Figures 23 and 24 compare KY-2 (a possible outlier) and OH-2. The horizontal components of the round sensor for KY-2 show unusually high peak velocity amplitudes relative to the square sensor. The high R component peak frequency of 56.8 Hz results in an acceleration of 1.01 g’s and the scatter plot of time-correlated peaks in Figure

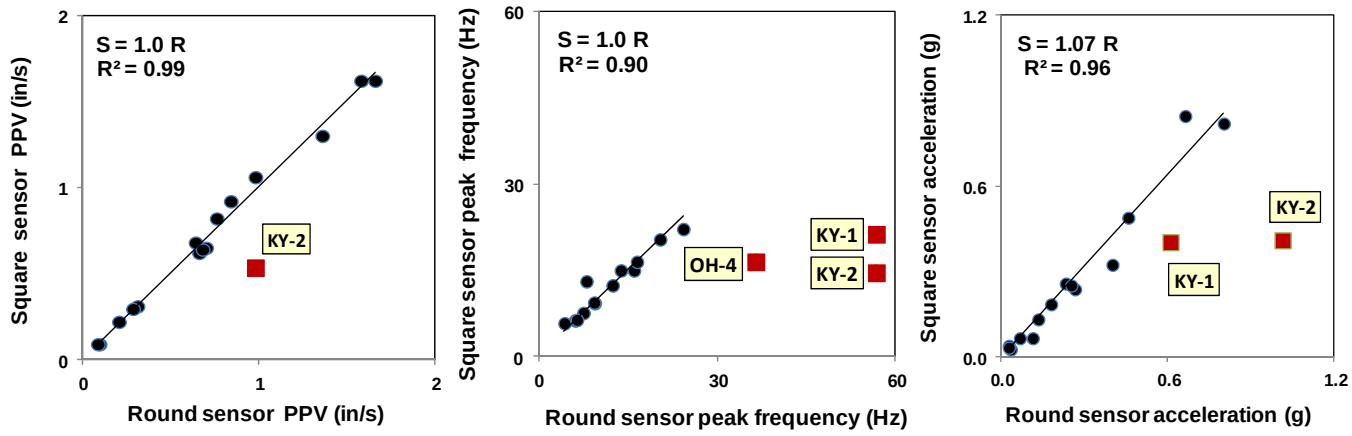

(a) (b) (c)

Figure 22 Response of round versus square spiked sensors for PPV (a), peak frequency (b), and computed acceleration (c) at 16 sites

23(b) indicates poor correlation. The T component peak frequencies are comparable while there is a slight round sensor enhancement, resulting in an acceleration of 0.57 g's. The squares sensor show consistent velocity and frequency peaks in all three components resulting in accelerations of 0.41 g's or less. The V component time-histories for the two sensor shapes show a near perfect correlation. Vertical motions are somewhat independent of edge shape effects.

Time history and scatter plots for OH-2 show excellent correlation and no differences between the two spiked sensors are apparent. This is the case with most other blast sites.

It is concluded that

- Shape is most likely not a factor contributing to difference in geophone response.
- Rather, the differences are attributed to poor spiking for the round sensor at blast site KY-2, allowing the sensor to laterally rotate about the spike resulting in lateral enhancement of R and T component peaks.
- The net effect is ground motion R acceleration that is nearly two times higher than it may have been if proper coupling had been exercised.

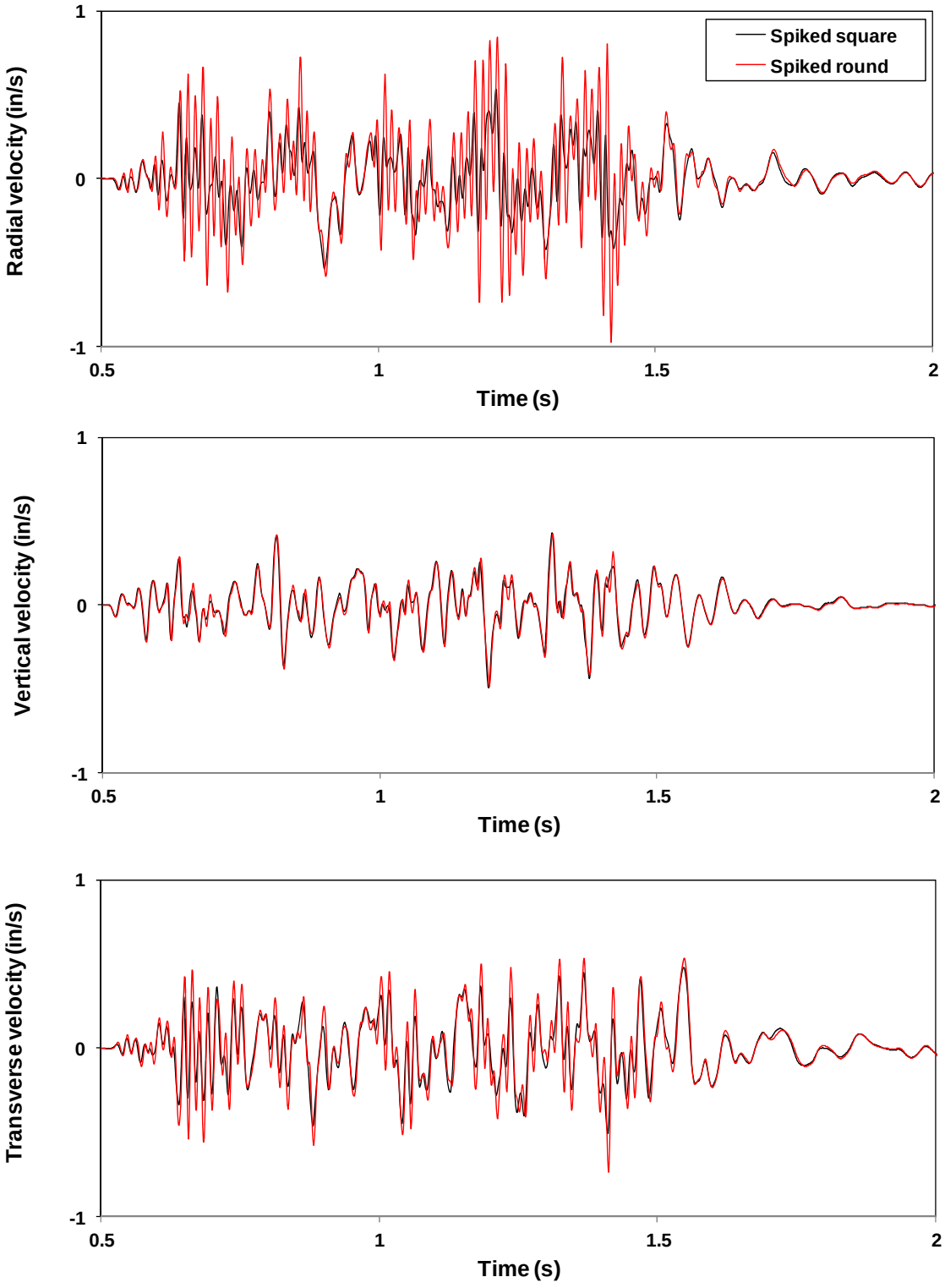

(a)

Figure 23 Component time histories (a) and scatter plots (b) for site KY-2

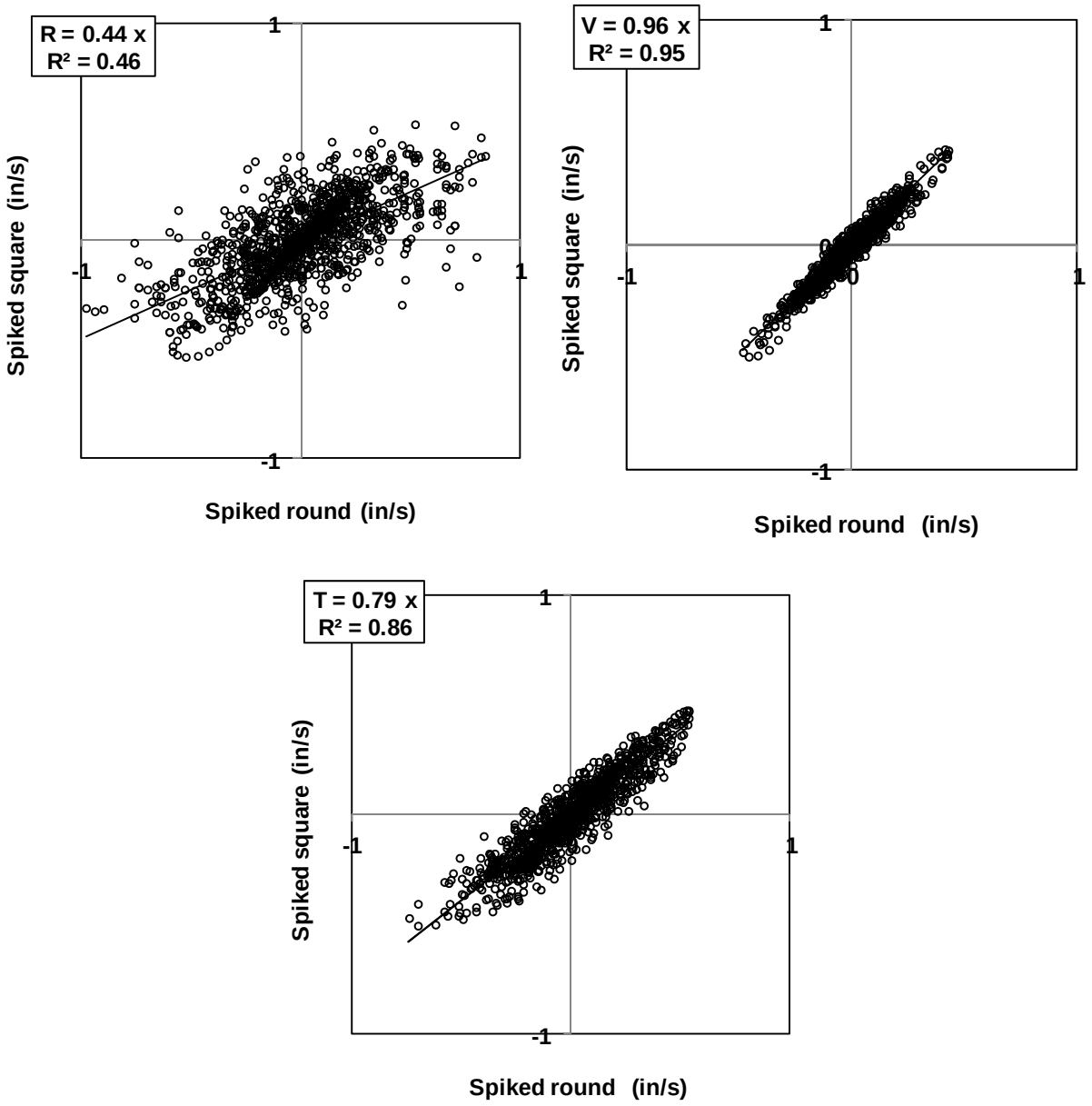

(b)

Figure 23 (cont.) Component time histories (a) and scatter plots (b) for site KY-2

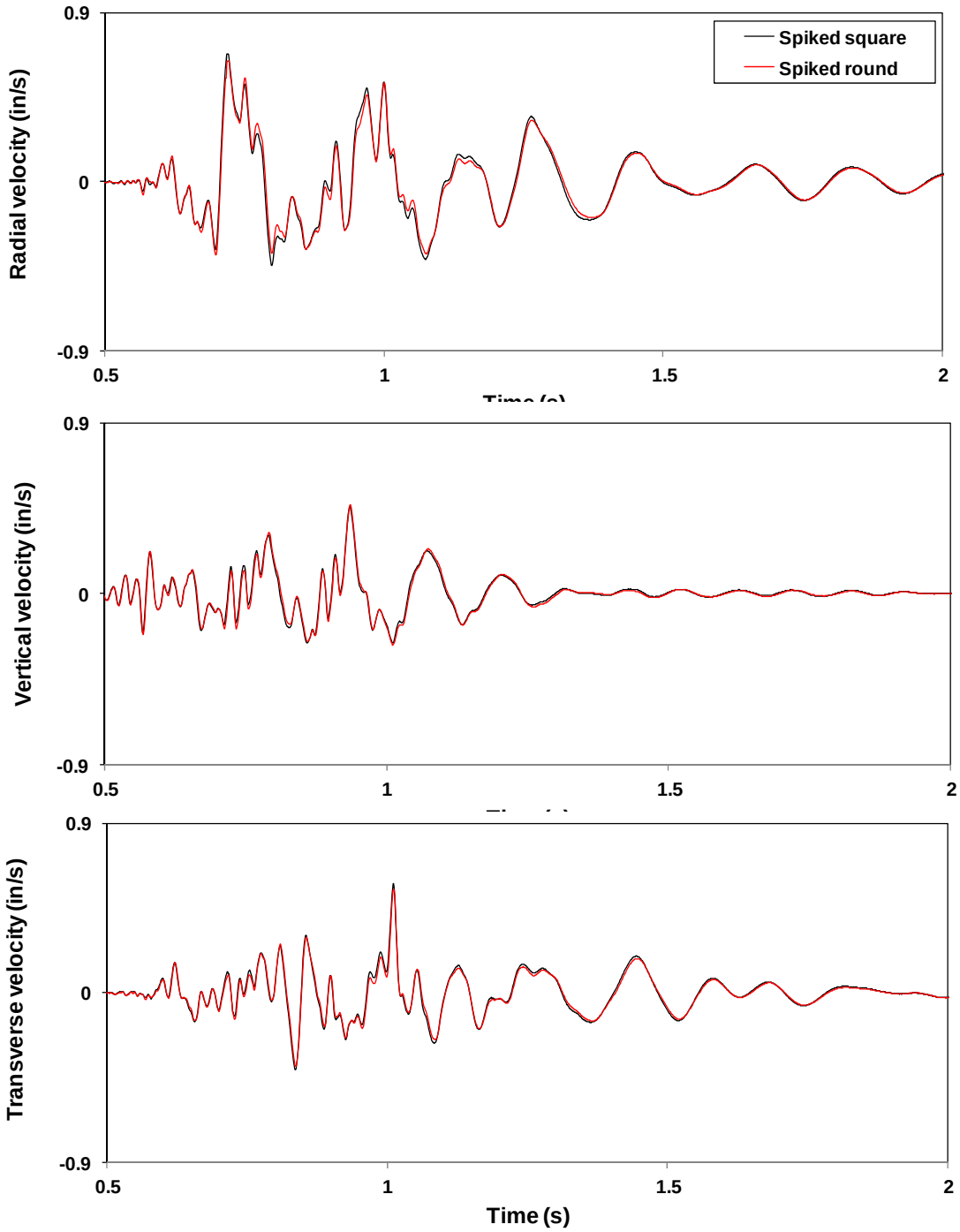

(a)

Figure 24 Component time histories (a) and scatter plots (b) for site OH-2

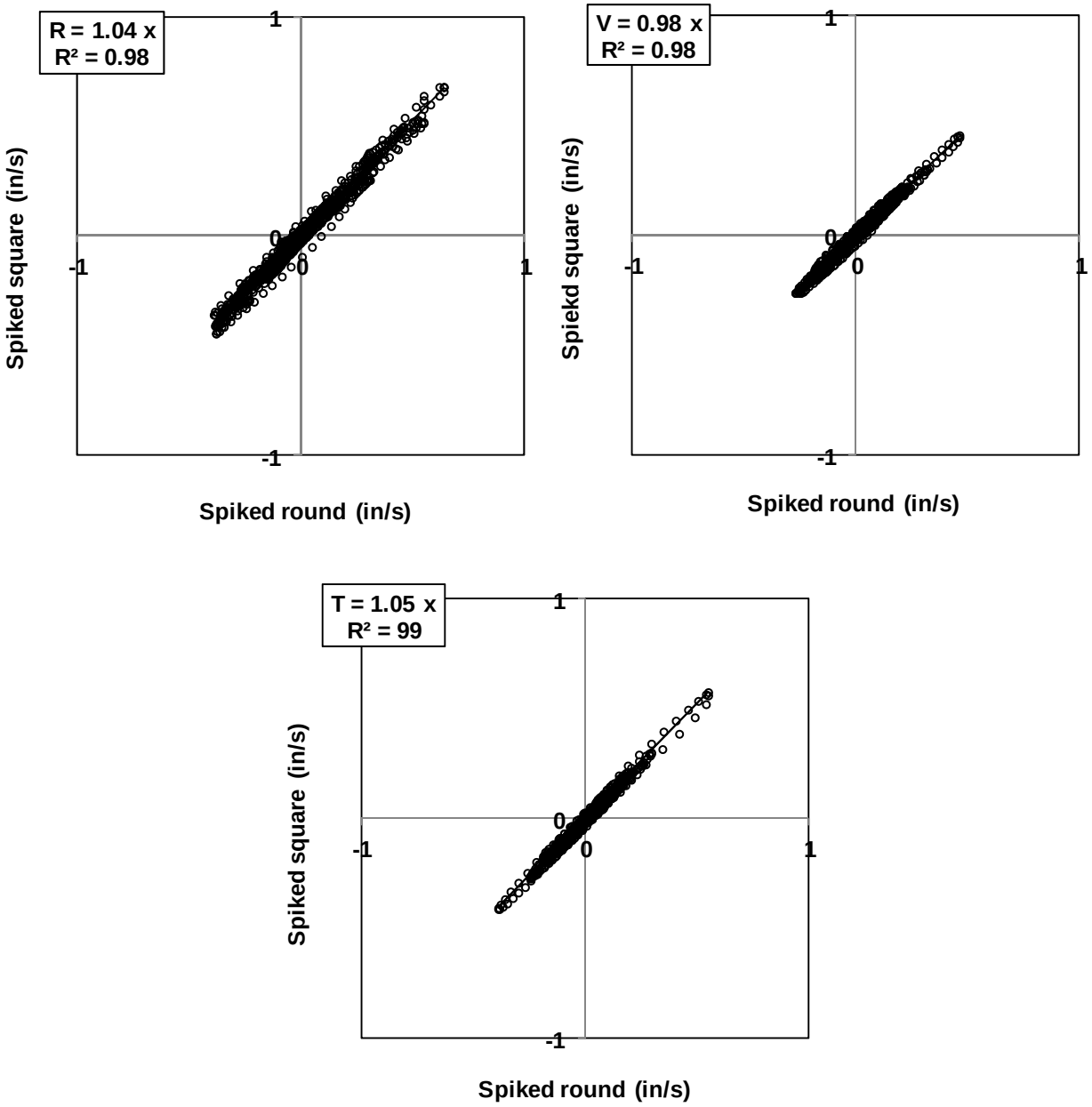

(b)

Figure 24 (cont.) Component time histories (a) and scatter plots (b) for site OH-2

a. Buried, spiked and combined spiked and buried sensor (8 sites)

Comparisons of three coupling methods at eight blast sites are provided in Figure 25 in which the performance of buried geophones are compared with spiked sensors and spiked sensors that were buried. Outliers were removed from the data set for regression analysis when comparing combing spiked and buried sensor with spiked and with buried sensors.

In all cases with the exception of PPV comparisons, the burial or spiking of sensors alone produced slightly higher peak frequencies and computed accelerations that for the combined spiked and buried sensors. The differences are considered to be minor and for the most part can be ignored. Based on the regression statistics and ignoring possible outliers for IL-1, KY-4 and KY-5, correlations with the combine method is very good. In particular, adding spikes to sensors that are buried has no advantage when compared with non-spiked buried sensors in terms of PPV (upper left figure).

Time histories and scatter plots are provided in Figure 26 through 29 for blast sites IL-1, IN-1, KY-4, and KY-5 representing the three outliers noted in Figure 25 and one possible non-outlier (IN-1). Time-history plots are provided for all three coupling methods for R, V, and T components. Scatter plots are arranged similar to Figure 25 in which combined spiked and buried sensors are correlated with each spiked and buried sensors for R, V, and T components.

Time-histories in Figure 26(a) for IL1 show enhancement for spiked sensors and well-correlated peak for buried and combined spiked and buried sensors. The spiked sensor horizontal components (R and T) show distinct time lags in peaks that produce random scatter plots in Figure 26(b) with little or no correlation.

Site IN-1 given in Figure 27 shows only minor peak enhancements in the T component time-histories and slightly lower scatter plot correlation between spiked and the combined methods. The best-fit line slope for the T component is 0.89 shown in the lower right plot in Figure 27(b). Spiking alone provided slight peak enhancement over the high-frequency wavelets superimposed on the lower frequency, broad peaks of Figure 27(a), top.

The influence of frequency on velocity amplification for spiked sensors is shown in Figure 28(a) for site KY-4. Scatter plots show lower correlation of spiked response with the combined method (e.g. regression slopes of 0.92 and less). The peak frequencies for buried and combined coupling were 7.4 Hz while the spiked sensor peak frequency was 64 Hz most likely due to lack of coupling. PPV for all three sensors occurred in the T component.

A similar comparison is made in Figure 29 for site KY-5 for overall higher frequencies (22 Hz for combined method and buried and 43 Hz for spiked). In this case, the higher frequencies contribute to far more random amplifications. Spiked sensor frequencies

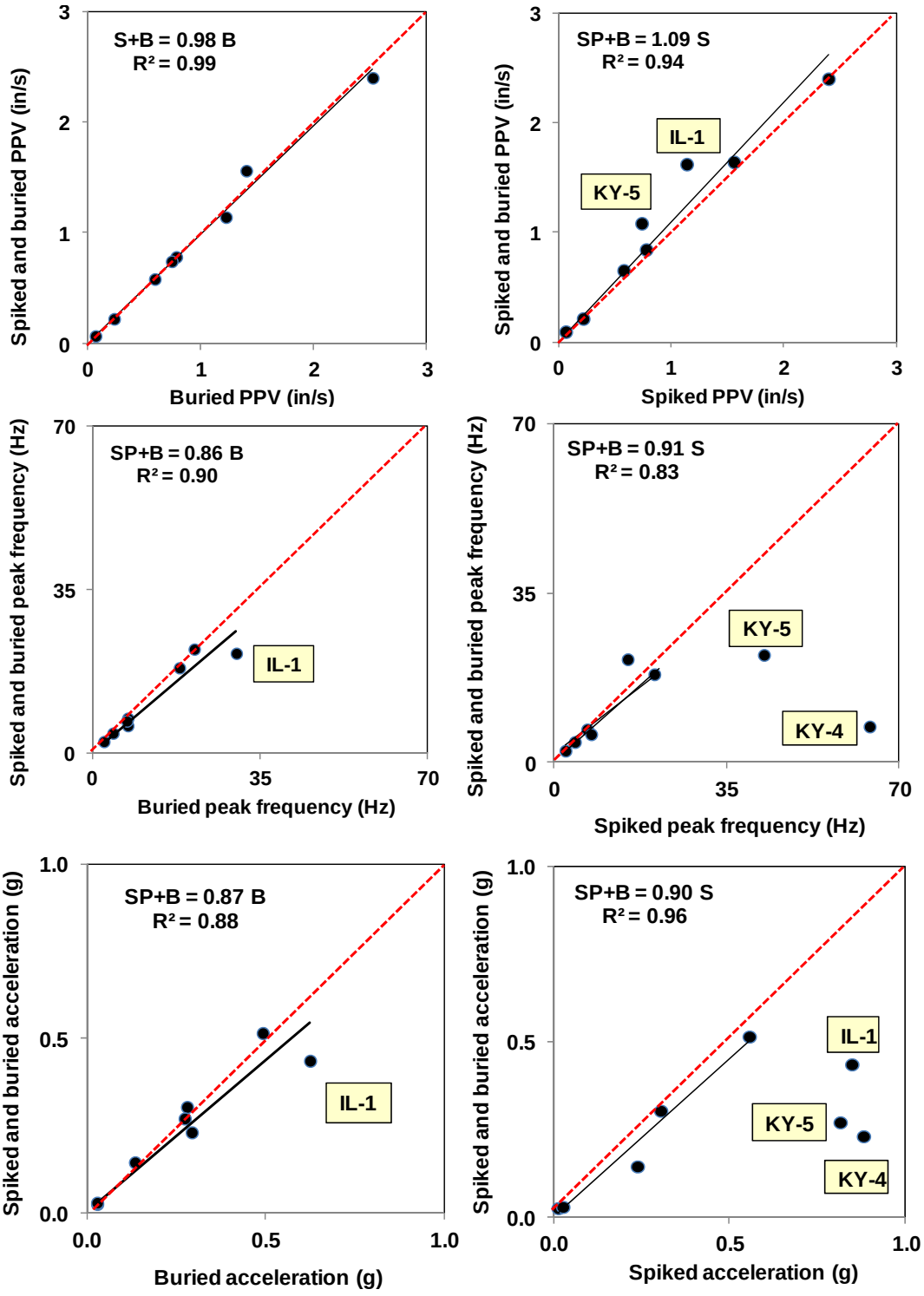

Figure 25 Response of buried, spiked, and combine spiked and buried sensors for PPV (top row), peak frequency (middle row), and computed acceleration (bottom row) at 8 sites

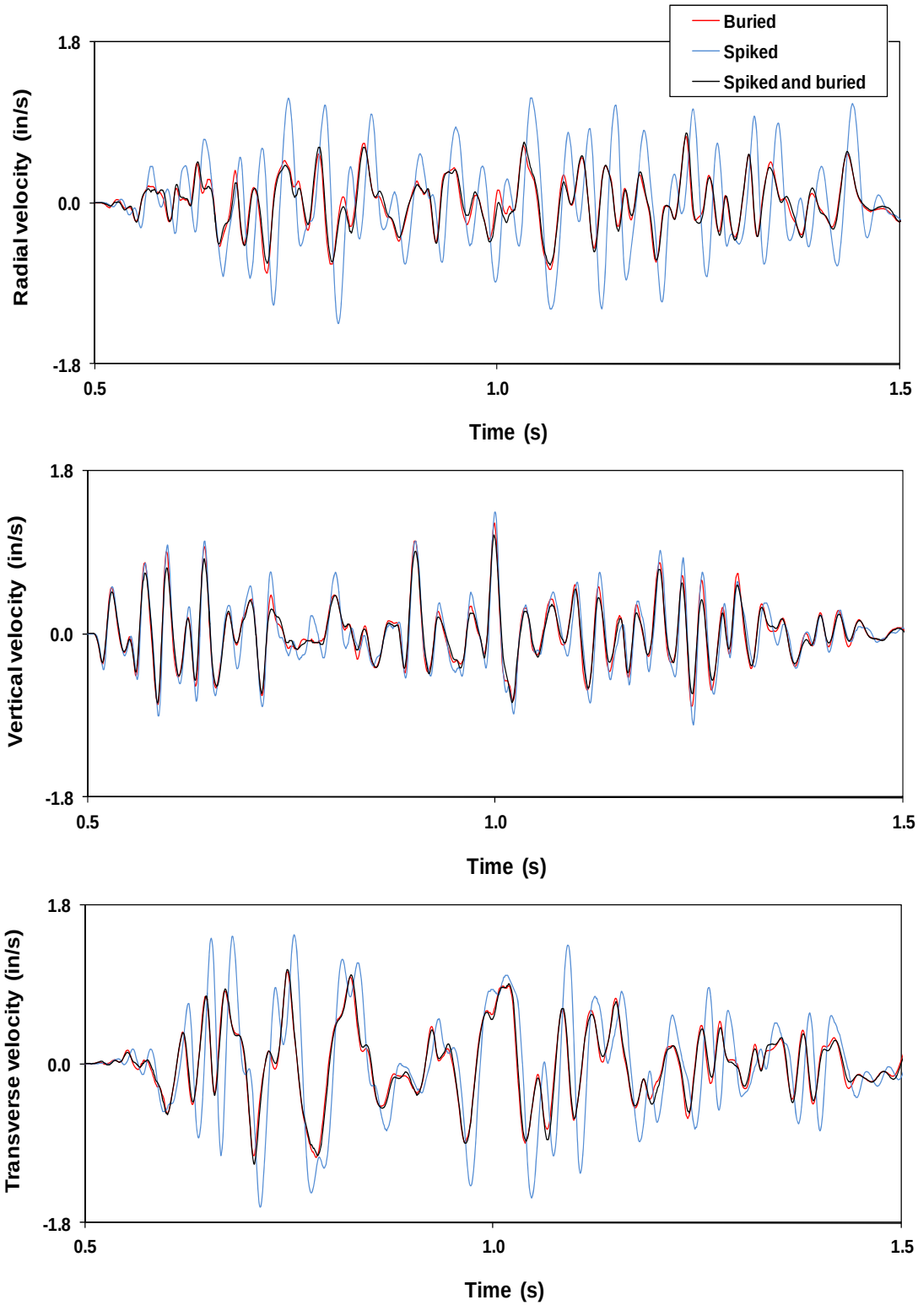

(a)

Figure 26 Component time histories (a) and scatter plots (b) for site IL-1

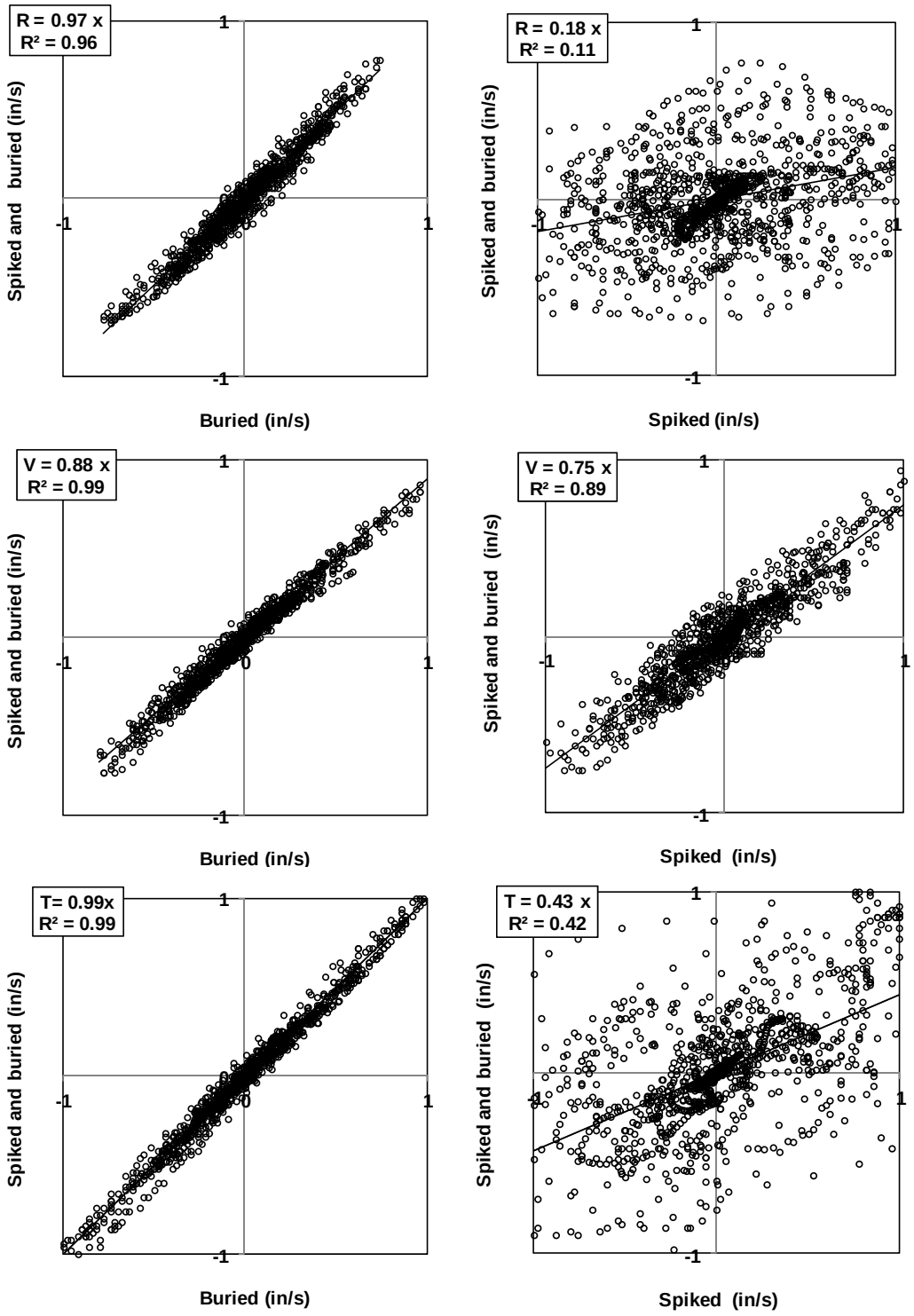

(b)

Figure 26 (cont.) Component time histories (a) and scatter plots (b) for site IL-1

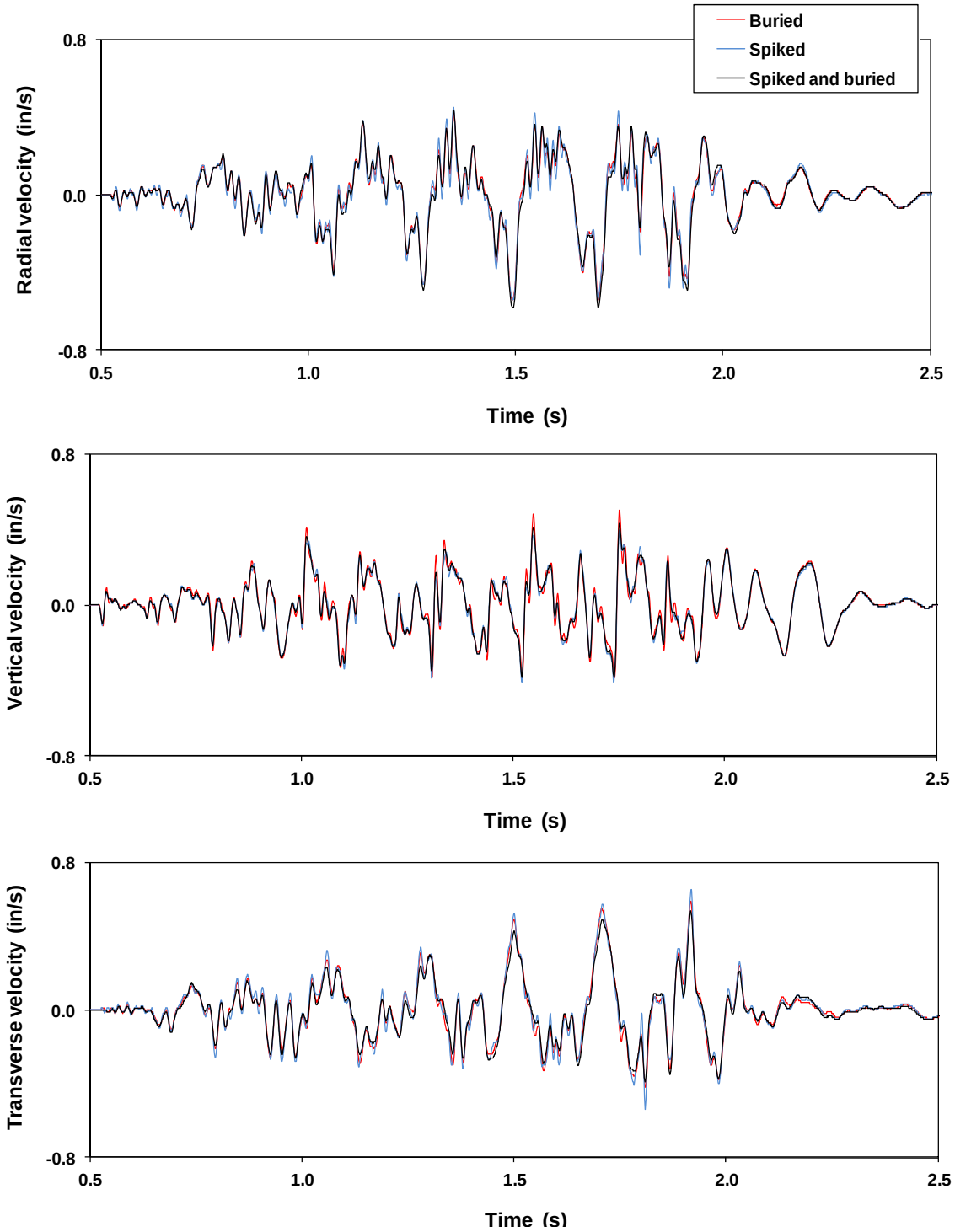

(a)

Figure 27 Component time histories (a) and scatter plots (b) for site IN-1

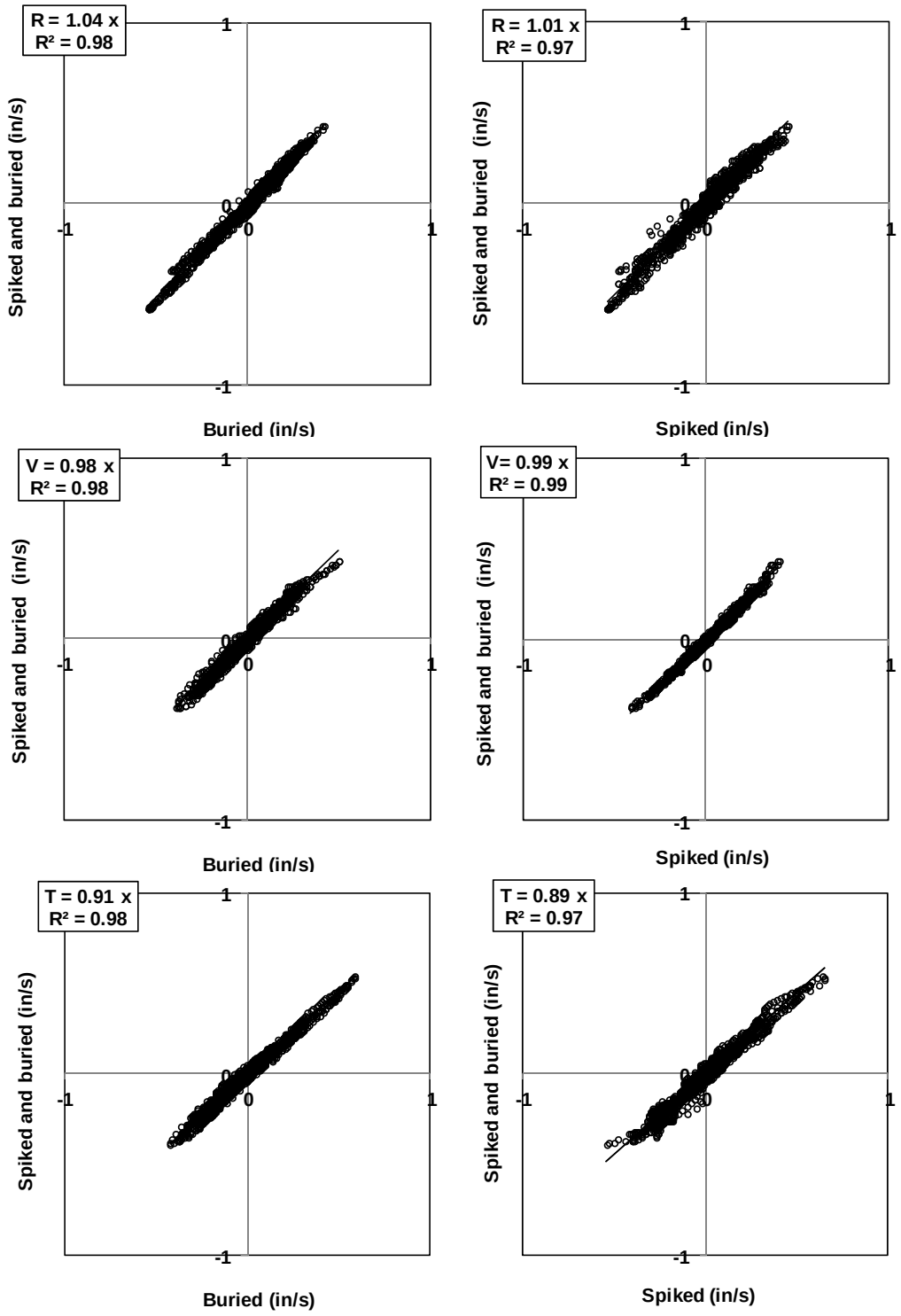

(b)

Figure 27 (cont.) Component time histories (a) and scatter plots (b) for site IN-1

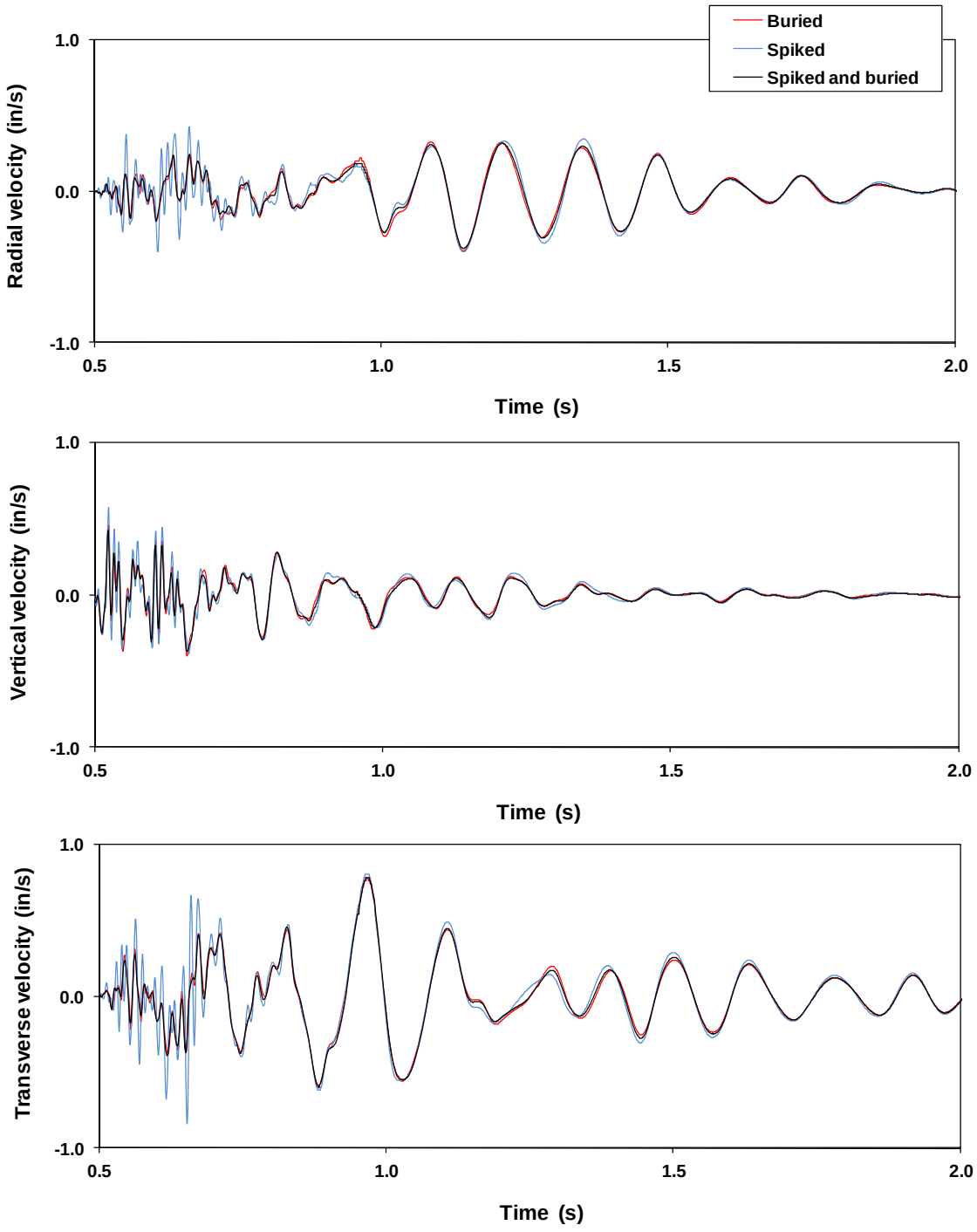

(a)

Figure 28 Component time histories (a) and scatter plots (b) for site KY-4

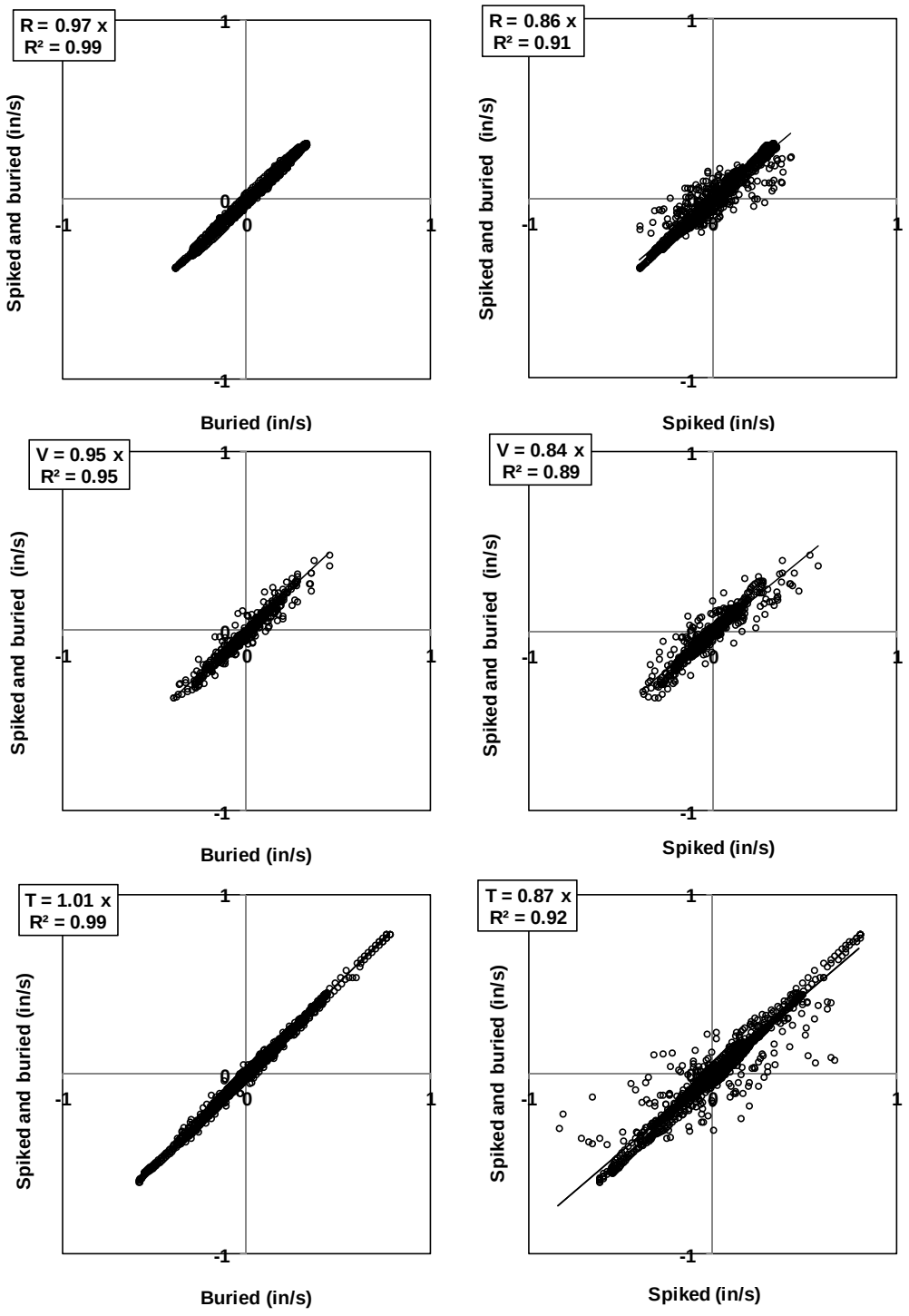

(b)

Figure 28 (cont.) Component time histories (a) and scatter plots (b) for site KY-4

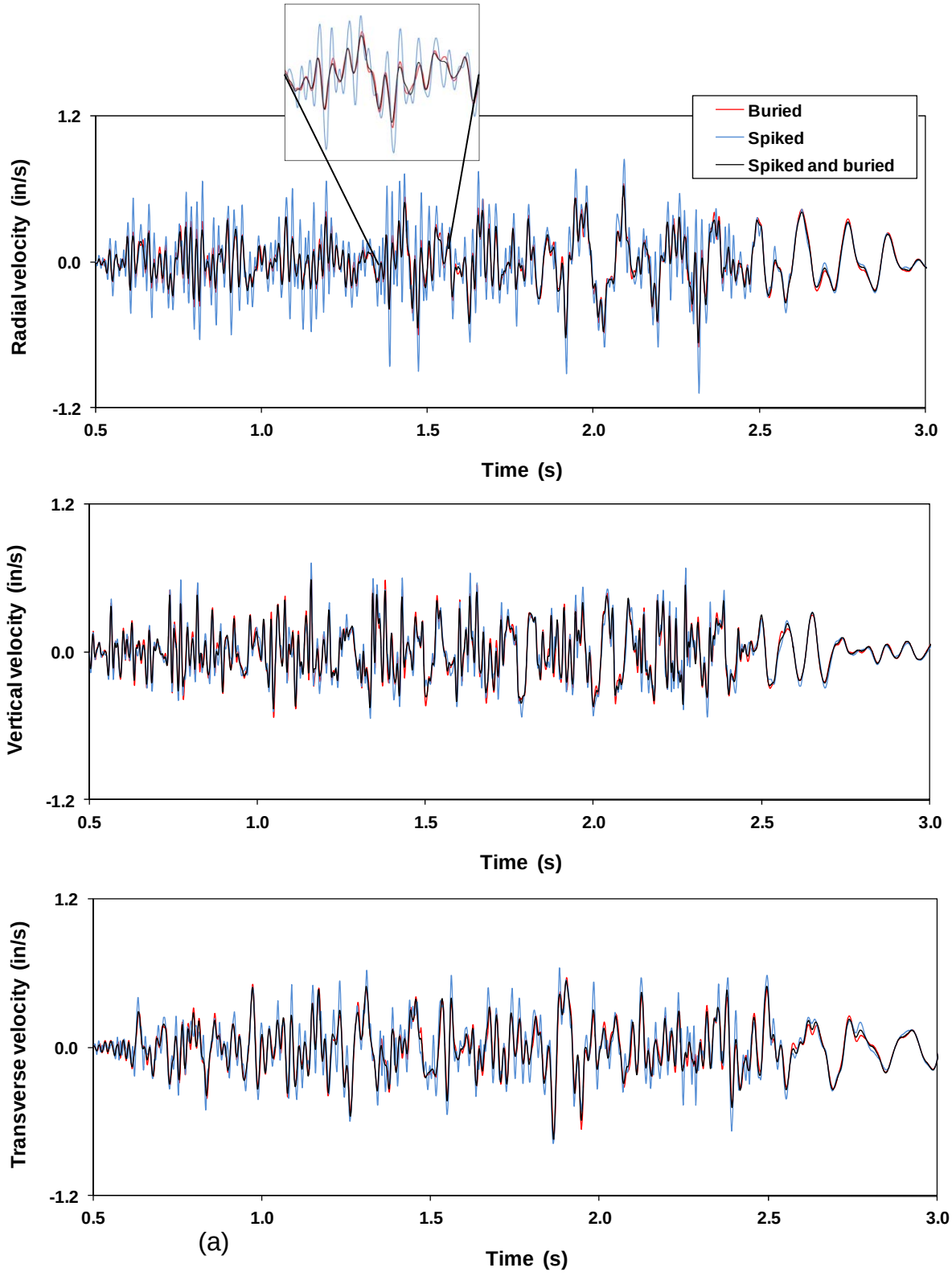

Figure 29 Component time histories (a) and scatter plots (b) for site KY-5

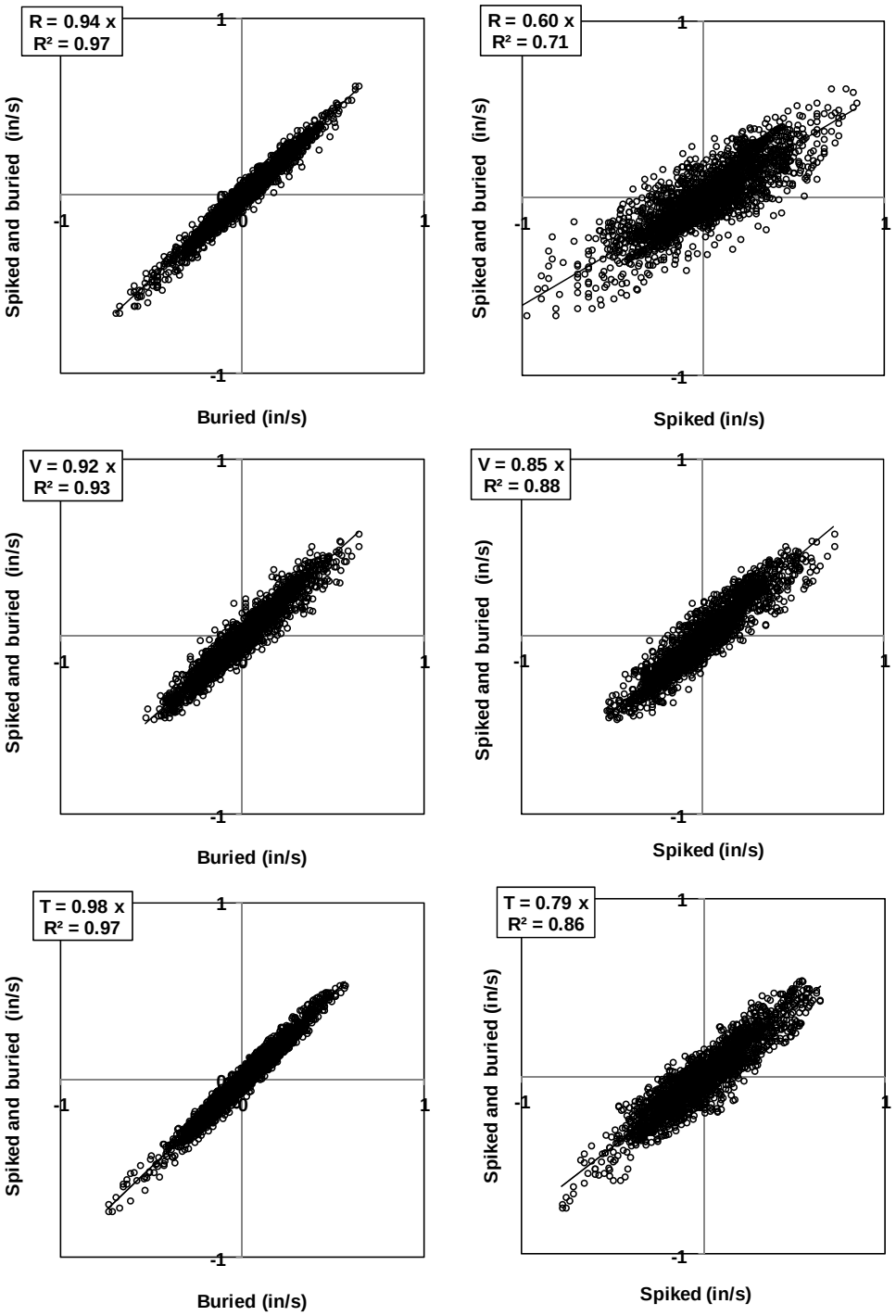

(b)

Figure 29 (cont.) Component time histories (a) and scatter plots (b) for site KY-5

produced a larger number of complete zero-crossings whereas the buried methods produced higher frequency wavelets on lower frequencies. This is shown in the radial expanded time-history window inset at the top of Figure 29 between 1.4 and 1.6 s. As a result, the R scatter plot for spiking exhibited random behavior, particular over the low, negative amplitude.

Findings from these comparisons at eight sites are as follows:

- Average PPV amplitudes for spiked sensors were 14% higher than for buried methods while average peak frequencies were over 67% greater.

- Spiked sensors placed on the ground surface exhibited more random frequency behavior compared with buried along and combined spiked and buried.

- The addition of spikes to a buried sensor does not provide better coupling compared with a buried sensor without spikes and results in the same geophone performance in terms of PPV, peak frequency and calculated acceleration.

    d. Buried, spiked, sandbag, and combined spiked and sandbag sensors (25 sites)

Comparisons of four coupling methods are shown in Figure 30 in which buried sensors are compared with spiked, sandbag, and combined spiked and sandbag in terms of PPV, peak frequency and computed peak acceleration. The best-fit trend lines are shown and do not include data highlighted that are assumed to represent potential outliers. Outliers are indicted for sites IL-1 and KY-1 (each previously suspected as decoupled) and KY-8, OH-3, OH-5, WV-2, and NM-4.

Figures 31 through 35 provide time-histories and scatter plots for five representative sites including IL-1 and KY-8 indicated as possible outliers. The other sites include WV-2, WY-5, OH-1. A sixth site, NM-7, is included for comparisons. However, a combined spiked and sandbag sensor was not used. Appendix C contained the data for PPV, peak frequency and computed acceleration for all blast sites.

Figure 31 shows time histories and scatter plots for IL-1 represented by a high frequency and high velocity amplitude site. PPVs for surface attachments were contained in the T component and in the V component for the buried sensor.

The lack of agreement in peak amplitudes and time of the peak are shown in the horizontal components. The buried sensor PPV was 1.22 in/s which was amplified by 33% and 54% for sensors with spikes and with a sandbag, respectively. Peak frequencies for surface mounted sensors were less than 50% of the buried sensor. The highest acceleration of 0.85 g’s occurred for the spiked sensor and was 37% greater than the acceleration for the buried sensor. Sensors using a sandbag showed a decreased acceleration averaging 0.49 g’s.

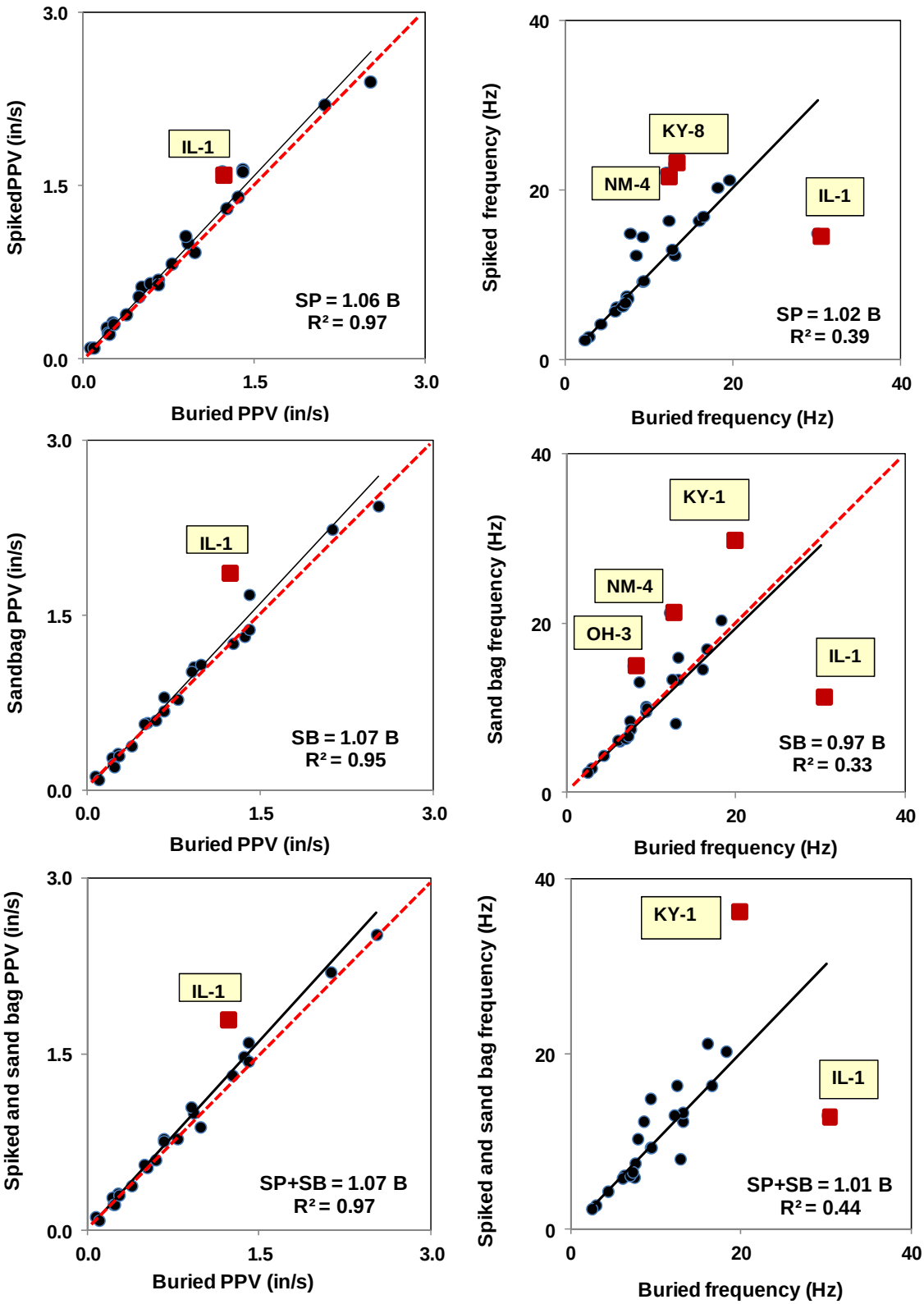

Figure 30 Response of buried, spiked, sandbag, and combined spiked and sandbag sensor comparisons for PPV (left) and peak frequency (right) at 25 sites

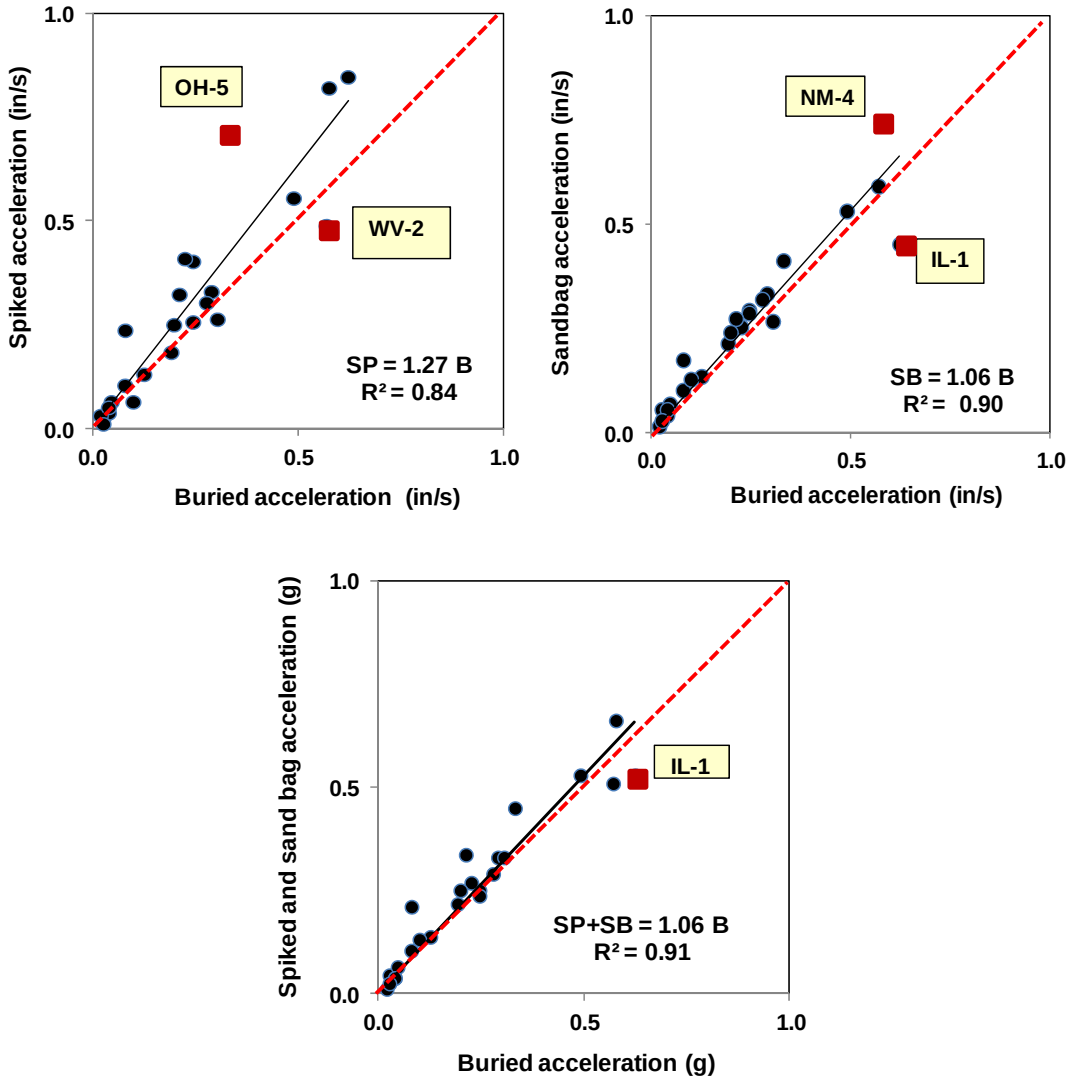

Figure 30 (cont.) Response of buried, spiked, sandbag, and combine spiked and sandbag sensor comparisons for acceleration at 25 sites

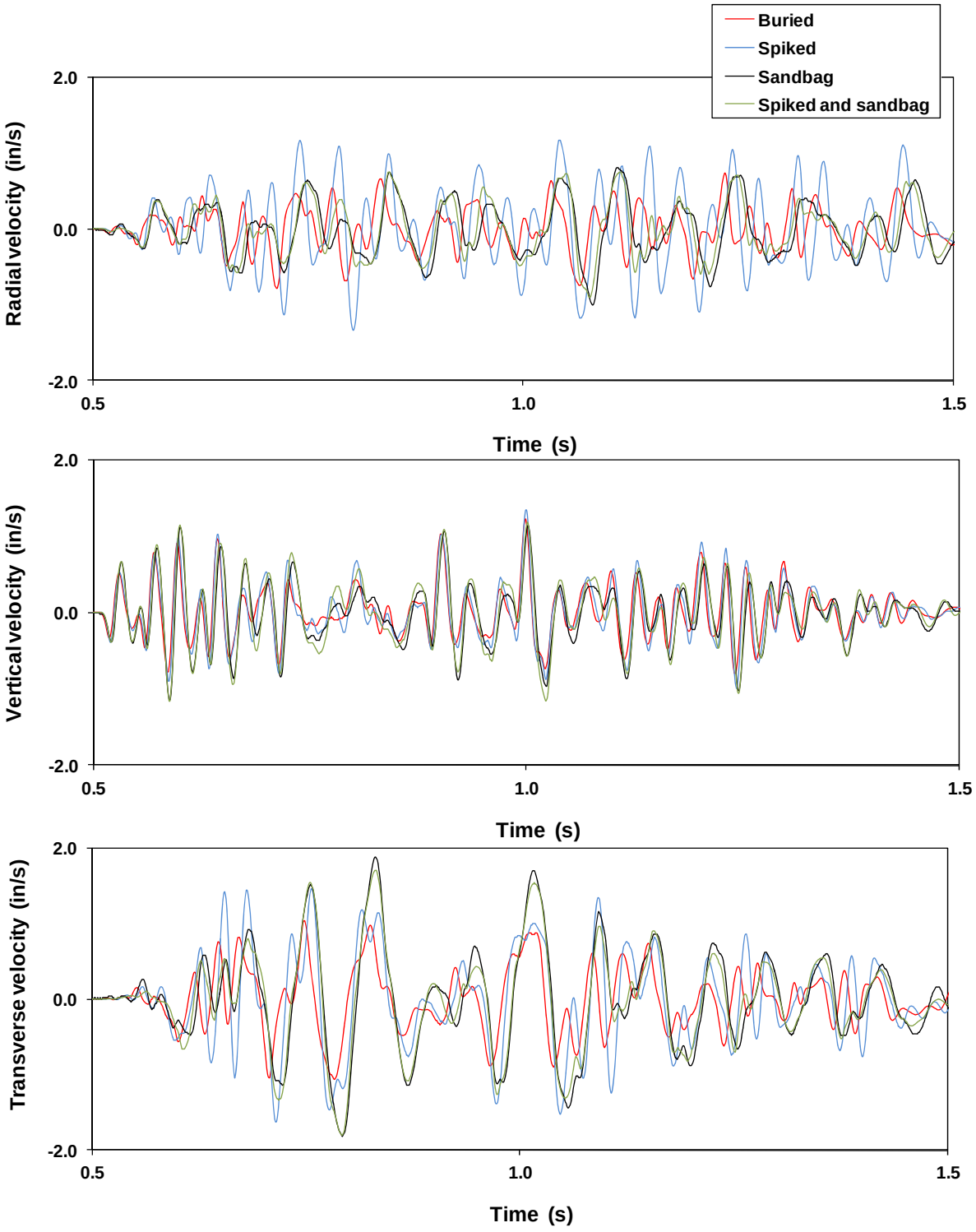

(a)

Figure 31 Component time histories (a) and scatter plots (b) for site IL-1

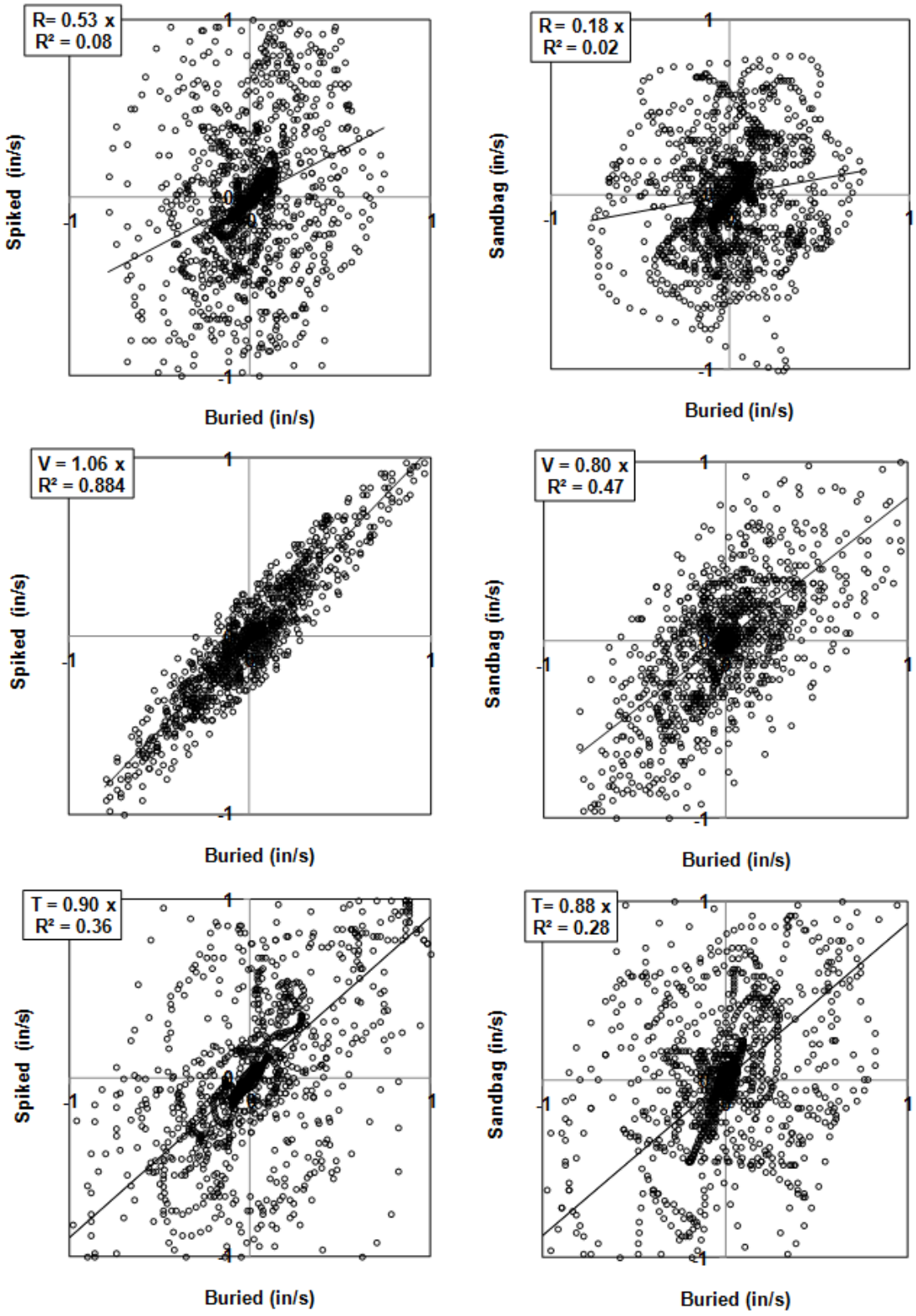

(b)

Figure 31 (cont.) Component time histories (a) and scatter plots (b) for site IL-1

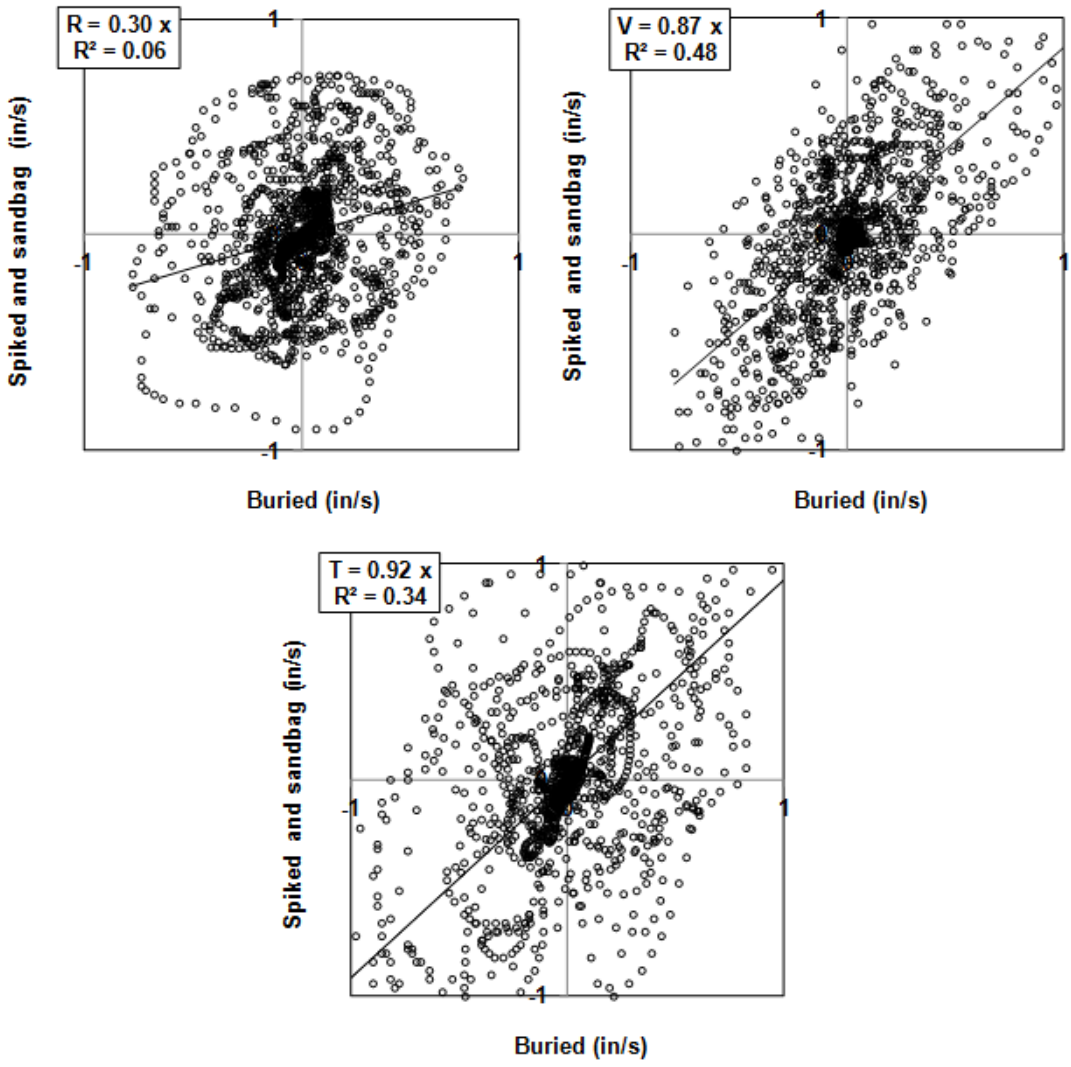

(b)

Figure 31 (cont.) Component time histories (a) and scatter plots (b) for site IL-1

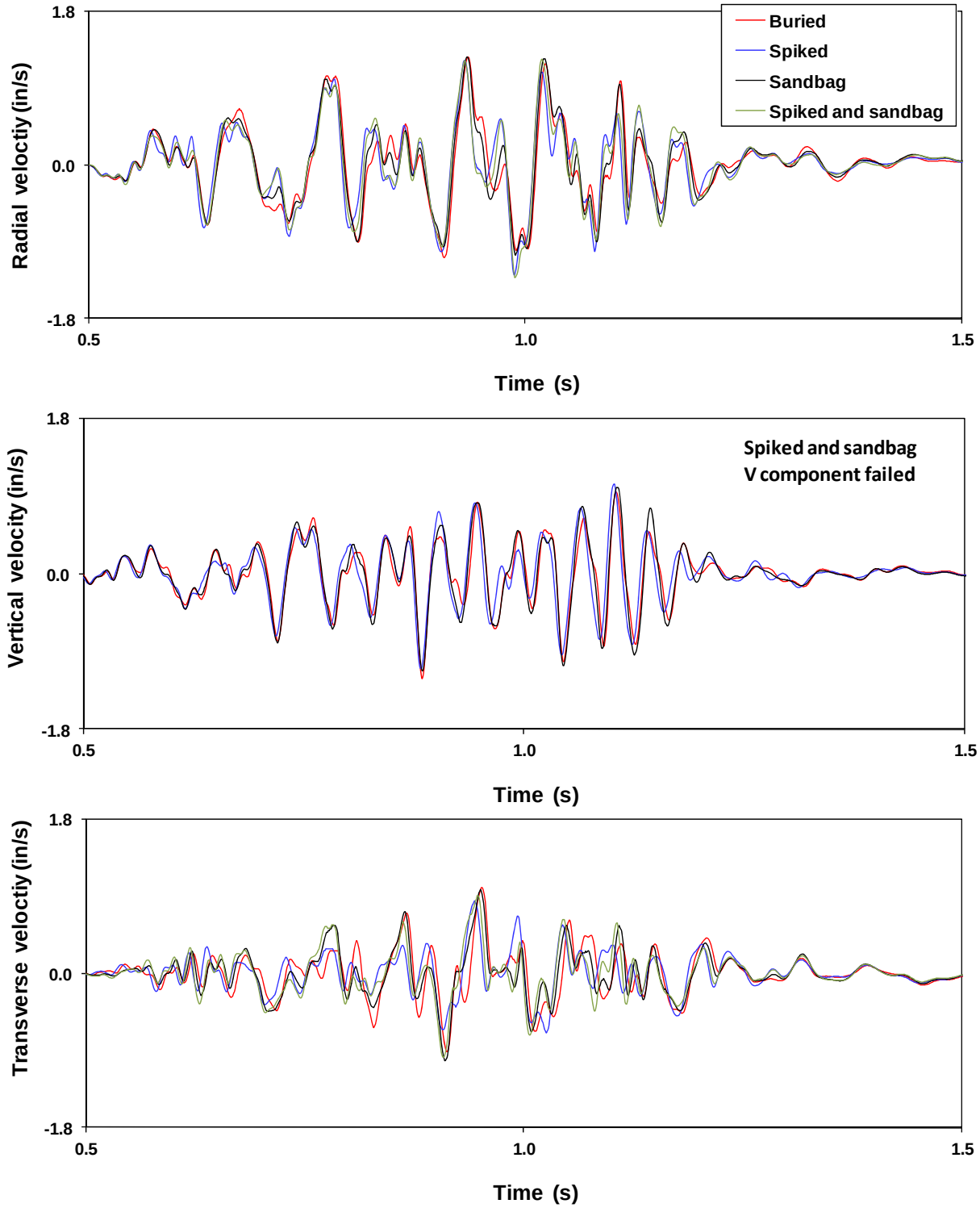

(a)

Figure 32 Component time histories (a) and scatter plots (b) for site WV-1

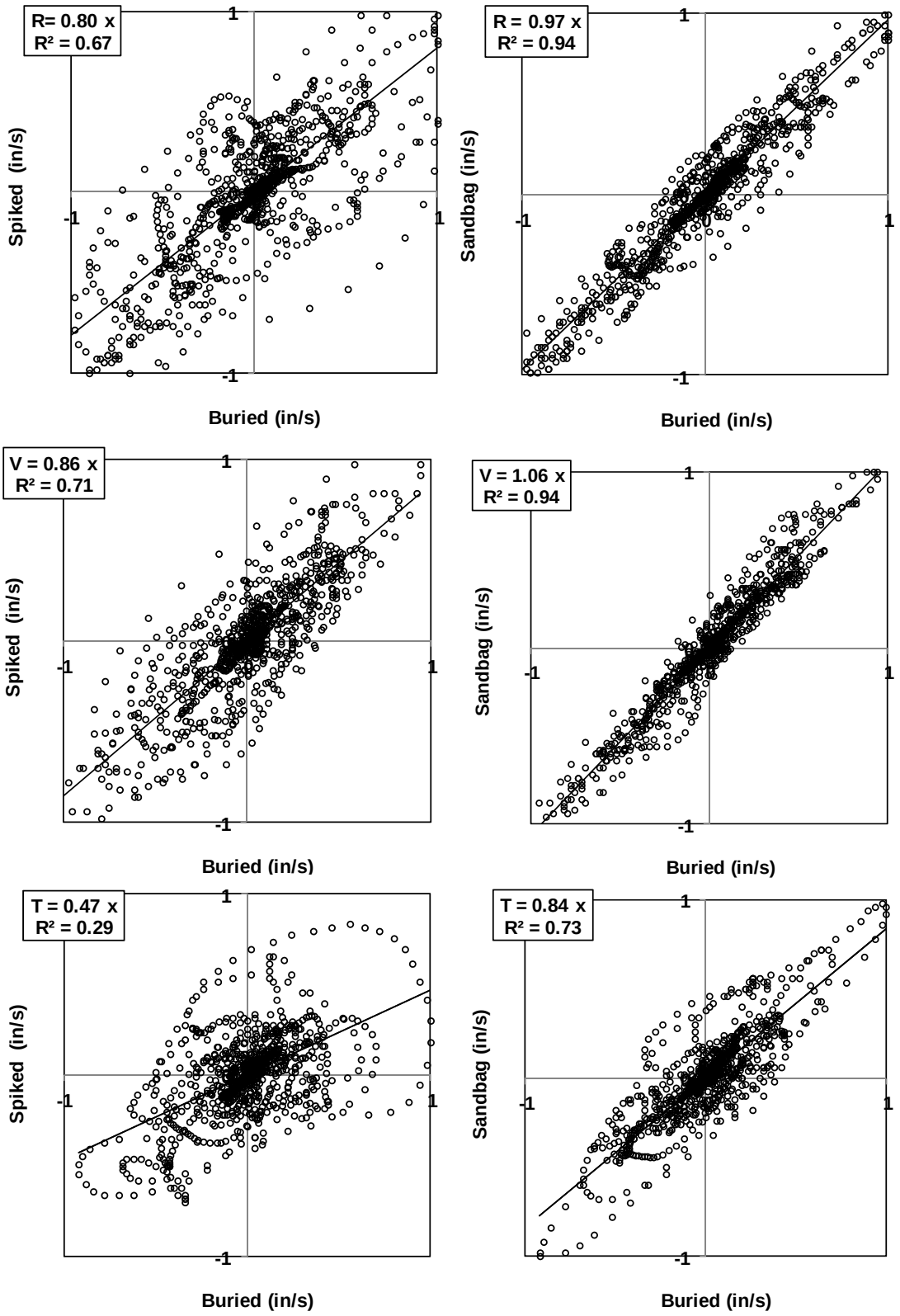

(b)

Figure 32 (cont.) Component time histories (a) and scatter plots (b) for site WV-1

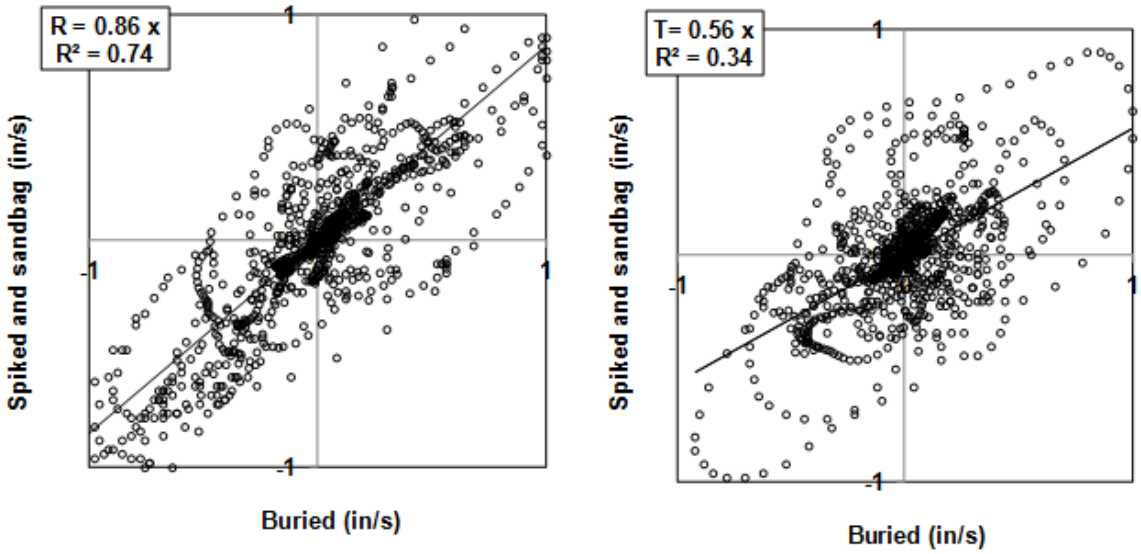

(b)

Figure 32 (cont.) Component time histories (a) and scatter plots (b) for site WV-1

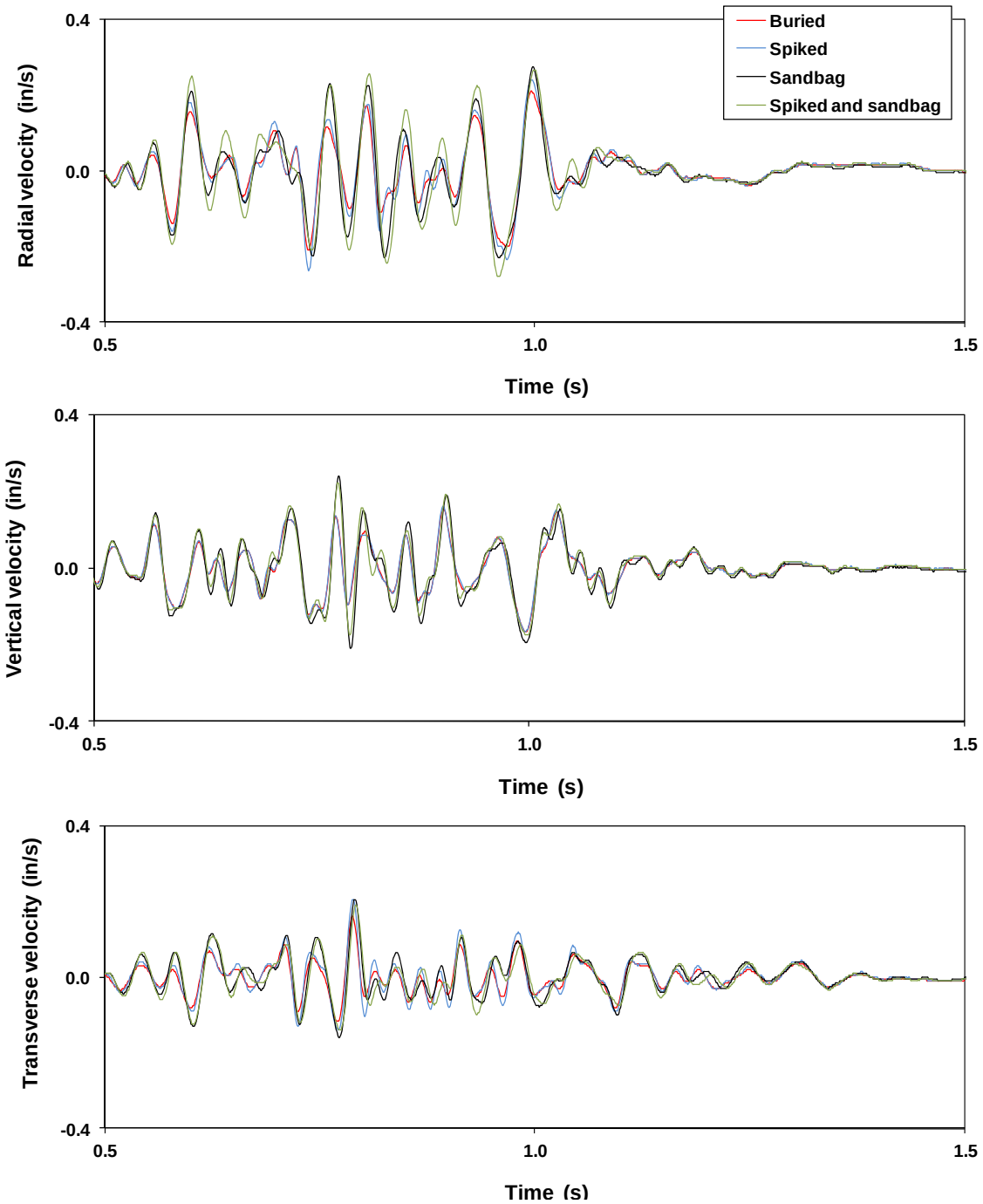

(a)

Figure 33 Component time histories (a) and scatter plots (b) for site KY-8

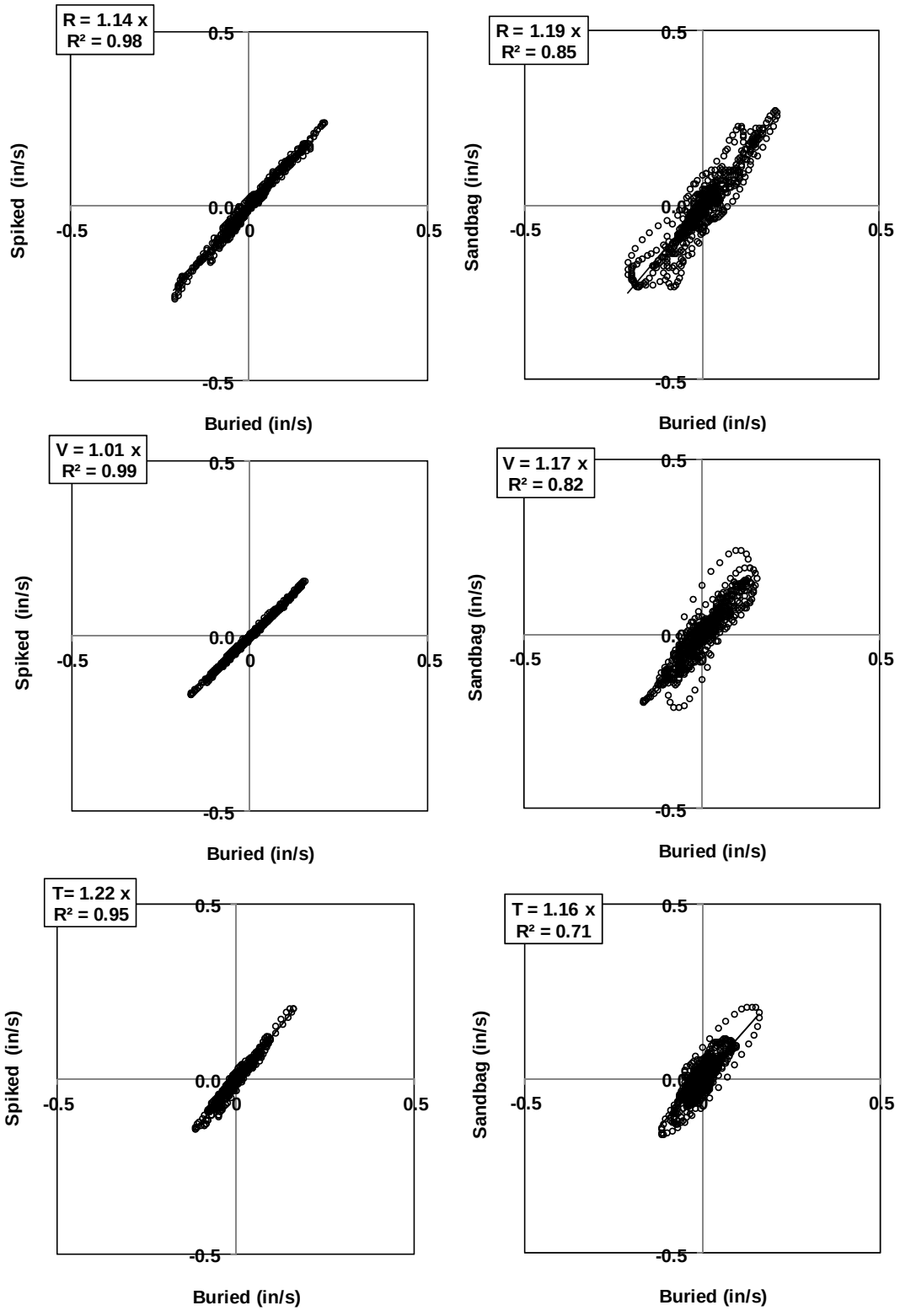

(b)

Figure 33 (cont.) Component time histories (a) and scatter plots (b) for site KY-8

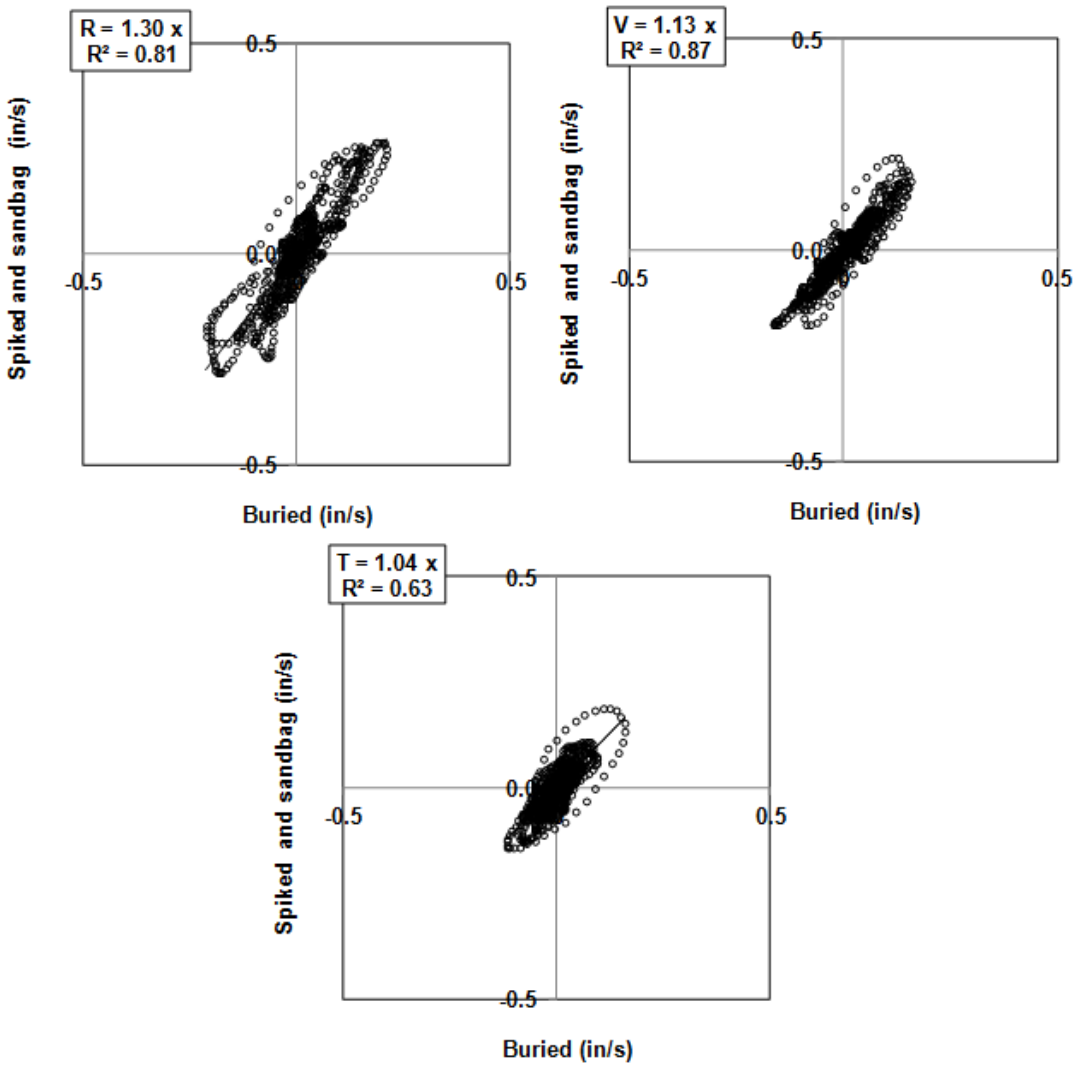

(b)

Figure 33 (cont.) Component time histories (a) and scatter plots (b) for site KY-8

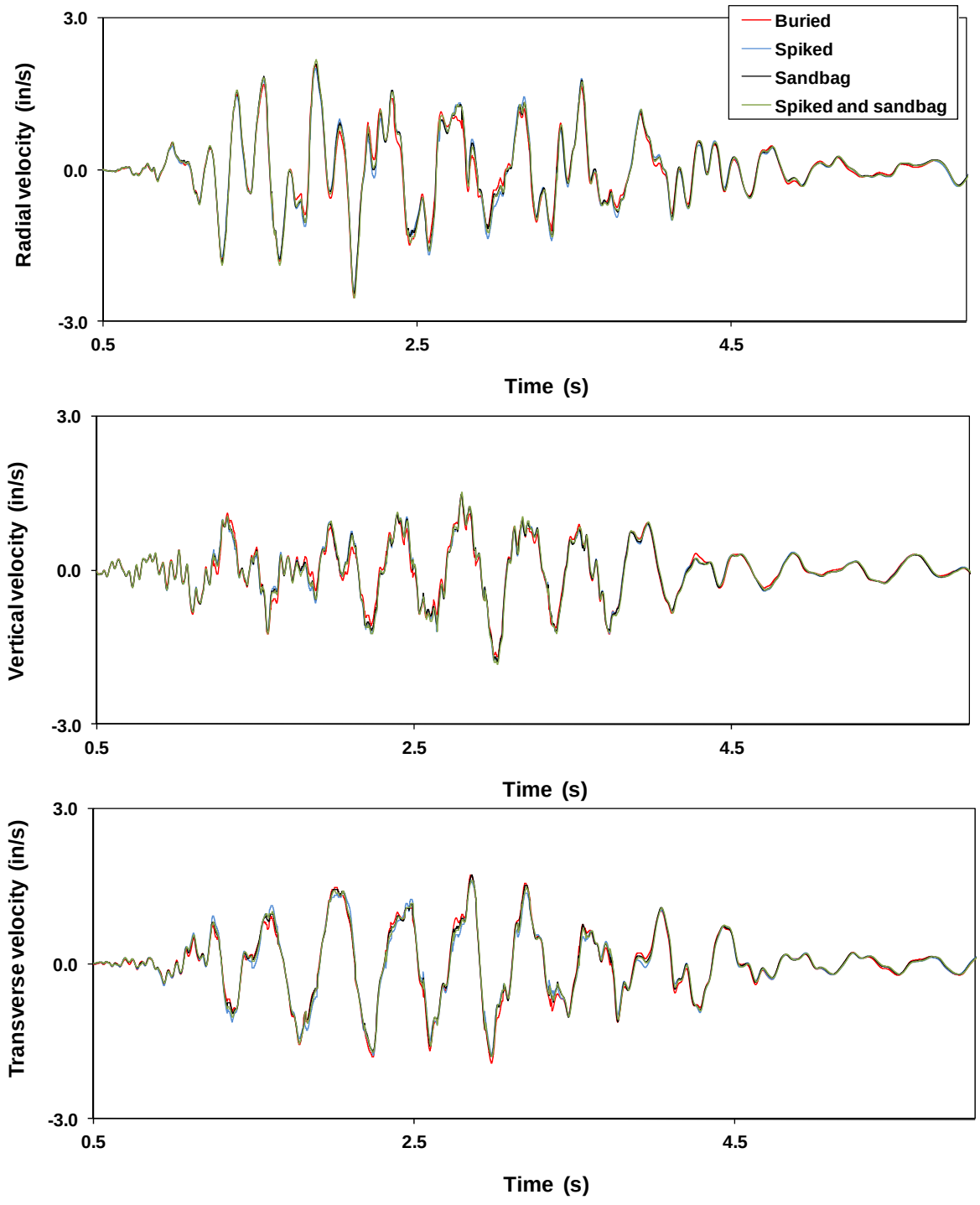

(a)

Figure 34 Component time histories (a) and scatter plots (b) for site WY-5

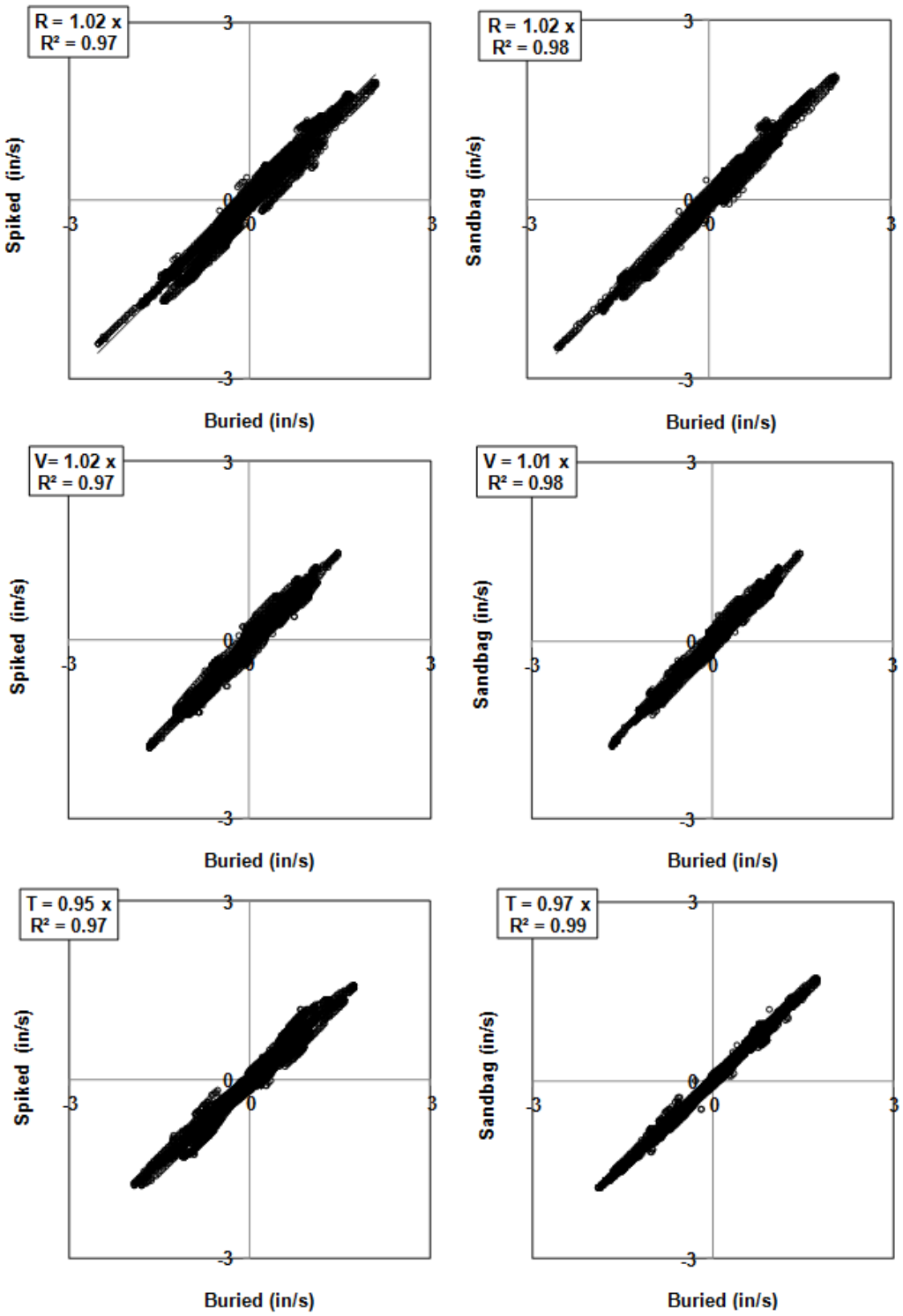

(b)

Figure 34 (cont.) Component time histories (a) and scatter plots (b) for site WY-5

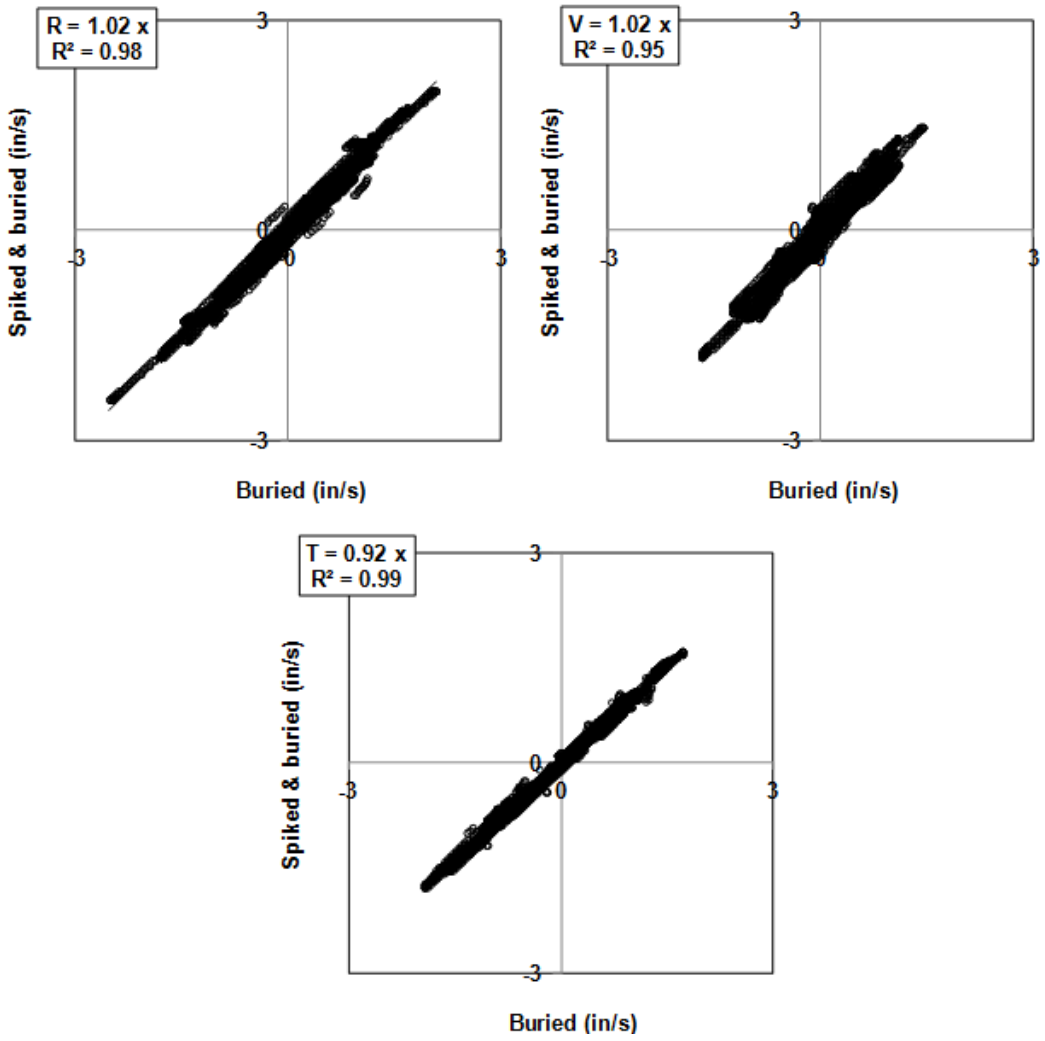

(b)

Figure 34 (cont.) Component time histories (a) and scatter plots (b) for site WY-5

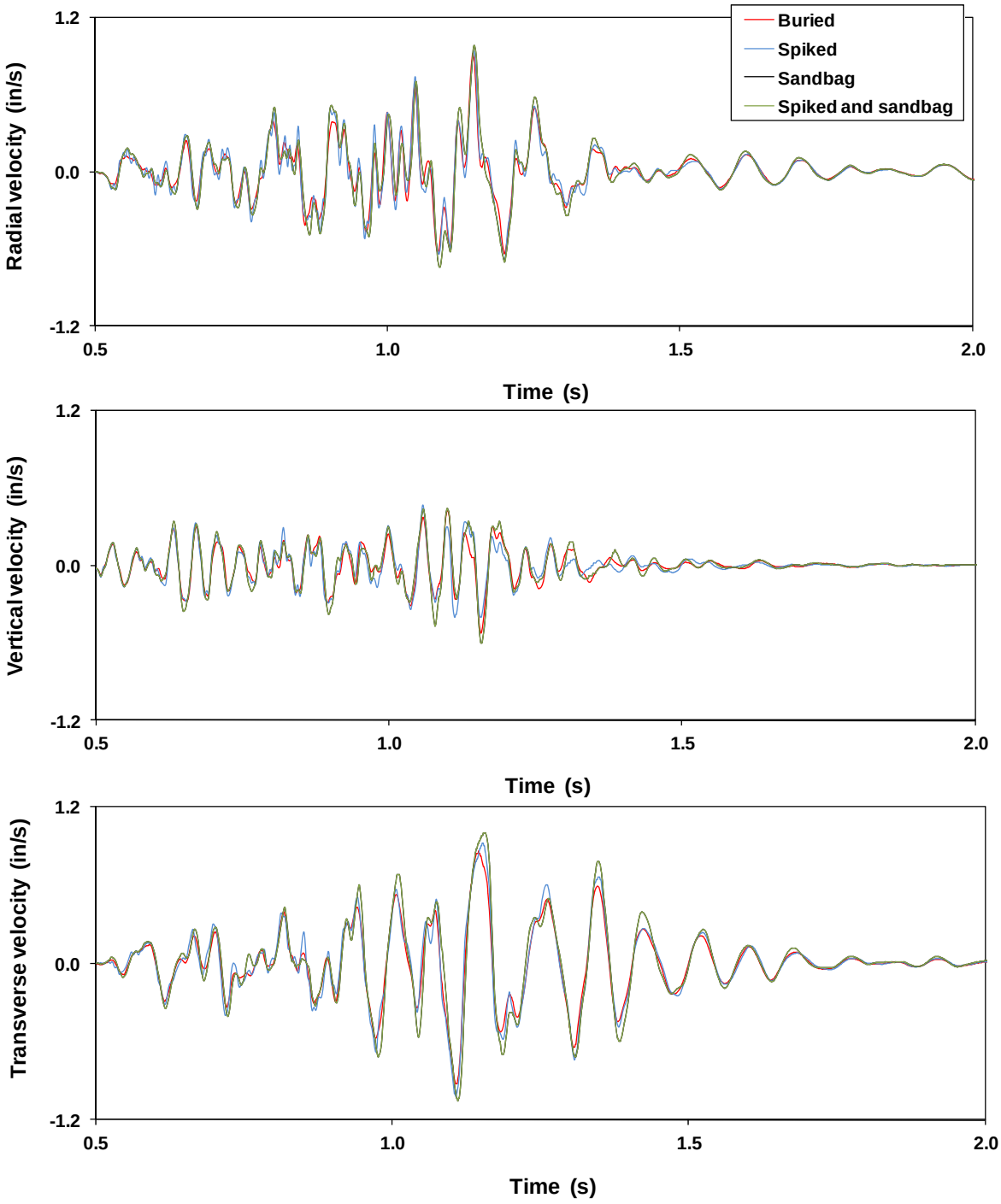

(a)

Figure 35 Component time histories (a) and scatter plots (b) for site OH-1

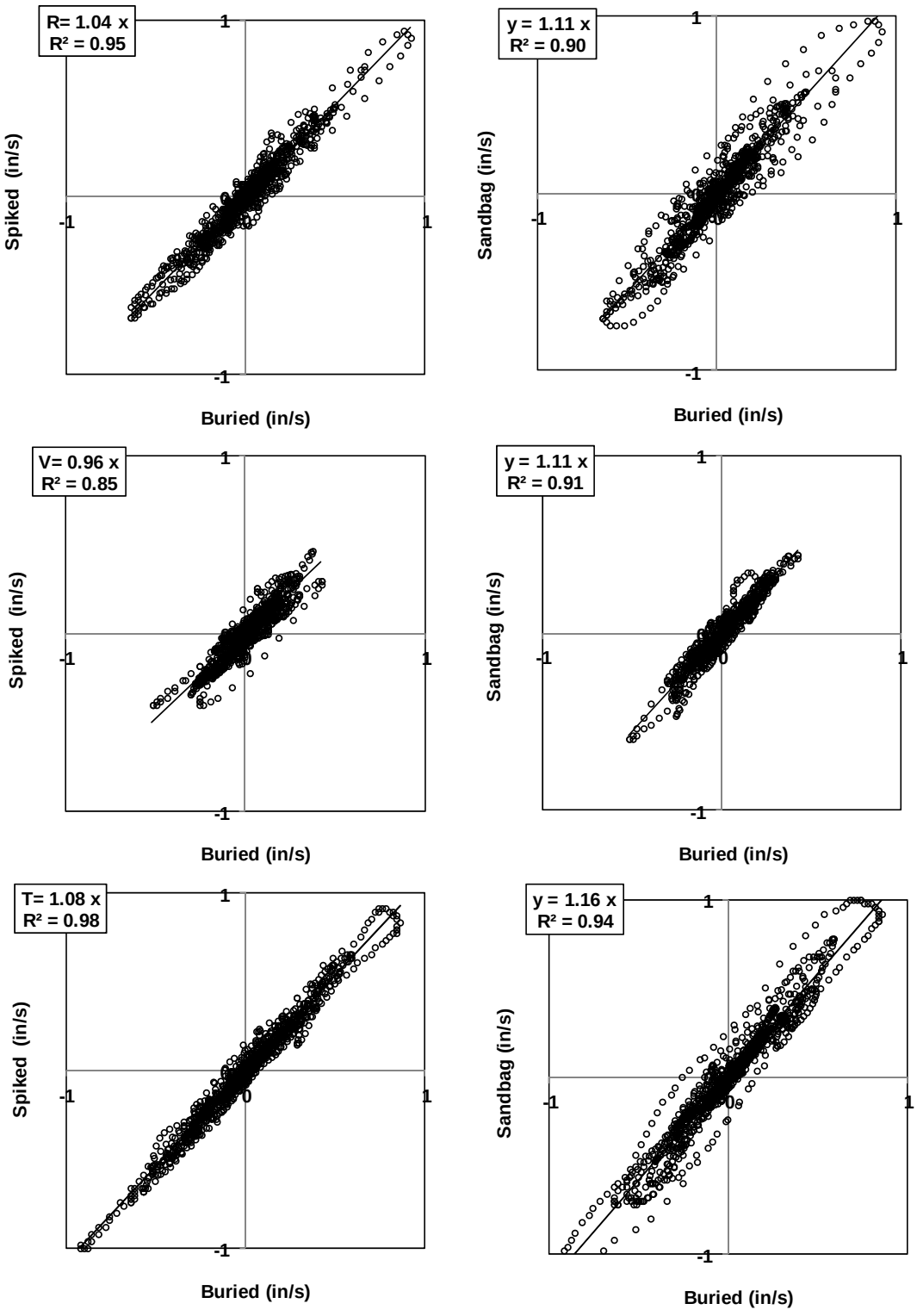

(b)

Figure 35 (cont.) Component time histories (a) and scatter plots (b) for site OH-1

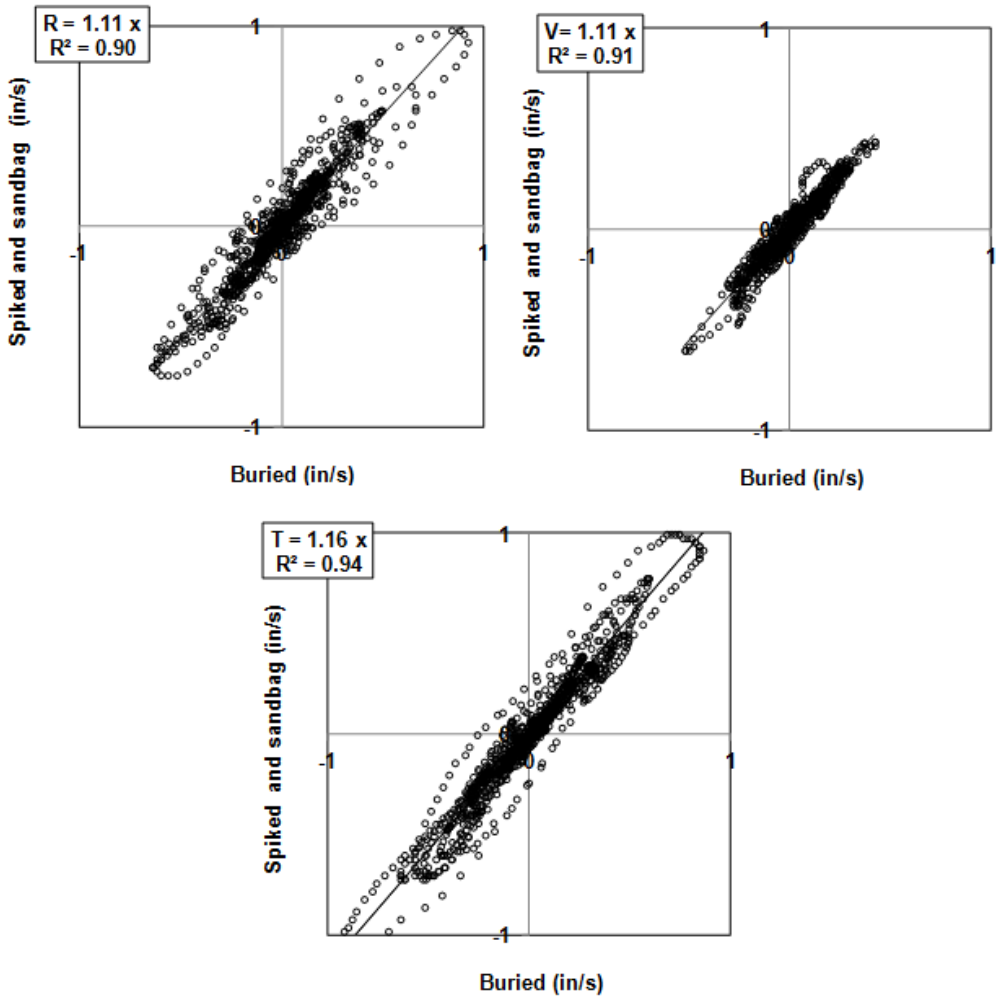

(b)

Figure 35 (cont.) Component time histories (a) and scatter plots (b) for site OH-1

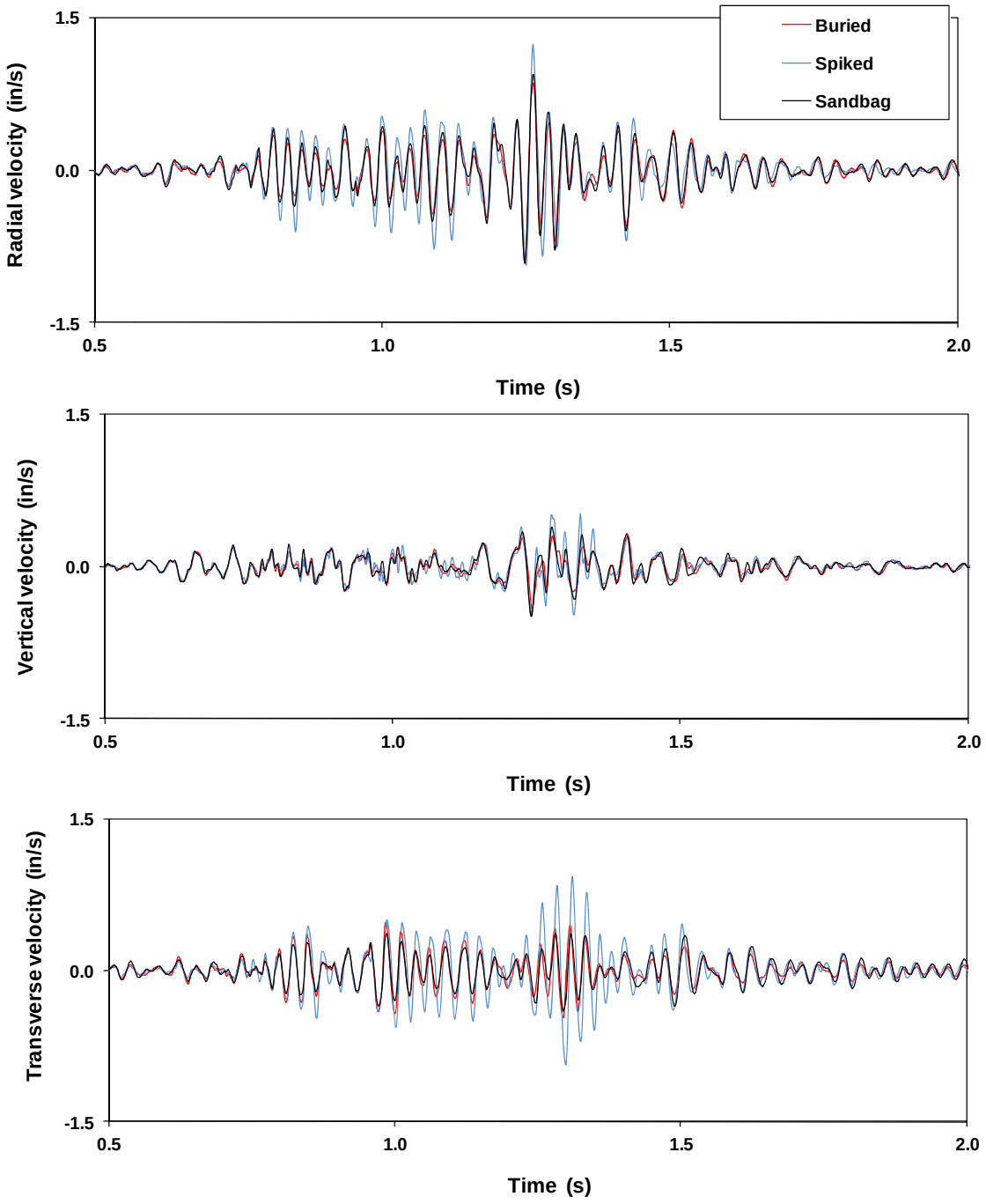

(a)

Figure 36 Component time histories (a) and scatter plots (b) for site NM-7

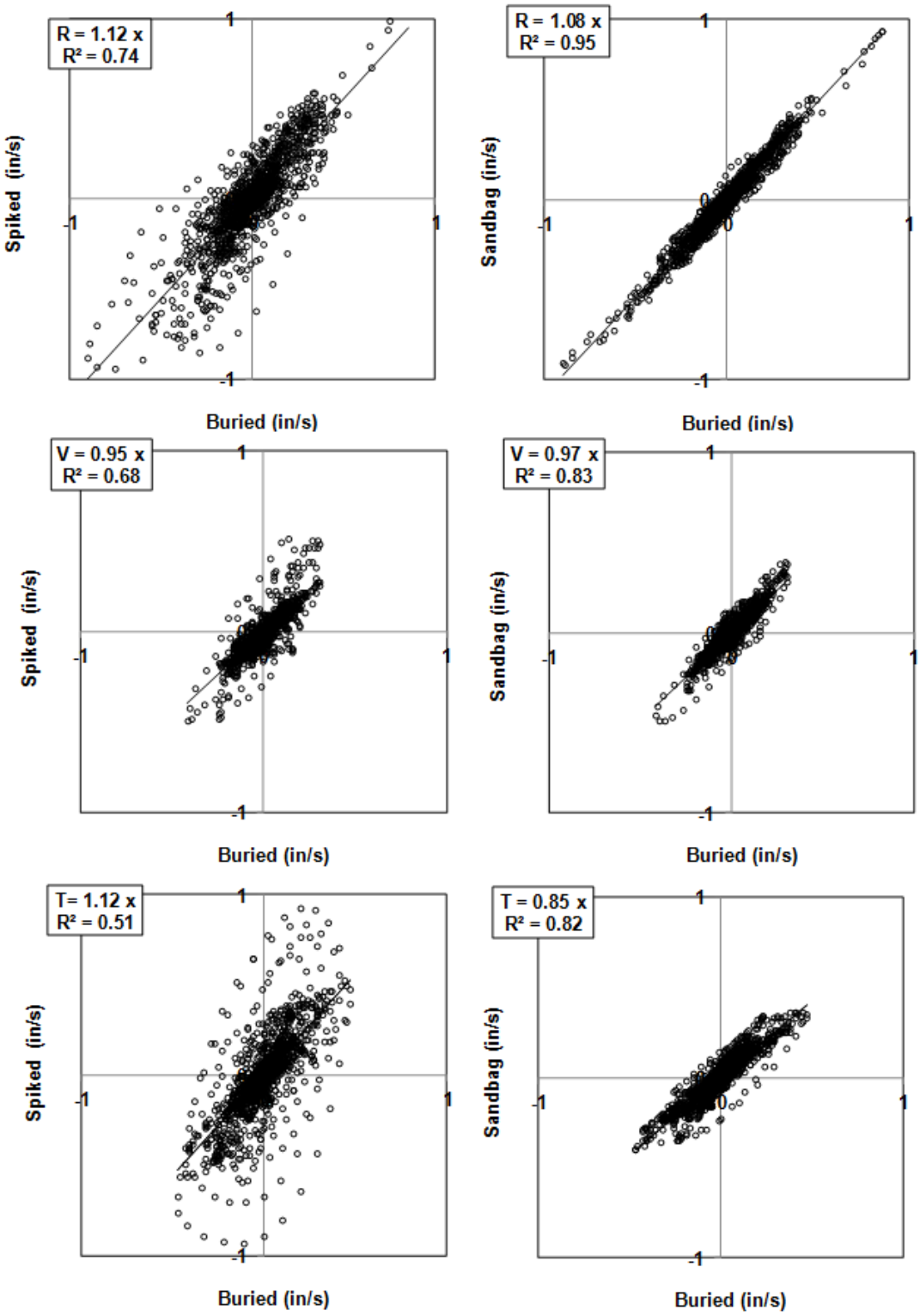

(b)

Figure 36 (cont.) Component time histories (a) and scatter plots (b) for site NM-7 as indicated by the slope.

Scatter plots given in Figure 31(b) indicate little or no correlation between the horizontal components of the buried sensor and surface mounted attachments. The only fair correlation that exists is the V component between buried and spiked sensors. It appears that all surface mounted sensors may have decoupled for blast site IL-1.

Time-histories for high velocity amplitude and moderate frequency site WV-2 are shown in Figure 32(a). Peak times are slightly offset for the T component while the R and V peak time tend to agree. Data in Appendix C suggest little or no decoupling with respect to PPV with less than 5% difference in PPV among all four methods. There is a 33% increase in peak frequency for sensors with spikes over the buried sensor.

The higher frequencies for the spiked sensors (spiked alone and spiked with a sandbag) is apparent in the scatter plots in Figure 32(b) with low data correlation and low slope showing reduced amplitude for surface mounted sensor relative to the buried sensor. This is most evident in the T component.

A good correlation exists between time-history scatter plot data for a sensor with the use of a sandbag and the buried sensor with only minor variations in peak amplitudes.

Time histories for KY-8 are given in Figure 33(a). Data in Appendix C suggest this is a low velocity amplitude and moderate frequency site with frequencies similar to WV-2 and all PPVs resided in the R component. While the peak times of time-histories appears to agree, there is uniform 33% increase in peak component velocities for all three surface mounted sensors relative to the buried sensor. The peak frequency for the spiked sensor was 77% greater than for the buried sensor while the use of a sandbag increase the peak buried 23%. The use of spikes and a sandbag did not change the frequency compared with burial.

Scatter plots in Figure 33(b) indicate good time-motion agreement between the spiked and buried sensors with more random correlation of the sensor with sandbags. In this case, the behavior of data for the sensor with a sandbag alone and with combined spikes and sandbag are nearly identical indicating the influence of the use of sandbags when ground motions amplitude are low and peak frequencies around 13 Hz.

Low frequency high amplitude site WY-5 shown in Figure 34(a) exhibited high visual time-history agreement between the buried sensor and all surface mounts with little PPV amplifications. As such, high correlations are shown in the scatter plots in Figure 34(b). All PPVs resided in the R component. The use of a sandbag and spiked alone tended to lower the PPV by a maximum of 6% from the buried sensor PPV. Peak frequencies were identical and a 14% increase in computed acceleration for the spiked sensor over the buried sensor.

Quarry blast site OH-1, shown in Figure 35(a), is a low to moderate frequency and moderate PPV site. The use of a sandbag alone increase PPV and peak frequency over the buried sensor by 15% and 54%, respectively. Acceleration values agree among coupling methods.

Scatter plots in Figure 35(b) show agreement between buried and spiked sensors with slight enhancement in peak amplitudes for sensors mounted with sandbags.

Site NM-7 represents horizontal high, uniform frequency (above 32 Hz) and high amplitude construction blast shown in Figure 35(a). A sensor with combined spikes and sandbag was not used at this site. All PPV values resided in the R component. Time histories show spiked sensor peak enhancements chiefly in the T component with a slight time lag in the peaks.

Data in Appendix C indicate that he spiked sensor was most affected by the ground motion frequency content with PPV and acceleration increases of 38% and 32%, respectively. In this case, coupling methods did not influence peak frequency amplitudes.

The lack of correlation for spiked sensor peaks relative to the buried sensor is shown in the scatter plots of Figure 35(b), The peak amplitude differences between sensors covered with a sandbag and buried are fairly uniform.

From the previous analysis and assessment of the entire data base for 25 sites, the following observations are made:

- Twenty-five sites were grouped based on peak frequency for the buried sensor to compute the enhancement of spiked sensor PPV as a percentage of PPV for the buried sensor. The average and standard deviation were computed for each group based on frequencies up to 9 Hz, between 9 and 13 Hz, and above 13 Hz. These ranged provided the lowest standard deviation when considering all 25 sites for comparison.

- Eight sites with PPV amplitudes greater than 0.1 in/s and up to 2.52 in/s with moderate frequencies above 13 Hz affect the performance of spiked sensors that can enhance the PPV by 22.6% $\pm$ 14% (average of eight sites).

- The use of sandbags for the same site frequency range can enhance the PPV over burial by 27% $\pm$ 29.3%. The effects of adding spikes with the use of a sandbag were similar to the performance of a sandbag alone. The high standard deviation indicated highly random data and overall poor performance to ensure geophone coupling.

- Ten sites with low frequencies below 9 Hz with PPVs that range from 0.07 to 1.36 in/s, the increase in spiked PPV over buried PPV averaged 5.9% $\pm$ 5.1%. Using a sandbag, the average was 8.3% $\pm$ 7.6%

- The increase in PPV using a spiked sensor for seven sites with peak frequencies between 9 and 13 Hz was 9.4% $\pm$ 5.3% and for the use of a sandbag it was 8.2% $\pm$ 7.3%.

- When the same analysis was applied to the data set based on acceleration, there were no clear trends in acceleration enhancements for sensors with either spikes or sandbags relative to buried sensors.

- When buried sensor accelerations fell below and above 0.2 g's (the ISEE recommendations for spiking) the average and standard deviation for acceleration differences between spiked and buried sensor accelerations were 23.4% ±19.2% (11 sites with buried sensors <0.2 g's) and 15.1% ±9.0% (14 sites with buried sensor > 0.2 g's). The demarcation of 0.2 g's provided the lowest standard deviations for spiked sensors.

- For the same analysis, comparing sensors deployed using sandbags with sensors that were buried, the standard deviations were greater than the average values of the acceleration differences and no conclusions can be made.

- Similar numbers were computed when using 0.1 g's and 0.3 g's to divide the data set resulting in more standard deviation scatter.

- In summary, assessments of geophone performance based on coupling methods cannot be reliably performed based on the highly random nature of the all data sets that include potential outliers.

4.3.5 Coupling performance based on Combined Relative Standard Error

Error analysis was used to identify blasts for which specific coupling methods may indicate a possible outlier using error bounds computed as the combined relative standard error (RSE from Table 4). This was performed by using relative PPV or the ratio of PPV for two coupling methods. PPV was used because this attribute has the most significance for regulatory compliance where structure damage criteria are specified in terms of in-ground peak particle velocity (PPV).

Relative PPV was plotted by blast site as a function of increasing values of buried sensor PPV frequency. In this manner, the influence of ground motions frequencies on possible decoupling are readily be observed.

RSE bounds in the form of horizontal lines associated with each attachment method were placed above and below relative PPV = 1. In this manner, ratios outside the error bounds can be identified as possibly decoupled. As an example, the use of sandbags on the surface yielded a combined RSE of ± 10.15%. Therefore, a ratio of sandbag PPV to buried PPV ranging from -0.8985 to +1.1015 is within the expected error for human deployment and manufacture and calibration while outside these bounds, decoupling may be possible.

The first set of comparisons was performed for buried, spiked, and combined spiked and buried sensors. In the second set, PPVs of three common surface attachments (spiked, sandbag, and combined spiked and sandbag) were normalized with the PPV

response of the buried sensor in the same cluster. These comparisons assumed that the buried sensor provided a basis of coupling. Therefore, relative PPV was defined as the PPV of the surface attachment methods divided by the PPV of the buried sensor for the same cluster.

a. Spiked, buried and combine spiked and buried sensors

The effects of spiking, burial, and combined spiking and burial were investigated at eight sites. Vibration data are given in Table 10.

Figure 37 compares the three methods in terms of PPV ratios in which the denominator is presumed to be the method providing the better coupling to ground motions. These ratios are given in the legend. Error bounds are shown with blue dashed lines on either side of relative PPV = 1. In each plot, the RSE bounds for spiked sensors, $\pm$4.74%, was used and blast sites are arranged in increasing buried geophone peak frequency from left to right. In this manner the effect of increasing frequency can be observed.

Linear regression plots in Figure 30 indicated decoupled sensor at blast sites WY-4, IL-1, KY-4, and KY-5 based on comparisons of PPV and peak frequency. Figure 35 shows similar relative PPV amplifications for spiking when compared with burial for the same sites.

Table 10 Data used for relative PPV using three coupling methods (blast sites shown in order of buried geophone peak frequency from low to high values)

		Spiked and buried			Buried			Spiked		
Site ID	Scaled Distance	Peak particle velocity	Peak frequency	Acceleration	Peak particle velocity	Peak frequency	Acceleration	Peak particle velocity	Peak frequency	Acceleration
	(ft/lb$^{1/2}$)	(in/s)	(Hz)	(g's)	(in/s)	(Hz)	(g's)	(in/s)	(Hz)	(g's)
WY-3	51.3	0.22	2.4	0.03	0.23	2.4	0.03	0.21	2.4	0.01
WY-5	12.9	2.40	4.2	0.52	2.52	4.3	0.49	2.40	4.3	0.56
WY-4	9.7	1.56	6.8	0.30	1.40	7.2	0.28	1.64	6.8	0.30
KY-4	134.2	0.78	7.4	0.23	0.78	7.4	0.29	0.84	64.0	0.88
IN-1	23.6	0.58	5.8	0.15	0.59	7.4	0.13	0.65	7.6	0.24
IL-2	116.2	0.07	18.2	0.03	0.07	18.2	0.03	0.09	20.4	0.03
KY-5	51.5	0.74	22.2	0.27	0.74	21.3	0.27	1.08	42.6	0.81
IL-1	19.4	1.14	21.3	0.44	1.22	30.1	0.62	1.62	15.0	0.85

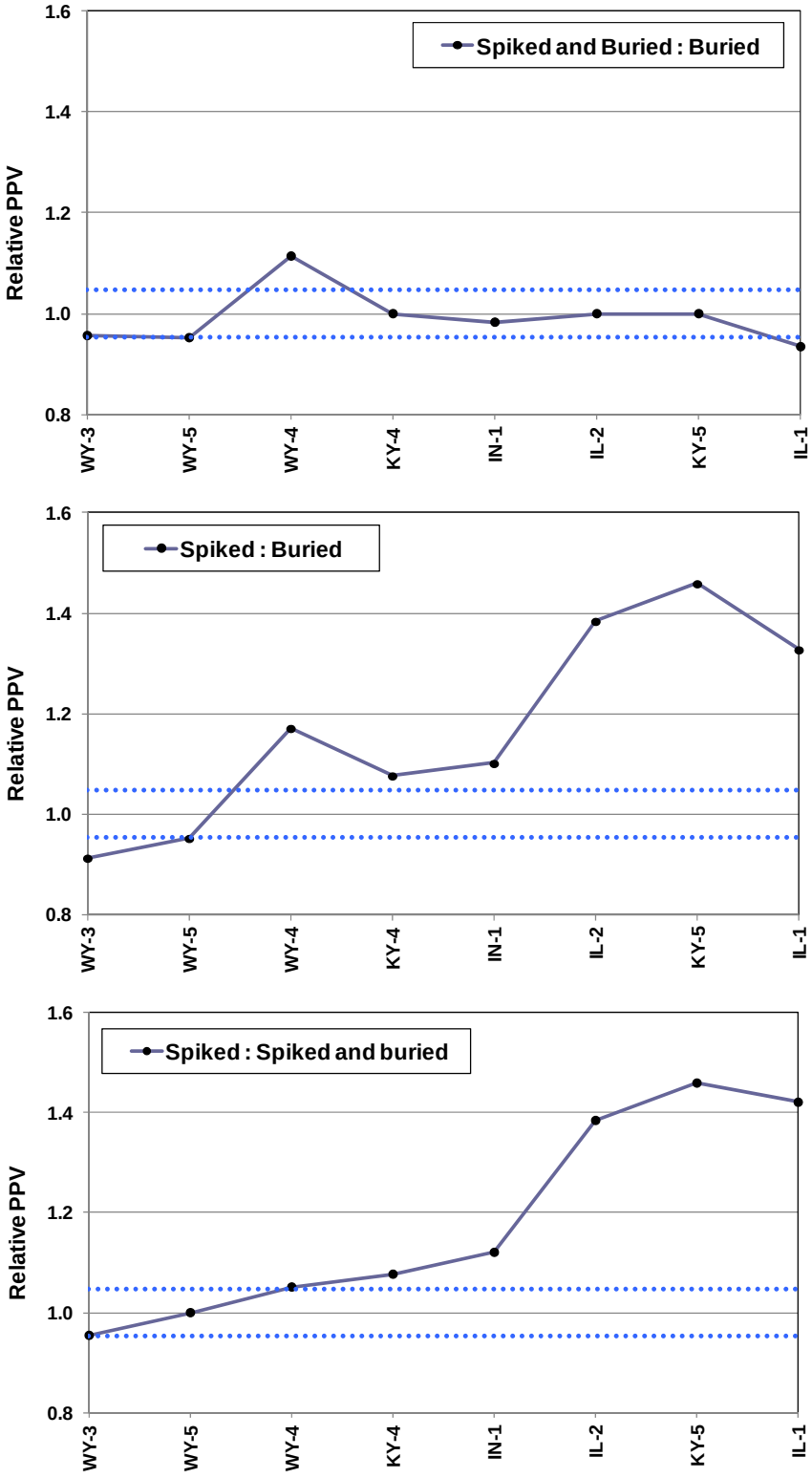

Figure 37 Relative PPV by blast site increasing in buried sensor peak frequency (left to right) for three coupling ratios

Combined spiked and buried sensors relative to buried sensors showed the lowest potential for decoupling at all sites tested with the exception of site WY-4 (Figure 37, top, where the ratio plots outside the error bounds). The lack of data outside the RSE error bound suggests spikes are not necessary when burying sensors as they do not provide any additional coupling benefit. The spiked sensors (both combined with burial and spiked on the surface) at siteWY-4 showed indications of decoupling relative to the buried sensor based on the high peak velocity (2.52 in/s), very low frequency (4.3 Hz) for the buried sensor.

The plots of relative PPV for spiking (middle and bottom plots) are similar indicating decoupling "agreement". The bottom plot was not used to detect decoupling but rather to verify the buried sensor and spiked and buried sensor behaved in a similar manner.

The response of combined spiked and buried sensors relative to that for the buried sensor at blasts sites IL-1, IL-2, and KY-5 (and possibly KY-4 and IN-1) are similarly decoupled. With the exceptions of IL-2 and IN-1, the most likely reason for decoupling is the high ground acceleration over 0.2 g's noted for the buried sensor response at sites KY-4, KY-5, and IL-1. This produced amplified spike sensor accelerations over 0.8 g's at these sites. However the PPV differences for KY-4 does not support decoupling of the spiked sensor as discussed below.

Both the IL and KY blasts represent two consecutive shots with sensors in each cluster remaining in place (e.g., only deployed once). At the IL site, the spiked sensors appeared decoupled for both blasts based on the velocity amplitude difference. For site IL-1, the spiked sensor peak was 33% greater than the buried sensor peak whereas for shot IL-2, the difference was 29%, although the velocity and acceleration amplitudes were extremely low. Using PPV ratios alone to determine decoupling may not tell the entire story for moderately high frequency response when accelerations are low.

On the other hand, the spiked sensor for KY-5 appears decoupled while decoupling is not as evident in Figure 35 for KY-4 (a pre-split shot). This is because the PPV differences are small (8%) while differences in accelerations and frequencies are large most likely due to the spiked sensor response to fast delays used for the pre-split shot.

From the above analysis, the following observations are evident:

- For buried sensor frequencies > 20 Hz (KY-5 and IL-1), spiked sensors clearly showed decoupling.

- The decoupling implications at high ground velocities are observed in Figure 38 in which the use of the spiked sensor resulted in a non-compliant measurement using the Office of Surface Mining (OSM) upper limit to PPV.

- The concept of relative PPV, although useful to assess decoupling, indicates IL-2 spiked sensor may be decoupled. This conclusion may be supported based on low ground motion accelerations.

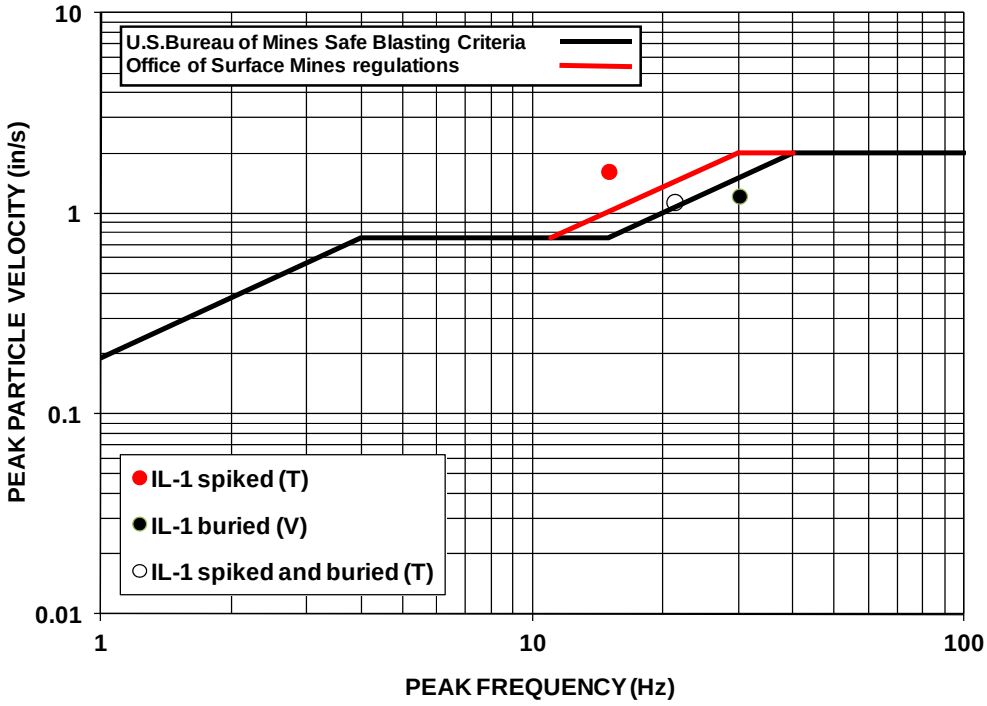

Figure 38 Peak particle velocity (PPV) versus frequency at the PPV showing data plotted for three coupling methods at blast IL-1

- The use of spikes when burying sensors does not appear to have any advantage over a well-coupling buried sensor without spikes.

b. Spiked, sandbag, buried, and combine spiked and sandbag sensors

The use of spiking, burial, sandbag placed on a surface-mounted sensor and combined spiking and sandbag were investigated at 25 sites. Vibration data are given in Table 11 by blast site listed by increasing buried sensor peak frequency.

Figure 39 shows plots of relative PPV for three methods of surface attachments normalized with buried geophone response. OH-2 and WY-4, both low frequencies, high velocity sites, show some decoupling of the sandbag and spiked and sandbag sensors. At higher peak frequencies, KY-6 and KY-8 show decoupling of all surface attachment methods. As previously noted, spiked sensors are decoupled at sites IL-1 and IL-2. However the use of sandbags with and without spiking also exhibited significant decoupling. Sites KY-2 and OH-6 showed evidence of possible decoupling for the combined spiked and sandbag sensor while decoupling is questionable with eh use of sandbag and spiking alone.

Table 11 Data used for relative PPV using four coupling methods (blast sites shown in order of buried geophone peak frequency from low to high values)

		Buried			Spiked and sandbag			Spiked			Sandbag		
Site ID	Scaled Distance	Peak particle velocity	Peak frequency	Acceleration	Peak particle velocity	Peak frequency	Acceleration	Peak particle velocity	Peak frequency	Acceleration	Peak particle velocity	Peak frequency	Acceleration
	($ft/lb^{1/2}$)	(in/s)	(Hz)	(g)	(in/s)	(Hz)	(g)	(in/s)	(Hz)	(g)	(in/s)	(Hz)	(g)
WY-3	51.3	0.23	2.4	0.03	0.22	2.4	0.03	0.21	2.4	0.01	0.20	2.4	0.03
WY-2	29.1	0.38	2.9	0.04	0.38	2.8	0.04	0.38	2.8	0.05	0.38	2.9	0.05
WY-5	12.9	2.52	4.3	0.49	2.52	4.4	0.53	2.40	4.3	0.56	2.44	4.4	0.53
WV-1	22.5	0.22	6.0	0.04	0.22	5.9	0.04	0.22	5.8	0.04	0.23	6.2	0.04
OH-2	26.8	0.66	6.2	0.19	0.78	6.2	0.22	0.68	6.3	0.19	0.80	6.1	0.21
WV-3	21.0	0.10	6.9	0.02	0.09	6.2	0.01	0.09	6.4	0.03	0.09	6.4	0.01
WY-4	9.7	1.40	7.2	0.28	1.60	6.6	0.29	1.64	6.8	0.30	1.68	6.7	0.32
IN-1	23.6	0.59	7.4	0.08	0.60	6.0	0.21	0.65	7.6	0.24	0.60	8.5	0.17
WY-1	16.8	2.12	7.5	0.30	2.20	7.6	0.33	2.20	7.3	0.27	2.24	7.5	0.27
OH-3	30.8	0.98	7.8	0.25	0.88	10.4	0.24	0.92	15.0	0.26	1.08	15.0	0.28
OH-1	22.4	0.92	8.5	0.29	1.00	12.4	0.33	1.00	12.4	0.33	1.06	13.1	0.33
KY-2	49	0.49	9.3	0.23	0.56	15.0	0.27	0.54	14.6	0.41	0.57	10.2	0.25
OH-6	13.1	0.90	9.3	0.20	1.05	9.4	0.25	1.06	9.3	0.25	1.02	9.6	0.24
KY-7	28.6	0.78	9.4	0.13	0.78	9.4	0.14	0.82	9.4	0.13	0.78	10	0.13
NM-4	14.4	1.40	12.1	0.58	1.44	13.1	0.66	1.62	22.2	0.82	1.38	21.3	0.74
WV-2	26.9	1.26	12.4	0.57	1.32	16.5	0.51	1.30	16.5	0.49	1.26	13.4	0.59
NM-5	29.1	0.27	12.8	0.10	0.30	8.1	0.13	0.30	13.1	0.07	0.30	8.2	0.13
KY-6	33.8	0.26	13.1	0.05	0.32	12.4	0.07	0.31	12.4	0.07	0.32	13.4	0.07
KY-8	27.3	0.21	13.1	0.08	0.28	13.4	0.11	0.27	23.2	0.11	0.28	16.0	0.10
OH-4	24.5	0.66	16.0	0.21	0.76	21.3	0.34	0.64	16.5	0.32	0.68	14.6	0.27
OH-5	16.4	1.36	16.5	0.33	1.48	16.5	0.45	1.40	17.0	0.72	1.32	17.0	0.41
IL-2	116.2	0.07	18.2	0.03	0.12	20.4	0.05	0.09	20.4	0.03	0.12	20.4	0.05
KY-1	52.9	0.52	19.6	0.25	0.54	36.5	0.25	0.62	21.3	0.40	0.58	30.1	0.29
IL-1	19.4	1.22	30.1	0.62	1.80	13.1	0.53	1.62	15.0	0.85	1.88	11.6	0.45
NM-7	40.8	0.90	34.1	0.56				1.24	32.0	0.74	0.94	34.1	0.57

(note: a combined sandbag and spiked sensor was not used at site NM-7)

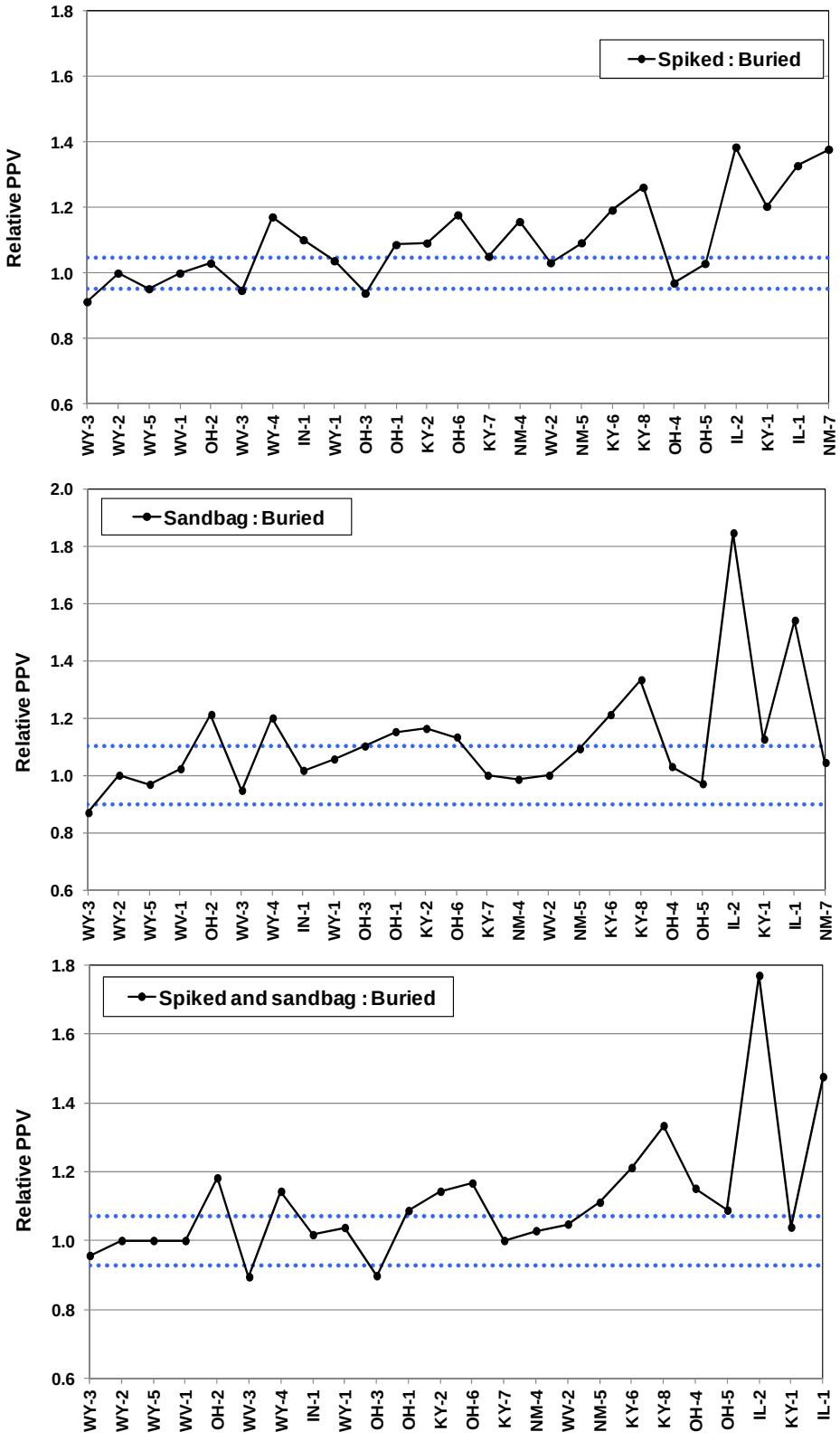

Figure 39 Relative PPV by blast site increasing in buried sensor peak frequency (left to right) for three surface attachment methods relative to geophone burial

The following observations are evident from the data plotted in Figure 39:

- The trend in relative PPV with blast site arranged in increasing peak frequency associates with the buried sensor suggests there may be a dependency of decoupling on frequency as shown in Figure 37.

- The trend in relative PPV for the use of sandbags is similar to the trend for combined sandbag and spiking suggesting that spiking does not contribute any added benefits to coupling when using sandbags.

c. Influence of ground acceleration and frequency on the likelihood of decoupling

From the previous analysis, there appears to be a correlation between ground motion frequency and the likelihood of geophone decoupling. ISEE recommendations for geophone ground attachment are based on acceleration. While acceleration is a good criteria, it is affected by both vibration amplitude and frequency. Since buried sensor PPV is used to normalize and compare all other coupled sensor PPVs, then frequency may represent a more fundamental attribute on which to judge decoupling rather than acceleration which is a derivative of velocity and frequency.

Buried geophone peak accelerations and peak frequencies are plotted in Figures 40 and 41, respectively, against blast site ID in increasing amplitudes of the two attributes. In each plot, sites with geophones showing possible decoupling are highlighted in red. Decoupling was suspect for one, two, or three deployment methods in a cluster representing spiking, sandbag, and combined spiking and sandbag.

The use of an attribute to set a criteria for coupling recommendations can be compared by assessing which attribute better demarks or separates sensors that are well-coupled from those that are not.

The 0.2 g's ISEE criteria is shown in Figure 40. Eight out of 15 blasts in which buried sensor accelerations were close to or above 0.2 g's resulted in possible decoupling. The remaining seven blasts did not exhibit decoupling. The utility of the 0.2 g's limit was effective for 53% of the blasts.

Four blasts exhibited sensor decoupling when buried sensor peak accelerations fell below 0.2 g's. This observation shows that decoupling may exist even at very low ground accelerations as low as 0.02 g's. Therefore, the burial of geophones should be exercised at all times.

Figure 41 make use of peak frequency at the PPV for the buried sensor to correlate with observed decoupled sensors. When the buried peak frequency was greater than 9 Hz, a total of 11 sites (79%) exhibited possible decoupling while 3 sites did not. Two sites showed possible decoupling when the peak frequency fell below 9 Hz. Below 13 Hz,

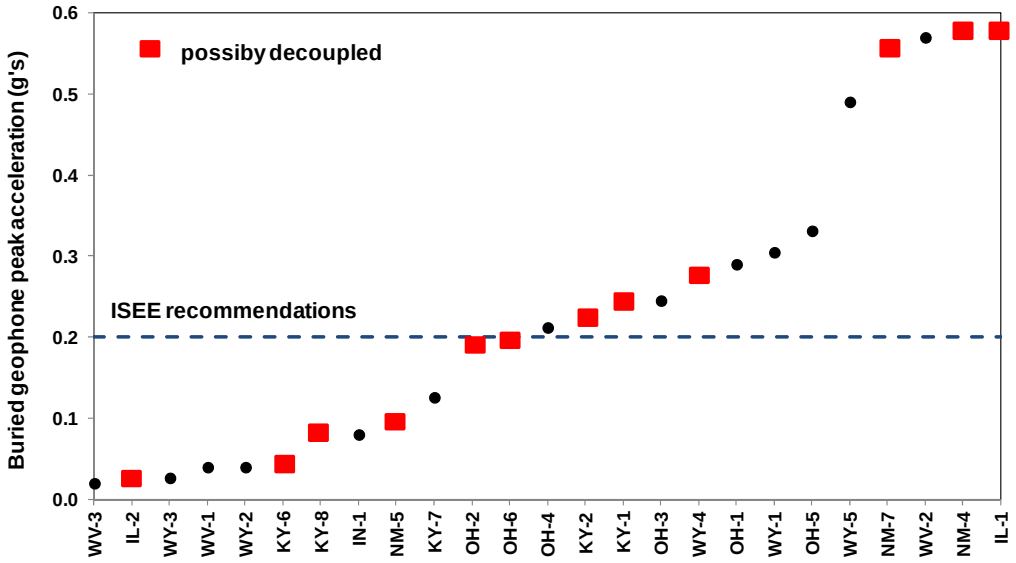

Figure 40 Buried geophone peak acceleration versus blast site showing sites with possible decoupled sensors for spiked, sandbag and combined spiked and sandbag; ISEE recommendation for attachment is shown as a horizontal dashed line at 0.2 g's

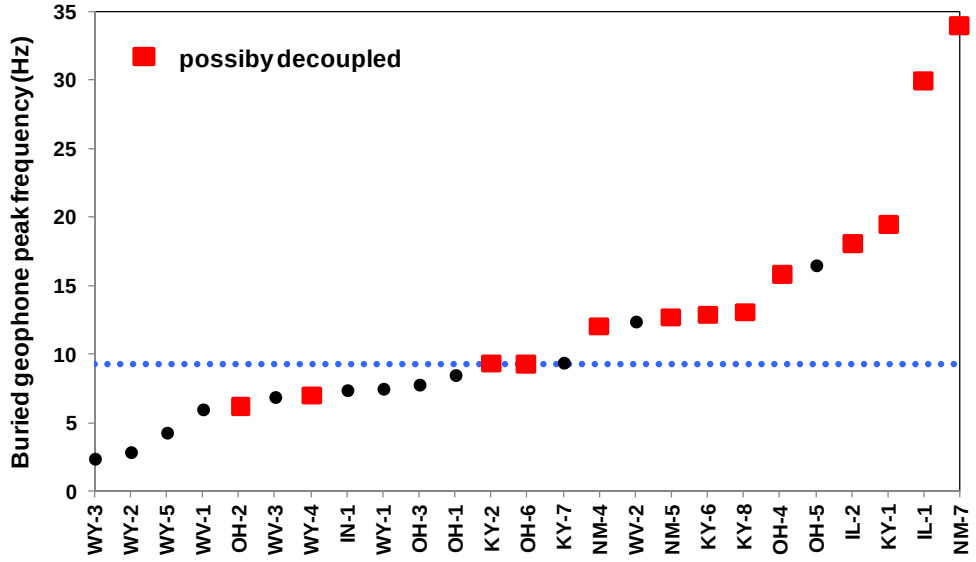

Figure 41 Buried geophone peak frequency versus blast site showing sites with possible decoupled sensors for spiked, sandbag and combined spiked and sandbag at buried frequency of 9 Hz or greater

decoupling was suspect for spiked sensors while above 13 Hz, the use of sandbags and spikes produced possible decoupling.

Comparison of Figure 40 and 41 suggests peak ground motion frequency may be a good indicator of decoupling and therefore frequency may be used as a possible basis of recommendations for attachment methods.

The use of sandbags when ground motion PPV is expected to be over 0.2 in/s with a peak expected frequency over 13 Hz should be discouraged. Spiked sensors may not be appropriate at peak frequencies above 9 Hz.

To emphasize the possible dependence of frequency on decoupling, relative PPV ratios for spiked and sandbag sensors were correlated with the predominant site frequency using Fast Fourier Transform, or FFT. The site frequency was computed as the average for all three components of the buried sensors for each cluster. In other words, Fourier spectrum peaks, computed using the seismograph software, were averaged for the R, V, and T components and compared with the relative PPV within the RSE bound for spiked ($\pm$ 4.74%) and sandbag ($\pm$10.15%) sensors. The FFT, or average frequency content over the entire time-history, was used rather than the peak frequency or zero-crossing at the PPV as it better reflects the periodic vibration energy in the ground or the entire time-history.

Figure 42 shows the resulting plot of sandbag and spiked sensors relative PPV for seismographs placed in the same cluster. The data base was expanded to 27 blasts sites to include a total of 70 measurement clusters at a wider range of scaled distances from 9.7 to 204 $ft/lb^{1/2}$.

The data spread in Figure 42 shows a high amount of scatter with evidence of possible decoupling at low frequencies. Trends observed in the data are summarized in Table 12.

Fifty-four percent of the spiked sensor relative PPV fall outside the error bounds with 32.9% and 21.4% falling above and below the RSE bounds, respectively. In general, at frequencies below 9 Hz, it is likely spiked sensors may show lower velocity amplitudes compared with buried sensors. Above 9 Hz, spiked sensor velocities are more likely to record higher readings than buried sensors.

Relative PPV measurements for over two-thirds of the sensors with sandbags fell within the RSE bounds. Very few (5.7%) data fell below the lower bound at 5 Hz and lower while 25.7% fell above the upper error boundary.

Both spiked sensor and sensors with sandbags show nearly the same likelihood of decoupling (21.4% and 25.7%, respectively) above error bounds. However, the magnitude of amplification is higher with sandbags relative to buried PPV than with spiked sensors.

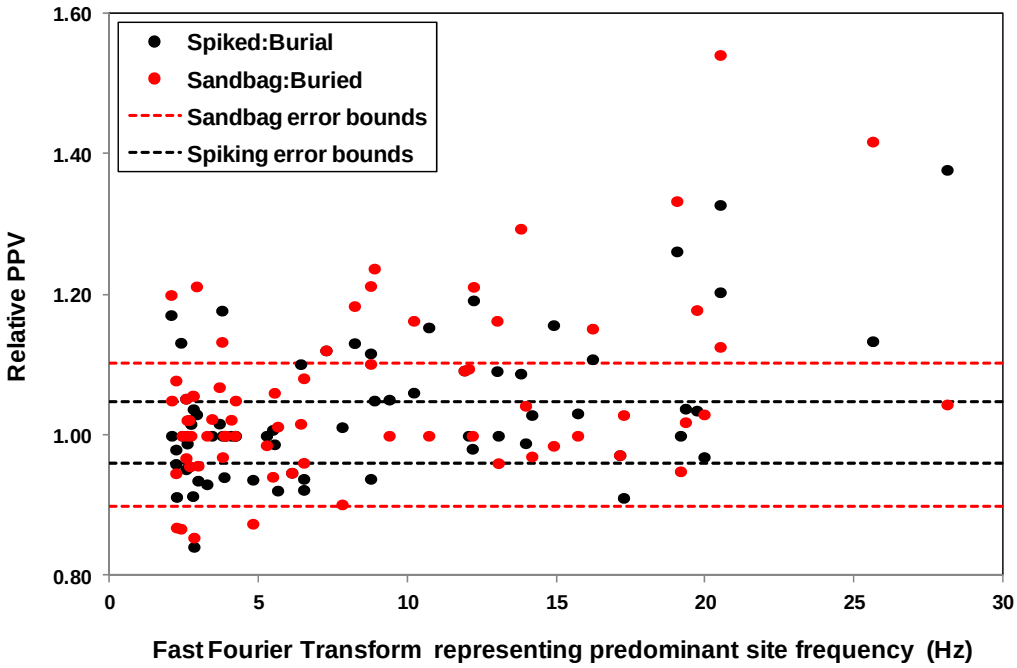

Figure 42 Relative PPV for sandbag to buried and spiked to buried ratios at 70 measurement clusters; RSE bounds for sandbag and spiking are shown

Table 12 Percentage of relative PPV data in Figure 42 that fall within and outside error bounds for spiked and sandbag geophones

Method	Percentage (%)		
	below error bound	above error bound	within error bound
Spiking	21.4	32.9	45.7
Sandbag	5.7	25.7	68.6

4.4 Effects of Soil Characteristics on Spiked and Buried Geophones

Kinney (2009) studied the effects of soil type on characteristic time histories from blasting using various seismograph geophone coupling methods. Soil samples were collected from 15 sites representing 21 blasts for laboratory testing and engineering classification according to the Unified Soils Classification System (USCS). Samples were taken from blast sites in New Mexico, Ohio, Kentucky, and West Virginia, at depths ranging from one to two feet below the ground surface.

The purpose of collecting soil samples was to study the effects different soil characteristics, such as water content and gradation, have on blast wave time-histories. Laboratory test were performed at New Mexico Institute of Mining and Technology and included water content (ASTM D2216), sieve analysis (ASTM D6913), hydrometer analysis (ASTM 152H), and Atterberg Limits (ASTM D4318).

Table 13 summarizes the result of laboratory tests and identifies each site by blast type and site ID. Percent clay size refers to the size fraction less than 2 μ-m. Soils were classified as poorly graded sandy silt (SP-SM), low plasticity organic silts (ML-OL), low plasticity silty clay (CL-ML), low plasticity silt (ML), poorly graded gravel (GP), poorly graded sand (SP), and well-graded sand (SW).

Component velocity time-histories were used to observe the influences of soil parameters among groups of three sites with similar ranges in peak velocity and frequencies. In each case, the geophones were considered to be well-coupled. Soil parameters of water content and grain size distribution defining soil classification were used as a basis of comparison between spiked and buried geophones because they were emplaced within surface soils. In all cases sandy, gravely granular soils were compared with soils having a high percentage of fines and clay materials with varying moisture content.

Table 13 Summary of laboratory tests on soil samples taken from 15 sites

Blast Type	Site ID	TEST RESULTS								
		Water Content	Gradation				Liquid Limit	Plastic Limit	Plasticity Index	USCS Classificaiton
		(%)	% Fines	% Sand	% Gravel	% Clay-size				
Construction	NM-4	14.4	2.7	73	24.3	0				SW
	NM-5	17.2	1.4	67.1	31.5	0				SW
	NM-6	3.22	8.2	91.2	0.6	8.0				SP-SM
	NM-7	3.12	6.3	92.9	0.8	11.6				SP-SM
Hard Rock Quarry	OH-1	23.14	1.3	57.9	40.8	0				SP
Coal	OH-2	35.70	88.0	0	0	25.3	44.4	29.1	15.3	ML-OL
	OH-3									
	OH-4									
	OH-6	28.82	1.2	33.8	65.0	0				GP
	OH-5	18.82	0.8	41.6	57.6	0				GP
	WV-1	5.90	3.8	70.2	26.0	0				SW
	WV-2	13.24	3.7	59.1	37.2	0				SW
	WV-3									
	KY-6	7.31	1.4	65.3	33.3	0				SW
	KY-7									
	KY-8	13.08	4.7	81.9	13.4	0				SW
	KY-3	20.10	79.2	0	0	23.4	23	16.8	6.2	CL-ML
	KY-1	21.00	93.1	0	0	7.5	29.2	24.1	5.1	
	KY-2									
	KY-4	27.50	72.0	0	0	9.6	30.6	28.2	2.4	ML
	KY-5									

4.4.1 Comparison of gravel, sand and silt sites at low frequency

Figure 43 (a) through (c) show time histories comparing high water content silts with high water content sandy gravel and dry well-graded sand. Component peak frequencies and moisture content are given in Table 14. Geophone clusters were placed at scaled distance from 26 to 28 ft/lb$^{1/2}$.

In all cases, spiked sensors behaved nearly identical to the buried sensors with some minor variations in the wet silt (OH-2) T component where the difference in peak between the two methods was 18.4%. Two distinct observations may be made.

- Wet soils (OH-2 and OH-6) produced PPV in the R component while the dry sand, the PPV was in the T component. The T component PPV for KY-7 was found to be unusual.

- The dry SW soil produced nearly sinusoidal wave shapes absent of high frequency wavelets on the low frequency waveforms that are present in the wet soils (OH-2 and OH-6).

- High frequency wavelets superimposed on lower frequency motion are most apparent in the wet silt (OH-2) and to a lesser extent in the wet sandy gravel (OH-6).

The interpretation of low frequency, harmonic time-histories showing superimposed higher frequencies is often difficult. Many references in the literature refer to these types of time-histories as ones indicating geophone decoupling. However, this may not be the case if it is assumed that the buried sensors are well coupled and both the spiked and buried sensor shows the same features. The natural frequency of wet soils with a high percentage of fines can produce underlying low frequency responses on which high frequency motions can superimpose. Hence, special care must be taken when assessing such time-histories as decoupling may not always be the cause of this phenomenon.

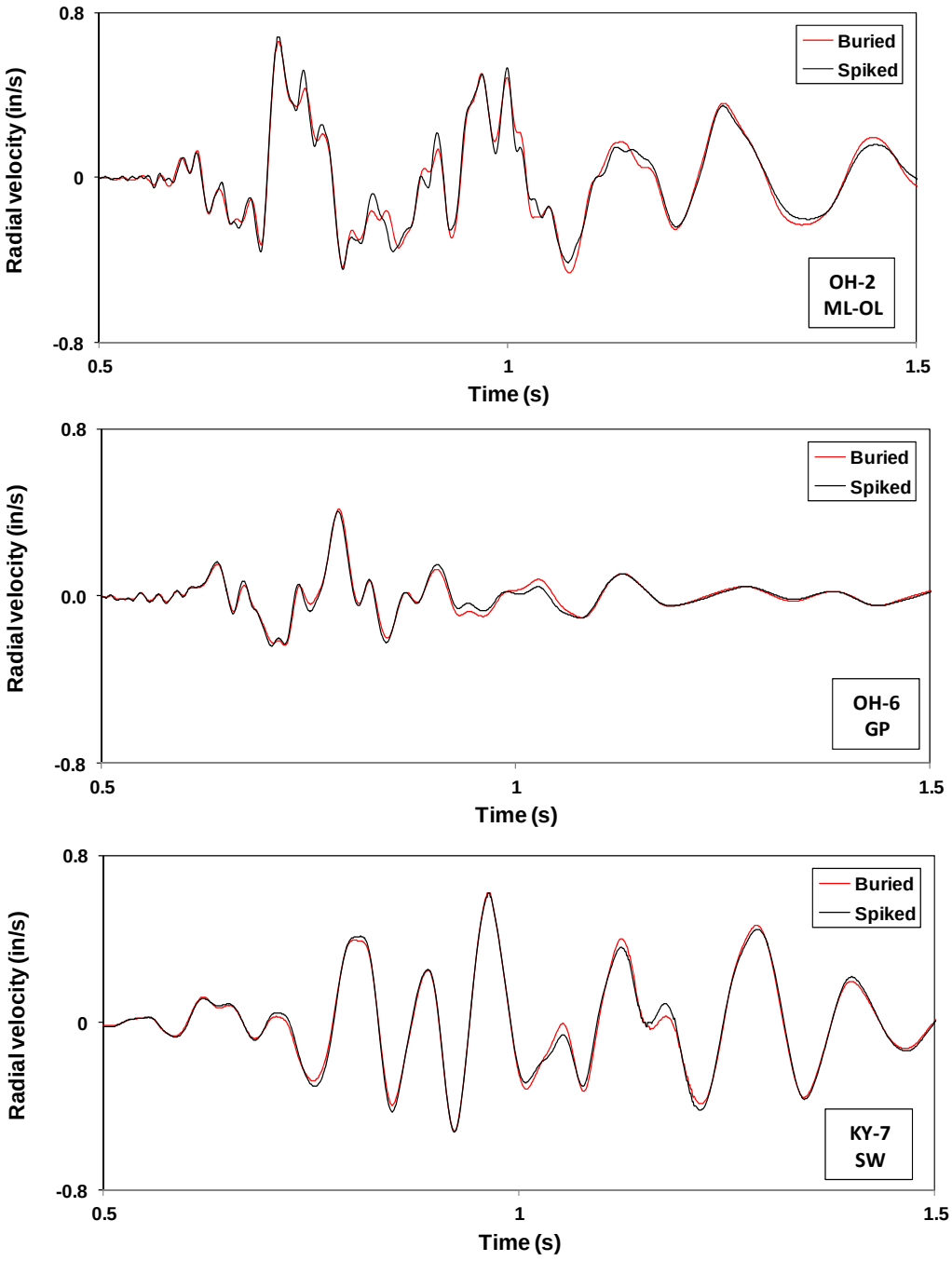

Figure 43 (a) Radial components for blast sites OH-2, OH-6, and KY-7

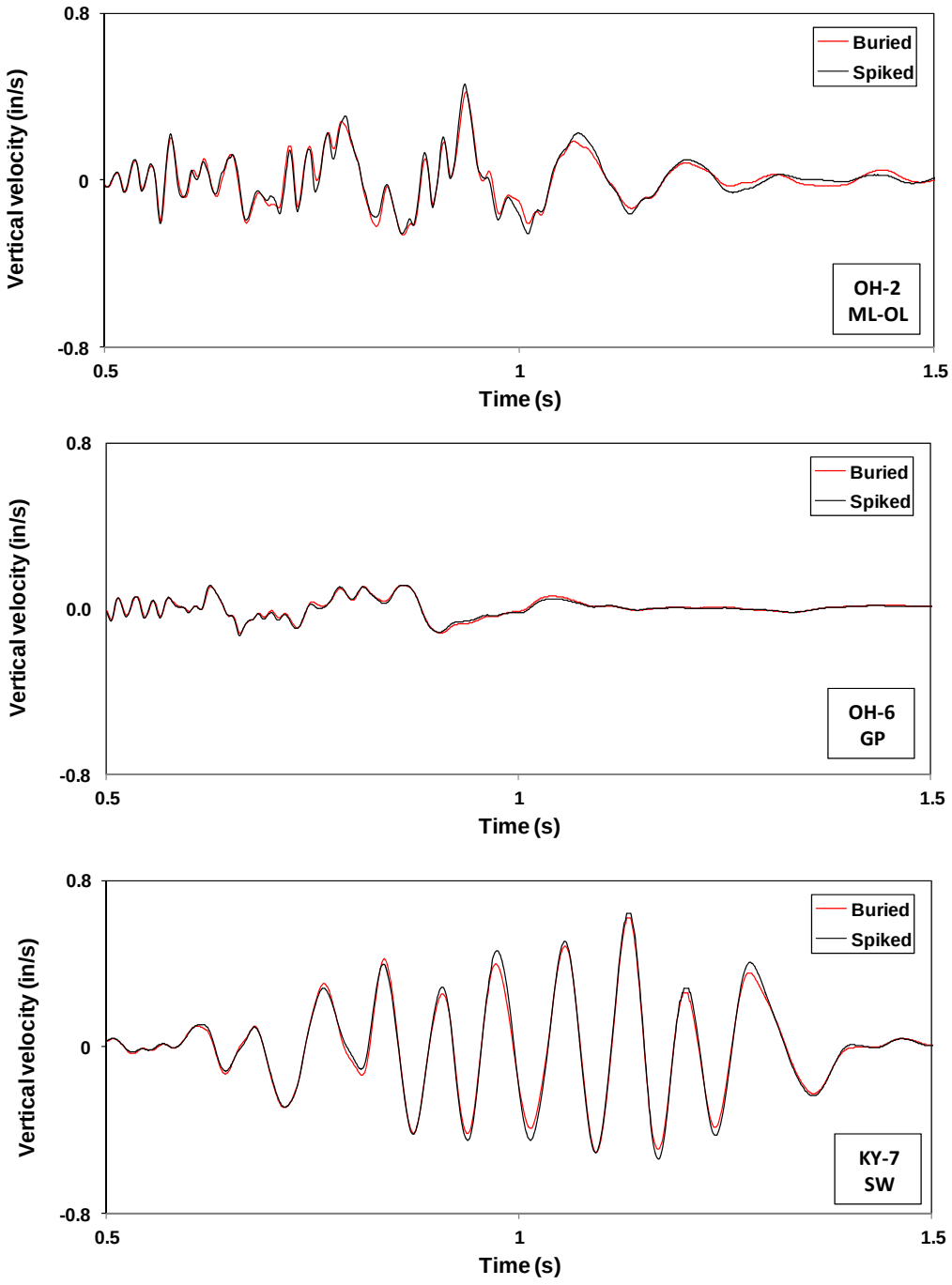

Figure 43 (b) Vertical components for blast sites OH-2, OH-6, and KY-7

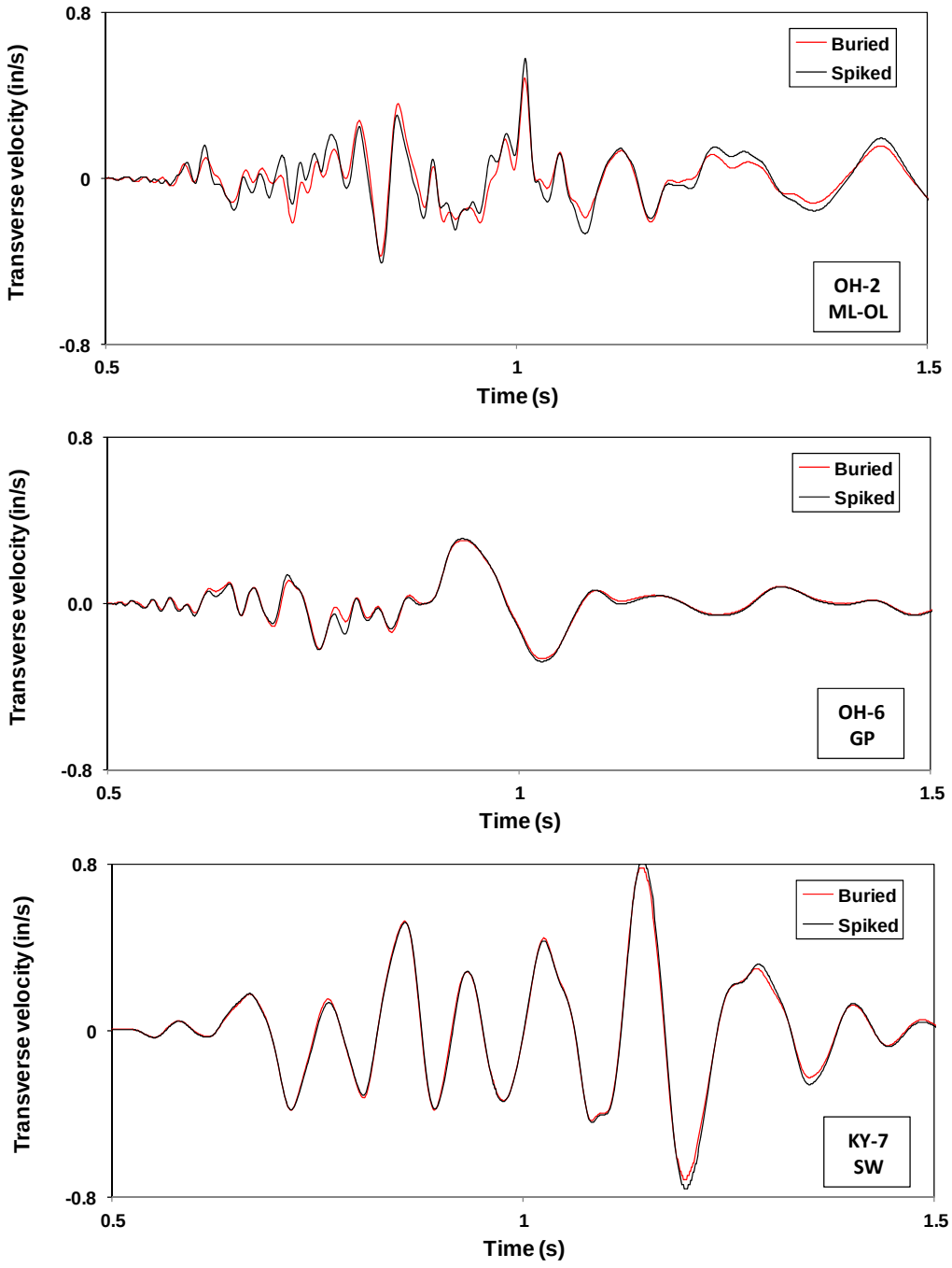

Figure 43 (c) Transverse components for blast sites OH-2, OH-6, and KY-7

Table 14 Site summary for OH-2, OH-6 and KY-7

Site ID	USCS Symbol	Water content (%)	Component frequency range (Hz)
OH-2	ML-OL	35.7	6-10
OH-6	GP	28.8	5-11
KY-7	SW	7.3	9-13

4.2 Comparison of sand and silt sites at moderate frequency, high velocity amplitude

Figure 44 (a) through (c) show time histories comparing high water content silts for a different blast with low to medium water content well-graded sands. Component peak frequencies and moisture content are given in Table 15. Geophone clusters were placed at scaled distance from 14 to 30 ft/lb$^{1/2}$.

The following observations are made:

- At elevated velocity amplitudes and frequencies, the high frequency wavelets superimposed on lower frequency motion is less apparent, particularly for OH-3 wet silt.

- For OH-3 the horizontal component spiked peaks were lower than the buried geophone peaks (9.6% and 5.9% for R and T, respectively) which is not the case for dry sandy soils.

- When sands contained higher moisture levels, as in the case of NM-4, high amplitude ground motion showed spiked sensor motions 25 to 35% higher than for buried sensors for the V and R components, respectively.

- As in the case for KY-7, NM-4 time-histories showed uniform frequency content.

- Site WV-2 exhibited velocity enhancement in all components for the buried sensor along with a time-lag in peaks in comparison with the spiked sensor. This may be caused by a lack of in-ground confinement within the dry sandy soils. This shows that it may be difficult in some dry granular soils with little or no fines to adequately compact and densify soils surrounding a buried sensor.

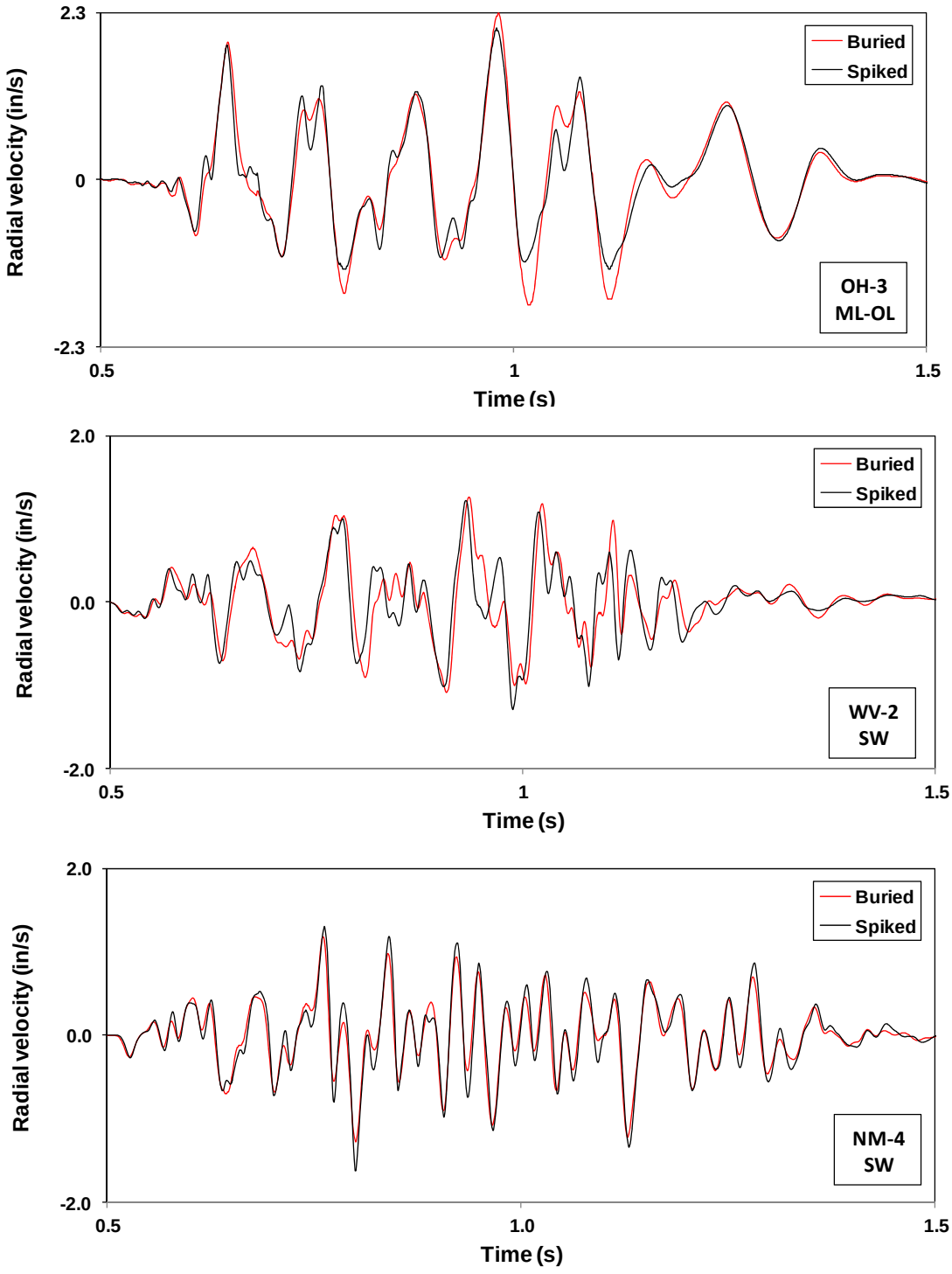

Figure 44 (a) Radial components for blast sites OH-3, WV-2, and NM-4

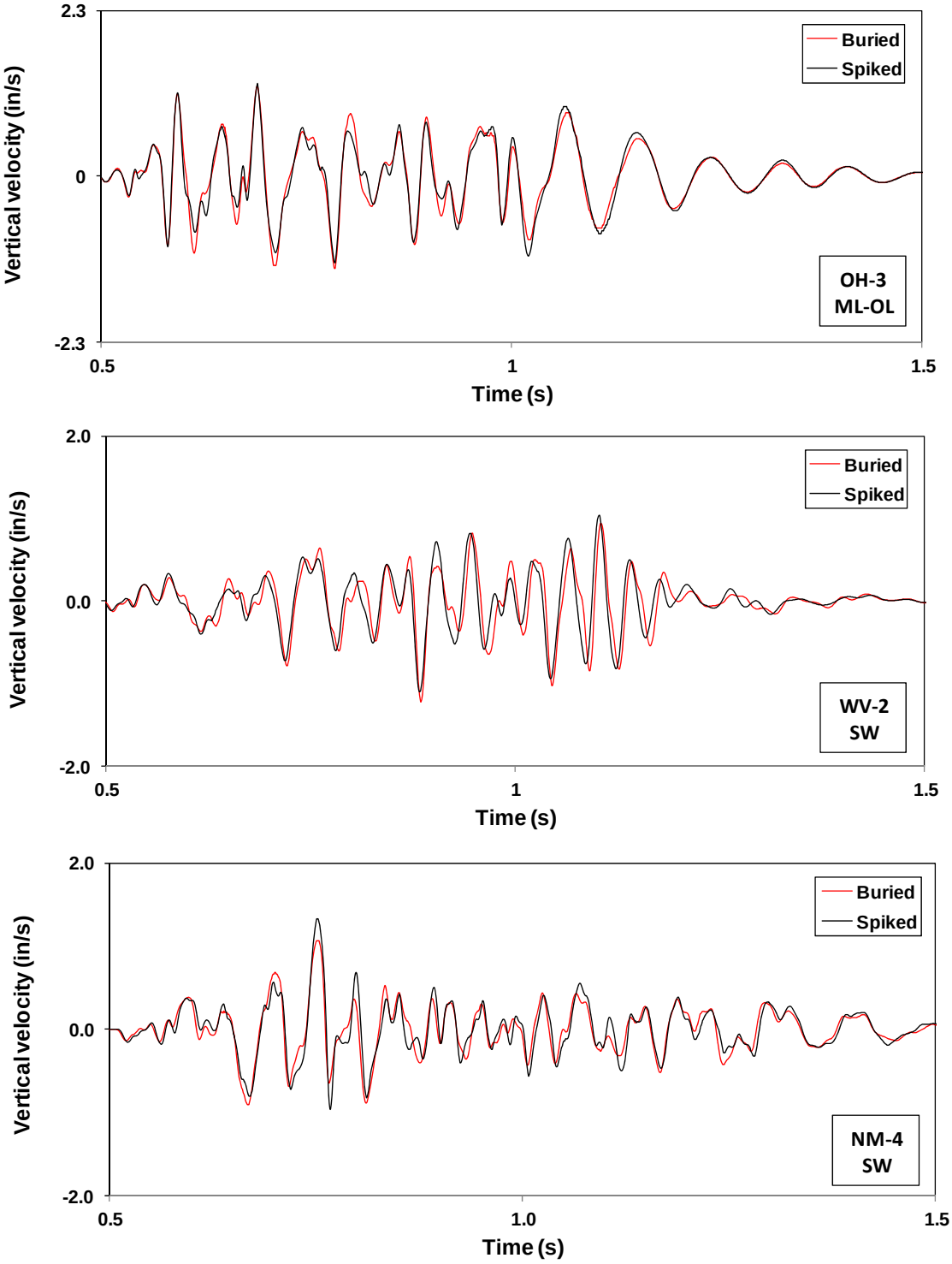

Figure 44 (b) Vertical components for blast sites OH-3, WV-2, and NM-4

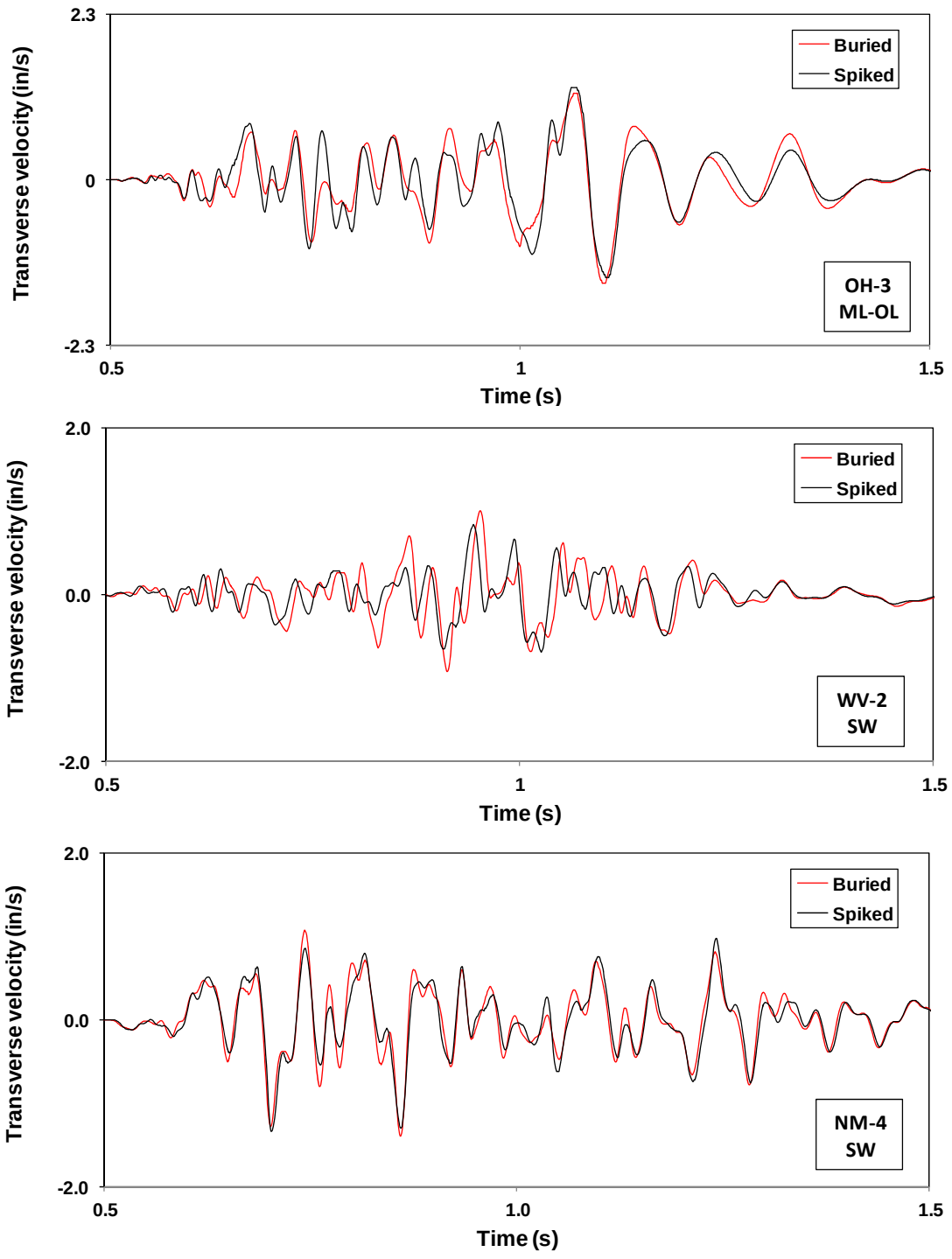

Figure 44 (c) Transverse components for blast sites OH-3, WV-2, and NM-4

Table 15 Site summary for OH-3, WV-2 and NM-4

Site ID	USCS Symbol	Water content (%)	Component frequency range (Hz)
OH-3	ML-OL	35.7	12-30
WV-2	SW	5.9	12.28
NM-4	SW	14.4	12.22

4.2.1 Comparison of clays, silts, and sand sites at high frequency, moderately high velocity amplitude

Figure 45 (a) through (c) show time-histories comparing ground motions at sites with moderately high water content silt and silty clay and low water content silty sand. Component peak frequencies and moisture content are given in Table 16 Geophone clusters were placed at scaled distance from 41 to 52 ft/lb$^{1/2}$.

The following observations are made:

- As before, the cohesive soils (sites KY-1 and KY-5) with moderate to high water contents exhibited a mixture of high frequencies superimposed on moderately lower frequencies in the horizontal components, chiefly in the T direction. The V components showed good amplitude and frequency correspondence between the two coupling methods.

- R component spiked sensor amplification was 54% in the wet silt compared with the buried sensor at site KY-5.

- There was no amplification noted in the wet silty clay soil at KY-1 for any component and the correspondence between the two methods was good.

- The T component for silty sand site NM-7 exhibited a slight time lag in the spiked sensor peaks. A 98% spiked sensor peak T velocity enhancement was noted over the buried sensor while the R component showed a 38% increase. V component frequencies were random and variable similar to NM-4.

- A buried sensor time lag was noted in the R component for NM-7 similar to the lag noted for WV-2.

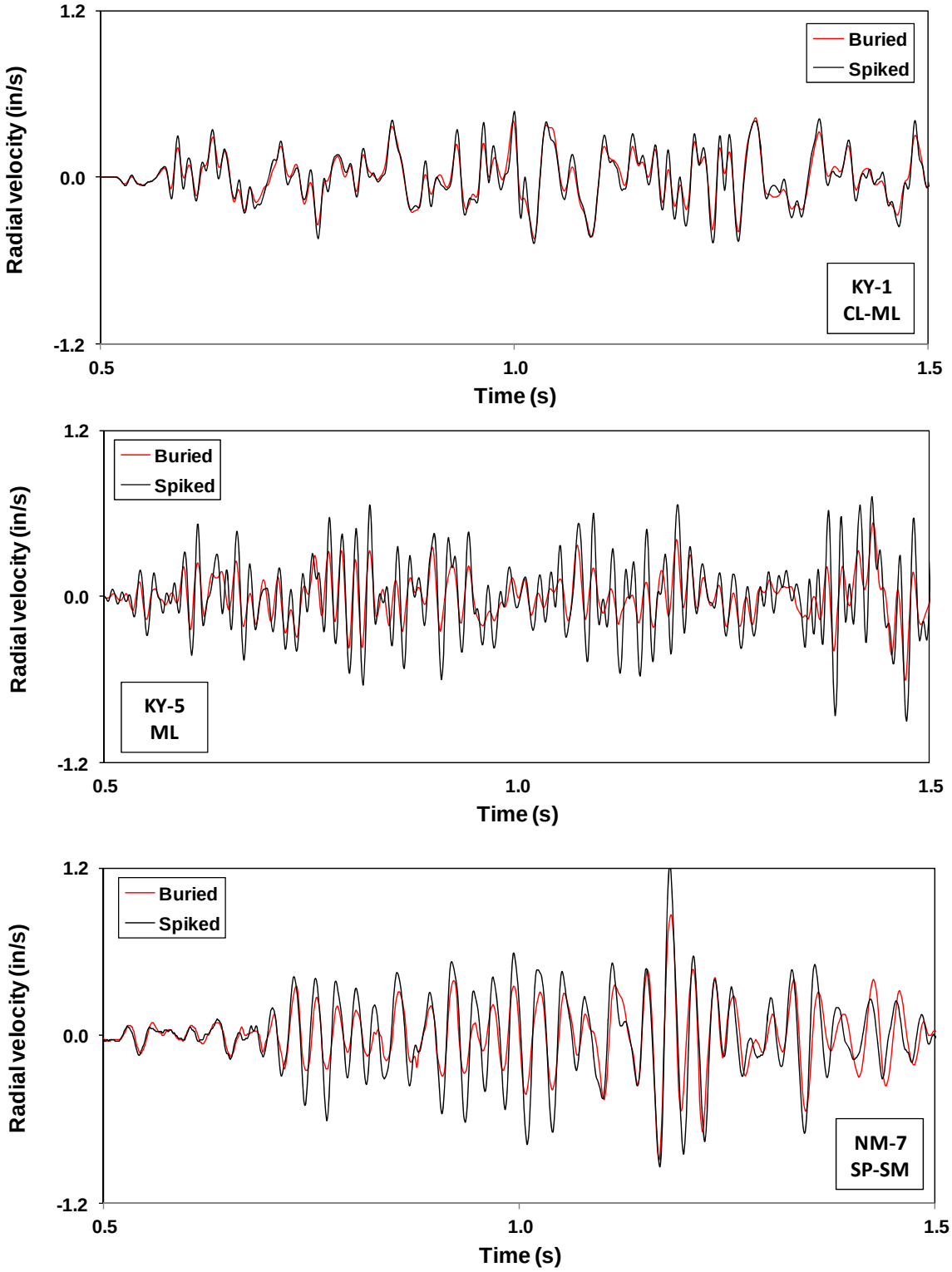

Figure 45 (a) Radial components for blast sites KY-1, KY-5, and NM-7

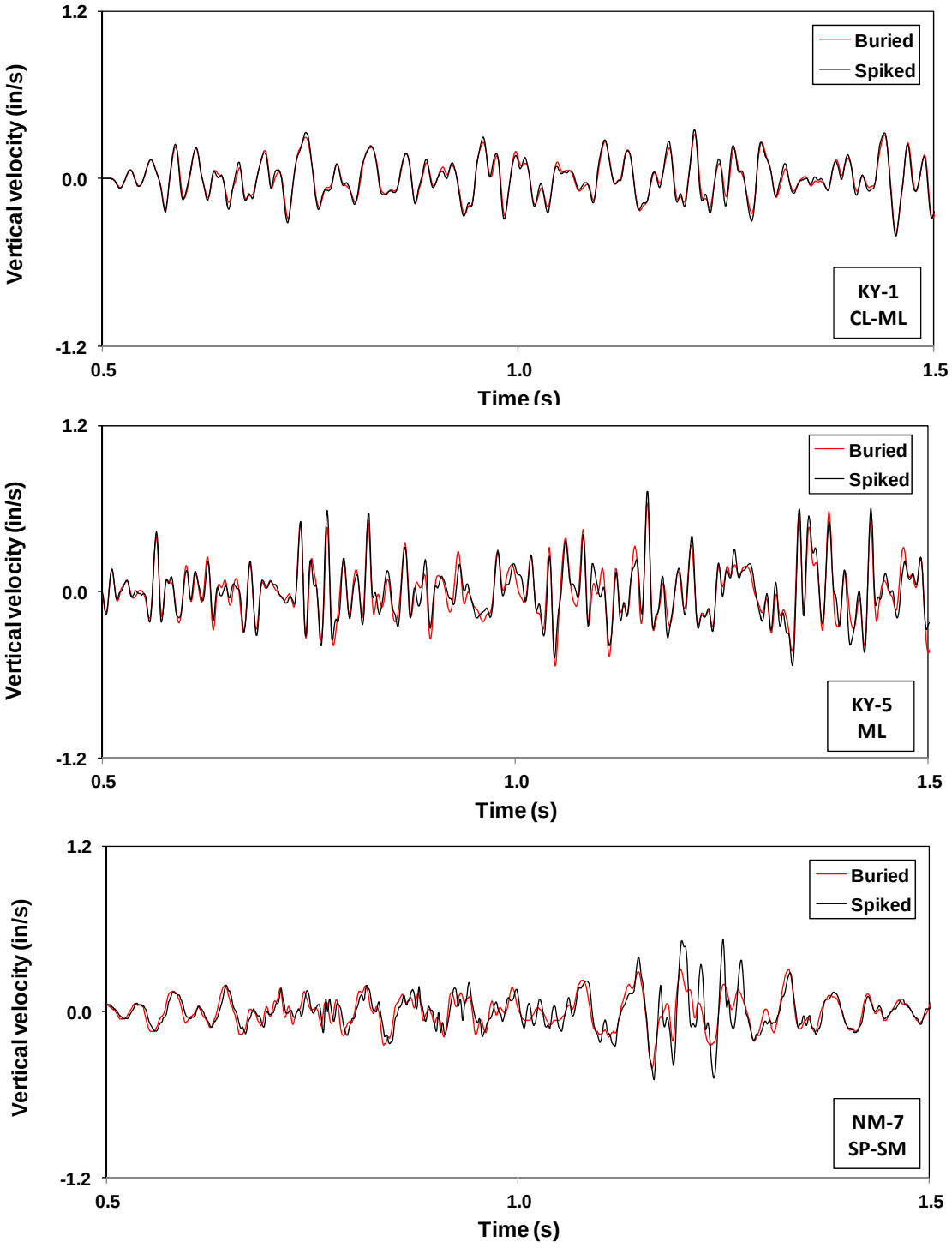

Figure 45 (b) Vertical components for blast sites KY-1, KY-5, and NM-7

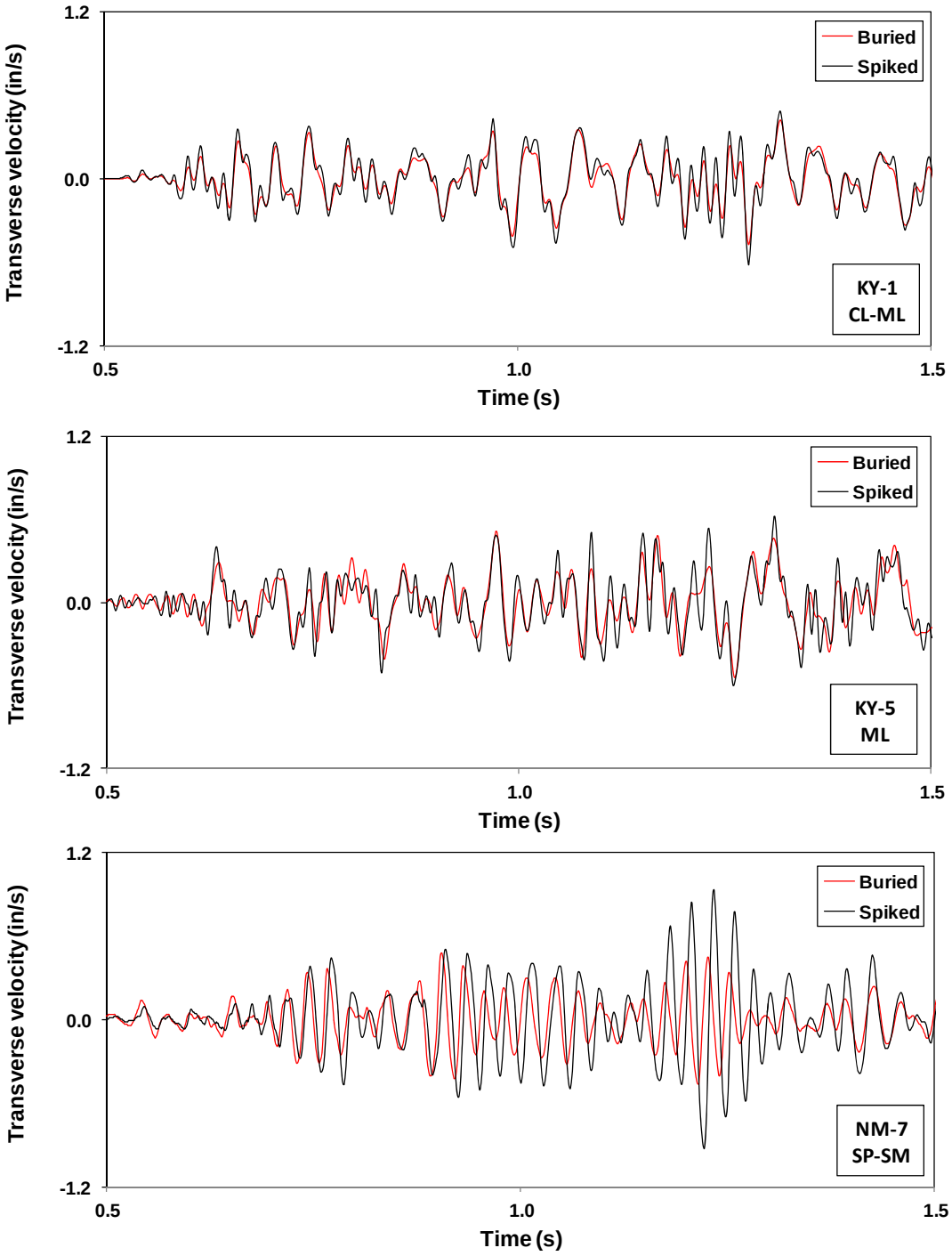

Figure 45 (c) Transverse components for blast sites KY-1, KY-5, and NM-7

Table 16 Site summary for OH-3, WV-2 and NM-4

Site ID	USCS Symbol	Water content (%)	Component frequency range (Hz)
KY-1	CL-ML	21.0	20-57
KY-5	ML	27.5	21-56
NM-7	SP-SM	3.1	23-40

4.4.4 Findings

There appears to be little correlation between geophone behavior with soil properties for buried and spiked geophones. There may be some influence of wet cohesive soils, such as slty clays and silts, on the observation of high frequencies superimposed on lower frequency horizontal ground motions that is independent of velocity amplitude and ground coupling method.

Difficulties compacting dry sandy soils when burying sensors may lead to amplification of peak velocities in all components. This may be caused by a lack of in-ground confinement within the dry sandy soils. This shows that it may be difficult in some dry granular soils with little or no fines to adequately compact and densify soils surrounding a buried sensor.

4.5 Attenuation of PPV with Scaled Distance

Figure 46 are plots of PPV as a function of scaled distance for all blast sites by coupling method for buried, spiked and sandbag geophones (a) and for all methods combined (b). Regression analysis best-fit (50-percentile) equations are given along with regression correlation coefficients (R^2) and are summarized in Table 17.

Although the data are scattered (combined data R^2 of 0.67), the attenuation fitting parameters, K-factor and slope “b”, are similar for the three methods and can be approximated by the equation for the combined data.

This shows that, *in the aggregate*, site geotechnical properties and blast methods are similar among all sites. The wide variation in rock types among the sites, including basalt, limestone, sandstone, shale, siltstone, and mudstone, do not significantly contribute to the overall trends on an based on coupling method. Variations in rock type may however contribute to the 67% data correlation.

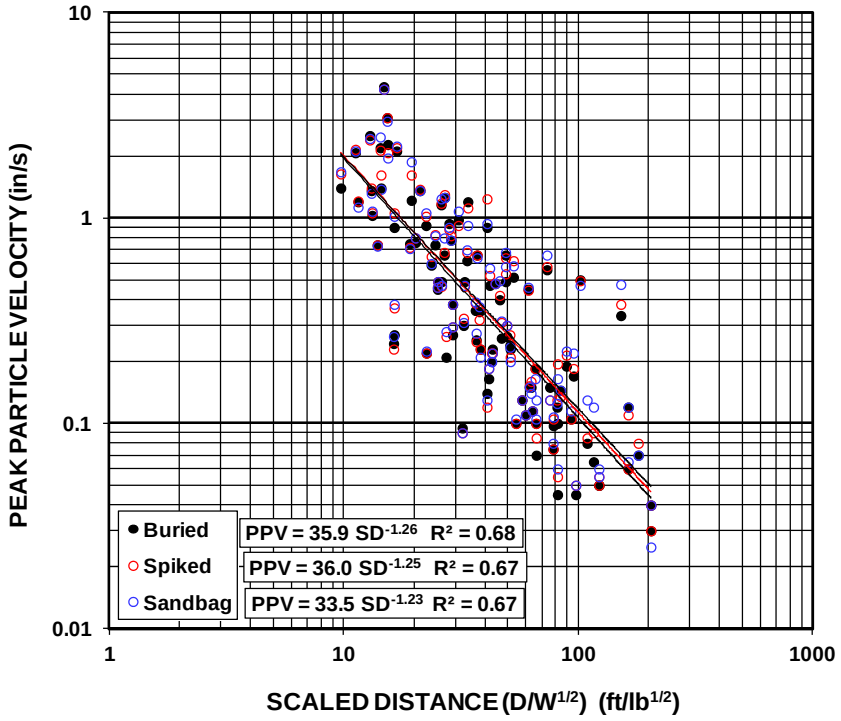

(a)

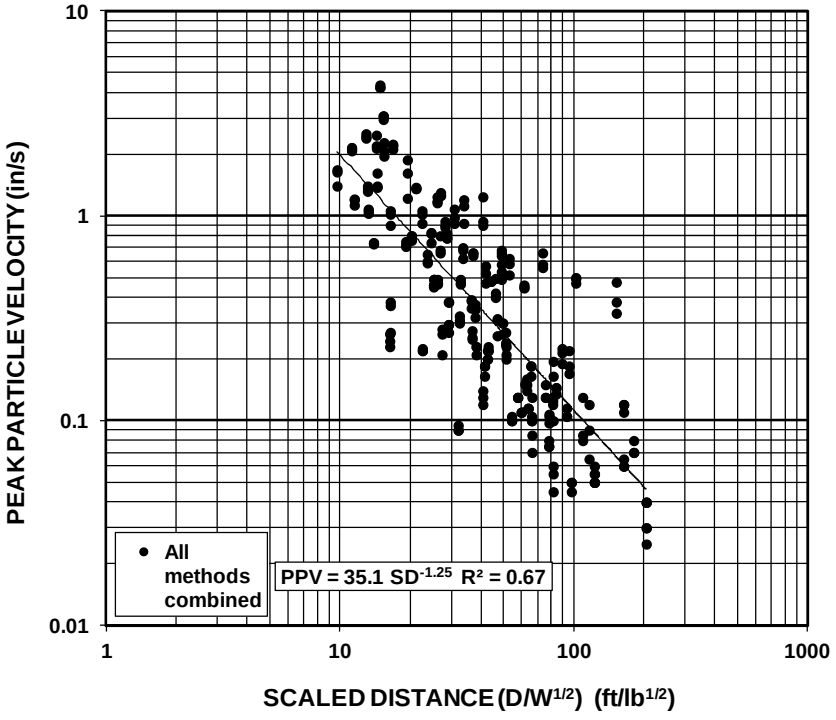

(b)

Figure 46 Peak particle velocity verses scaled distance for buried, spiked, and sandbag geophones

Table 17 Summary of regression analysis fitting parameters and correlation coefficient for attenuation plots

Method	K-factor	Slope, b	correltation coefficient R^2
Budial	35.9	-1.26	0.68
Spiking	36	-1.25	0.67
Sandbag	33.5	-1.23	0.67
All combined	35..1	-1.25	0.67

The agreement in attenuation fitting parameters does not negate the site-specific variabilities determined within each cluster. Rather, the findings indicate all methods provided similar PPV attenuation characteristics and scaled distance is not a factor influencing the performance of coupling methods.

5. CONCLUSIONS

TO BE SUBMITTED

6. REFERENCES

Taylor, B.N., and C. E. Kuyatt, 1994, Guidelines for Evaluating and Expressing the Uncertainty of NIST Measurement Results, NIST Technical Note 1297, 1994 edition, US Department of Commerce, National Institutes of Standards and Technology.

Adhikari, G., Venkatesh, H., Theresraj, A., Yor, S., Balachander, R., Jain, N., and Gupta, R., 2005, Role of Blast Design Parameters on Ground Vibration and Correlation of Vibration Level to Blasting Damage to Surface Structures, S&T Project: MT/134/02, National Institute of Rock Mechanics, Karnataka, India.

Aimone-Martin, C.T., Martell, M.A., McKenna, L.M., Siskind, D.E. and Dowding C.H., 2002, Comparative Study of Structure Response to Coal Mine Blasting, for the Office of Surface Mining, Pittsburgh, PA.

Armstrong, L.W., 2001, Evaluation of Parameters Effecting Blast Induced Vibrations, PhD Thesis, Faculty of Engineering, University of Wollongong.

Grogan, A., 1998, A Review of Suggested Geophone Attachments Methodologies From Commonly Referred to Monitoring Standards, Proceedings of the 24th Annual Conference on Explosives and Blasting Techniques, International Society of Explosives Engineers, New Orleans, pp. 105 -113.

International Society of Explosives Engineers, 2009, ISEE Field Practice Guideline Blasting Seismographs, Blast Vibration and Seismograph Section, Cleveland.

ISRM, 1992, Suggested Method for Blast Vibration Monitoring, International Journal of Rock Mechanics and Mining Science & Geomechanics Abstracts, Col., 29, No. 2, pp. 143-156.

Kinney, A., 2009, Effects of Soil Types on Geophone Measurements for Different Coupling Methods, M.S. project paper, New Mexico Institute of Mining and Technology.

Moser, T. B., 2010, Geophone Coupling – A comparative analysis of geophone response and ground vibration induced decoupling, M.S. thesis, New Mexico Institute of Mining and Technology.

Robertson, D. A., 1993, The Neglected Step to Accurate Blast Monitoring: Proper Coupling, Proceedings of the 9th Annual Symposium on Explosives and Blasting Research, International Society of Explosives Engineers, San Diego, pp. 83-91.

Stagg, M.S., and Engler, A.J., 1980, Measurement of Blast-induced Ground Vibrations and Seismograph Calibration, U.S. Bureau of Mines RI 8506.

Washburn, H. and Wiley, H., 1941, The Effects of the Placement of a Seismometer on its Response Characteristics, Geophysics, Vol. 6, Issue 2, p. 116.

Wheeler, R., 2004, The Importance of proper Seismometer Coupling, Proceedings of the 30th Annual Conference on Explosives and Blasting Techniques, International Society of Explosives Engineers, New Orleans, pp. 147-159.